40

DEGRADATION OF THE BETA-ALUMINA ELECTROLYTE IN A ZEBRA CELL

by

D P van Heerden

A thesis submitted to the Faculty of Engineering, University of Cape Town in fulfillment of the degree of Master of Science in Applied Science.

Department of Materials Engineering
University of Cape Town

[1988]

ACKNOWLEDGEMENTS

I would like to thank the following people who assisted me in this project:

My supervisors, Dr Ron Hutchings and Prof Anthony Ball for their encouragement, interest and advice.

Doctors Johan Coetzer, Roger Wedlake, Magriet Nolte and Tony Meintjies as well as Mr Sakkie Vlok of Zebra Power Systems (Pty) Limited for their interest, practical assistance and suggestions.

Mr Bernard Greeves and Mr James Peterson for their photographic expertise.

My fellow students within the department for their general assistance with the project.

The staff of the NIMR for the use of their facilities in compiling this thesis as well as their assistance with proof reading.

Mrs Sue Betz and Mrs Helgard Bohm for their assistance with the drawings and with compiling this thesis.

Dynamic Power Systems (Pty) Limited for financial support of this project.

ABSTRACT

Beta-alumina solid electrolytes studied were subjected to charge and discharge cycles in a secondary, high energy density Na/beta-alumina/$NaAlCl_4$/$FeCl_2$ cell (known as the Zebra cell) at 250^0 C. These electrolytes were studied by means of optical microscopy, as well as SEM and EDS analyses to establish possible failure modes.

After cycling little discolouration, or impurity pickup was found to have occurred in the electrolyte. The forms of degradation of the beta-alumina electrolyte identified appeared to be a result of inherent flaws in the beta-alumina electrolyte tube, problems due to protracted storage of the tubes, or an apparent interfacial film on the cathode/electrolyte interface.

A lead wetting agent was used in the cells to enhance the wetting of the beta-alumina electrolyte by the liquid Na. A study of the this coating after cycling of the cell showed that the coating was adherent irrespective of the number of cycles completed. The coating did not appear to influence cracking of the electrolyte during cycling.

Cracking of the beta-alumina electrolyte was found to have initiated from the Na/electrolyte interface. No evidence of crack initiation nor internal damage was found on the cathode/electrolyte interface.

The cracks through the beta-alumina electrolyte wall were found to have sealed by the formation of a plug consisting largely of Na and Cl. On the basis of EDS analyses of the fracture surface of the sealed crack possible sealing mechanisms are proposed.

CONTENTS

1. INTRODUCTION

The development of a high energy density battery system for load leveling and vehicle propulsion applications has, until recently, been largely reliant on the sodium/sulphur battery. In spite of intense research for almost twenty years the sodium/sulphur battery has not gone beyond the research stage due to inherent difficulties with respect to safety and reliability.

The recently announced Zebra cell (Coetzer; 1986) circumvents the pitfalls of the sodium/sulphur cell. The electrochemically active portions of the cell are a molten metallic sodium electrode and a porous electronically conducting iron electrode saturated with sodium aluminium chloride. The outer surface of the porous iron matrix is covered with a thin layer of iron chloride ($FeCl_2$). The electrodes are separated by a sodium ion conducting ceramic tube made of beta-alumina. The beta-alumina tube acts as the electrolyte of the cell: separating the reactants but simultaneously permitting sodium ion transfer. Beta-alumina conducts sodium ions, but is an electronic insulator. The cell operates at 250^0 C, well above the melting point of the sodium and the sodium aluminium chloride.

On connecting an external circuit to the cell the metallic sodium is ionized, giving off an electron to the anode current collector. The sodium ion then diffuses through the beta-alumina electrolyte to the cathode.

The reaction in the cathode is:

$$FeCl_2 + 2Na^+ + e^- \longrightarrow Fe + 2NaCl$$

Thus the overall cell in the Zebra cell during discharge is:

$$\begin{array}{rl} FeCl_2 + 2Na^+ + 2e^- \longrightarrow Fe + 2NaCl & \text{(cathode)} \\ \underline{2Na \longrightarrow 2Na^+ + 2e^-} & \underline{\text{(anode)}} \\ FeCl_2 + 2Na \longrightarrow Fe + 2NaCl & \text{(overall cell reaction)} \end{array}$$

The sodium aluminium chloride merely acts as a sodium ion transport medium (similar to the beta-alumina) and is not an electrochemically active portion of the cell. The cell thus operates simply by the electrochemical conversion of iron chloride to iron and sodium chloride during discharge of the cell, with the resultant chemical energy being converted to electricity. The reactions are reversible ie. the cell is fully rechargeable.

The cells have proved to be extremely reliable, with lifetimes of greater than 1000 cycles being reported (Coetzer; 1987). However premature cell failure and progressively decreasing cell capacities have occasionally been encountered.

Although there are several possible sources of degradation in the cell, this thesis will be predominantly concerned with the role of the beta-alumina tube in the degradation of the Zebra cell.

The aims of this project were:

1) To determine the role of the beta-alumina electrolyte in the degradation of cell performance in the Zebra cell
2) To determine the influence of the wetting agent used to enhance the wetting of the beta-alumina electrolyte by the liquid sodium on the cycling and degradation of the beta-alumina electrolyte tube.
3) To confirm the existence of, and determine the mechanism causing the crack sealing phenomena observed in beta-alumina tubes in Zebra cells as reported by Coetzer (1987).

All the cells studied were supplied by Zebra Power Systems (Pty) Limited. as part of their cell development program. The cells were thus not cycled to produce specific degradation modes but were set up to examine the performance of the cells.

This thesis is structured as follows:

1) The operation of the sodium/sulphur battery will be reviewed along with its known degradation mechanisms. Particular attention will be paid to the known degradation mechanisms in the beta-alumina electrolyte in these cells. Many of the processes in the sodium/sulphur battery are directly analogous to those in the Zebra cell and hence degradation in these cells should be similar to those of the Zebra cell.

2) Once the degradation modes in the sodium sulphur cell have been detailed, the Zebra cell will be discussed along with the known electrochemical processes occurring in it.

3) An investigation of the microstructure and phase content of an uncycled beta-alumina tube is reported. These results characterise the "as supplied" beta-alumina electrolyte.

4) The role of the beta-alumina in the degradation of the Zebra cell was investigated. Four beta-alumina electrolytes from cells showing different failure modes were examined and compared to a cell which had shown no degradation of cell performance with cycling, and to an uncycled electrolyte. Chemical, physical and microstructural changes in the chosen samples were investigated and interpreted.

5) The wetting of beta-alumina is enhanced by coating the of the sodium/electrolyte interface with a thin layer of lead. A study of the influence of this lead coating on the cycling and degradation of the beta- alumina electrolyte was undertaken. The sodium/electrolyte] interfaces of electrolytes from cycled cells were examined to determine the distribution of the Pb coating after cycling. The chemical compositions of fracture surfaces of cracks in the beta-alumina electrolyte was determined to assess whether the lead coating influences cracking of the electrolyte.

6) Several of the beta-alumina electrolytes extracted from cycled cells were found to contain cracks running through the wall from the sodium cathode to the cathode without internal shorting occurring. The physical appearance and chemical compositions of the interiors of these cracks were examined to determine whether crack sealing had occurred. Information from this investigation could be used to propose a possible crack sealing mechanism.

7) Finally the research conclusions will be summarised, and recommended future research areas relating to the degradation of Zebra cells suggested.

2. THE SODIUM/SULPHUR CELL

The structure, cycling and degradation of the Na/S cell will be discussed first, with a description of the Zebra cell following in chapter 5. Though the cathode design and composition of the Na/S cell differs from that of the Zebra cell, the principles involved in the operation and design are analogous. Furthermore many of the failure mechanisms in the Na/S cell are directly applicable to the Zebra cell as they are a result of the inherent properties of the beta-alumina electrolyte rather than the cathode composition.

The two electrodes of the Na/S Cell are molten sodium and molten sulphur. A beta-alumina tube simultaneously separates the liquid electrodes and acts as the electrolyte. The cell operates at temperatures between 300^0 and 350^0 C.

Several different configurations of the Na/S cell have been devised. One of the most widely used configurations (and the one used for most of the Zebra cells studied in this thesis) is shown in figure 2.1. The anode consists of a central molten sodium electrode (*) contained in a polycrystalline, sintered beta-alumina tube. The cathode is made up of liquid sulphur ($) contained between the outer surface of the tube and the outer casing of the cell.

At the top of the beta-alumina tube is an -alumina ring which is sealed to the beta-alumina with a borosilicate or alumino-borate glass. The ring acts as an electronic insulator between the cathode and anode. It is sealed to the respective container halves by an aluminium compression gasket.

---

* The liquid sodium will be referred to throughout this thesis as the anode: it acts as an electron donor during discharge of the cell.

$ The liquid sulphur will be referred to throughout this thesis as the cathode: it acts as an electron accepter during discharge of the cell.

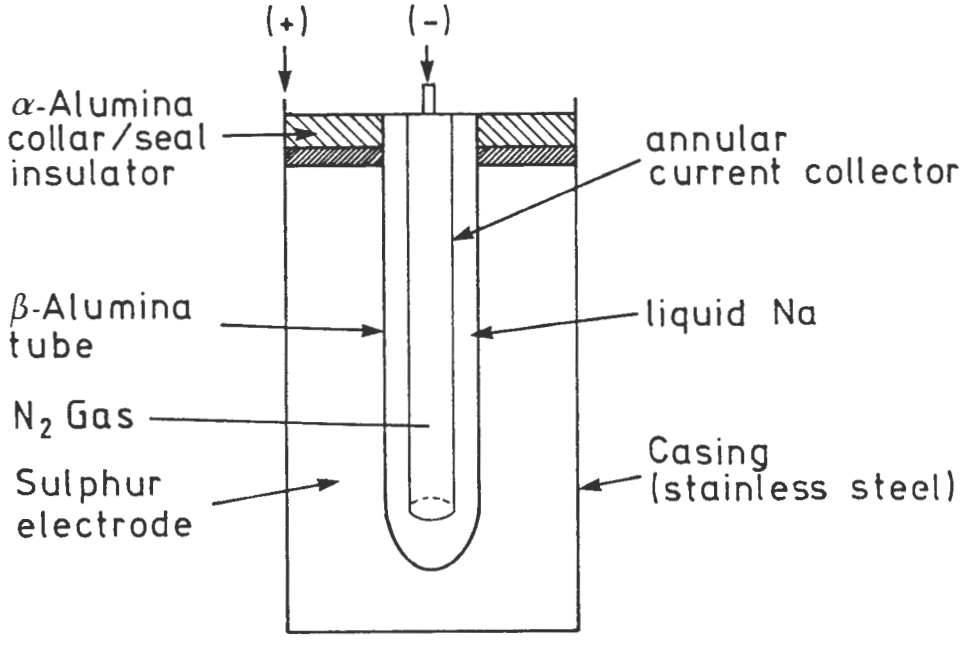

FIGURE 2.1. A SCHEMATIC REPRESENTATION OF A NA/S CELL.

During cell discharge the sodium is oxidised at the cell anode via the half-cell reaction:

$$Na \longrightarrow Na^{+} + e^{-}$$

The Na^{+} ions are transported through the beta-alumina electrolyte to the cell cathode where the sulphur is reduced via the half-cell reaction:

$$2e^{-} + S^{0} \longrightarrow S^{2-}$$

Electrons flow through the external circuit to produce the power. On charging of the cell the above reactions are reversed.

The electrolyte used is polycrystalline beta-alumina. Beta-alumina was chosen due to its low ionic resistivity and relative ease of manufacture. The crystal structure and ionic conductivity of beta-alumina will be discussed in section 3.

2.1 THE SULPHUR ELECTRODE.

The reaction of S with Na+ ions forms a variety of polysulphides (Na_2S_x). Some of the polysulphides formed are immiscible with liquid S, whilst others are solid and insoluble in the sulphur. This severely restricts the amount of discharge of the cell which may be allowed to

occur. Generally the cell is not discharged beyond a cathode composition 2Na:3S.

Molten S is an electronic insulator. To ensure that electronic extraction is possible from the cathode a graphite felt is added.

Space is provided at the sulphur side of the electrolyte for expansion due to polysulphide formation during discharge.

2.2 The SODIUM ELECTRODE.

Na does not wet beta-alumina below 300^0 C (Gibson; 1977). Bad wetting of the beta-alumina by the Na has been found to cause an interfacial resistance rise in Na/S cells.

Good wetting can be achieved by heating Na in contact with beta-alumina to a temperature between 350^0 and 400^0 C. Once good wetting of the beta-alumina by the liquid Na is achieved it is maintained at temperatures as low as 200^0C. Wetting is improved by cell cycling. However the presence of moisture on the beta-alumina surface has an adverse effect on the wetting of the surface (Viswanathan et al;1982).

Surface treatments of the beta-alumina were developed to improve wetting at the beta-alumina/Na interface. The smallest contact angle between the beta-alumina and molten Na was obtained by rubbing the surface with metallic lead (Demott et al.;1985). In practice the surface of the beta-alumina is coated with lead acetate using a saturated aqueous solution. The lead acetate is then decomposed to metallic Pb by heating to 250^0 C for several hours. Coating the surface with Pb was found to be only partially successful in preventing an interfacal resistance rise in the cells. Adding an oxygen getter (typically Ti or Al) to the Na in addition to the Pb coating is more successful in stabilising the cell resistances (Demott et al.;1985).

To ensure that no current concentration occurs in the electrolyte, the Na must be in contact with the entire inner surface of the beta-alumina tube during both charge and discharge of the cell. Several different designs have been developed to ensure that this occurs. In all the cells studied in this thesis, complete surface contact between the beta-alumina and the molten Na was ensured by forcing the Na from the reservoir by means of gas pressure (see figure 2.1).

3 The Electrolyte

The electrolyte used in Na/S cells (and in the Zebra cell) is a polycrystalline sodium-beta alumina tube.

Beta-alumina is made up of two phases: β-alumina and β"-alumina (*). Both β-alumina and β"-alumina are superionic conductors ie. the skeletons of their structures offer a number of vacant sites which may be occupied by mobile ions. The ions are easily able to jump the energy barrier between sites and migrate from one equivalent site to another along preferred pathways (Collongues et al; 1984).

3.1. β-ALUMINA

β-Alumina is the "historical" name of a sodium hexaluminate with a stoichiometric formula $Na_2O.11Al_2O_3$. β-Alumina has a hexagonal crystal structure with a space group $p6_3/mmc$ and lattice parameters:

a=5.587 $^{+}/_{-}$ 0.0004 Å
c=22.61 $^{+}/_{-}$ 0.002 Å

The crystal structure is made up of alternating layers of "spinel blocks" and "conduction planes". The crystal structure is illustrated in figure 3.1.(a).

Notice that there are two conduction planes and two spinel blocks per unit cell. The spinel blocks are made up of four close packed cubic layers of oxygen in which Al^{3+} ions occupy the octahedral and tetrahedral cation positions. The spinel blocks are stacked with a two fold screw symmetry as shown in fig 3.1.(b) (Yamaguchi et al.; 1968).

---

* Throughout the thesis beta-alumina will be used to refered to when no distinction is made between the β and β" phases β-alumina, or β will be used when the beta phase specifically
β"-alumina, or β" will be used when referring to the β" phase specifically.

FIGURE 3.1.(a) THE CRYSTAL STRUCTURE OF β-ALUMINA
(b) THE STACKING MODE OF THE SPINEL BLOCKS IN β-ALUMINA

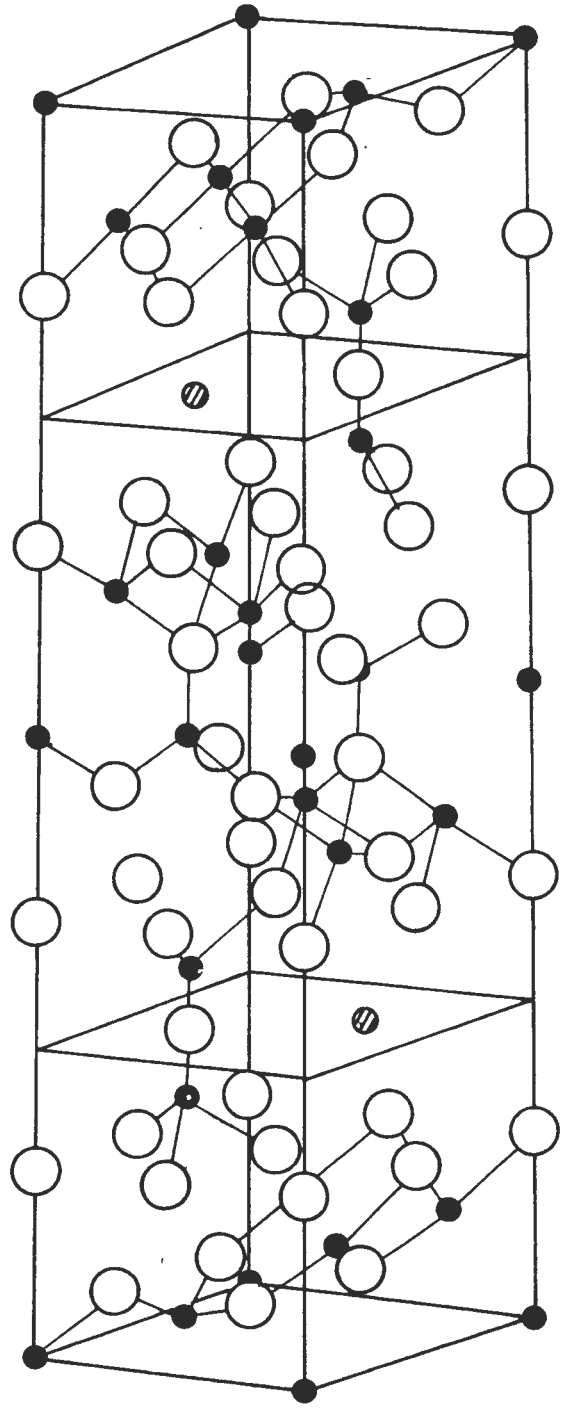

(A)

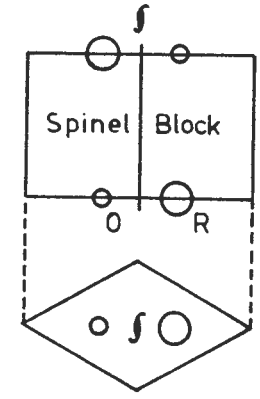

(B)

● Al^{+++}
⊘ Na^{+}
○ O^{--}

The conduction planes are situated between the spinel blocks. They contain Al-O-Al "spacers" binding the spinel units together. The conduction planes are mirror planes and contain the vacant sites for the migration of Na^+ ions. The possible Na^+ ion migration sites in each conduction plane in a unit cell are shown in figure 3.2. Notice that there are three types of sites in which the cation can be positioned, the Beevers-Ross (BR), anti-Beevers-Ross (aBR) and the mid-oxygen (mO) sites.

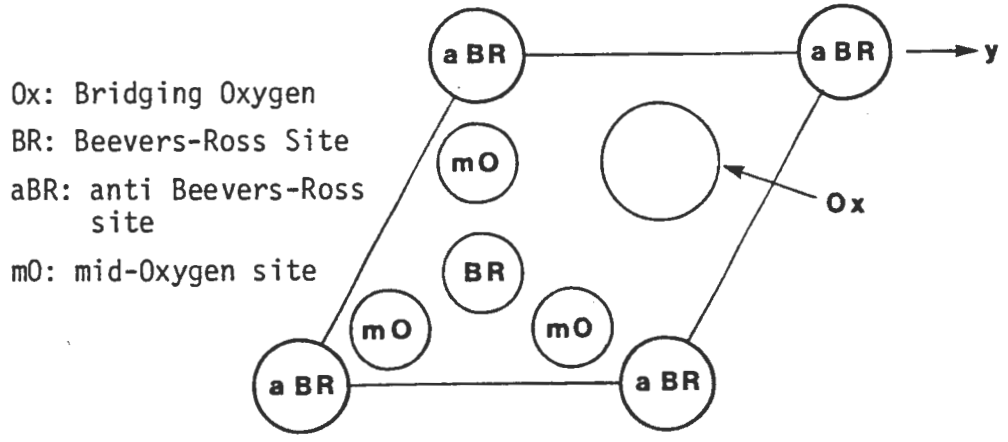

FIGURE 3.2. A SECTION THROUGH THE CONDUCTION PLANE OF β-ALUMINA SHOWING THE SITES AVAILABLE FOR Na^+ ION OCCUPATION.

The stoichiometric formula for β-alumina in the crystal structure shown in figure 3.1.(a) is $Na_2O.11Al_2O_3$ ie. one Na^+ ion per conduction plane per unit cell. As can be seen from the Na_2O/Al_2O_3 phase diagram in figure 3.3. β-alumina is found in the range $Na_2O:Al_2O_3$ 1:5.3 to 1:8.5 ie. stoichiometric β-alumina does not exist in the stability range of β-alumina.

In a neutron diffraction study of β-alumina carried out by Roth et al.(1976) defects were found containing an interstitial oxygen atom at a mid-oxygen position in the conduction plane. This interstitial oxygen attracts two Al^{3+} ions, displacing them from their lattice positions and leaving Al vacancies in the spinel ie. a v_{Al}-Al_i-O-Al_i-v_{Al} defect is formed (where v_{Al}-Al_i represents a vacancy interstitial pair). Two extra Na^+ ions are associated with the oxygen to preserve electroneutrality. Two BR sites are found to be vacant: the Na^+ ions normally associated with them occupy two nearby mO positions. This implies that in total four Na^+ ions are found close to mO positions associated with the oxygen interstitials. Thus more Na^+

ions are accommodated in the lattice than was stoichiometrically predicted.

Due to the presence of the oxygen interstitials, at 350^0 C, 59% of the Na^+ ions are on BR, 36% on mO, and 5% on aBR sites (Roth et al.,1976).

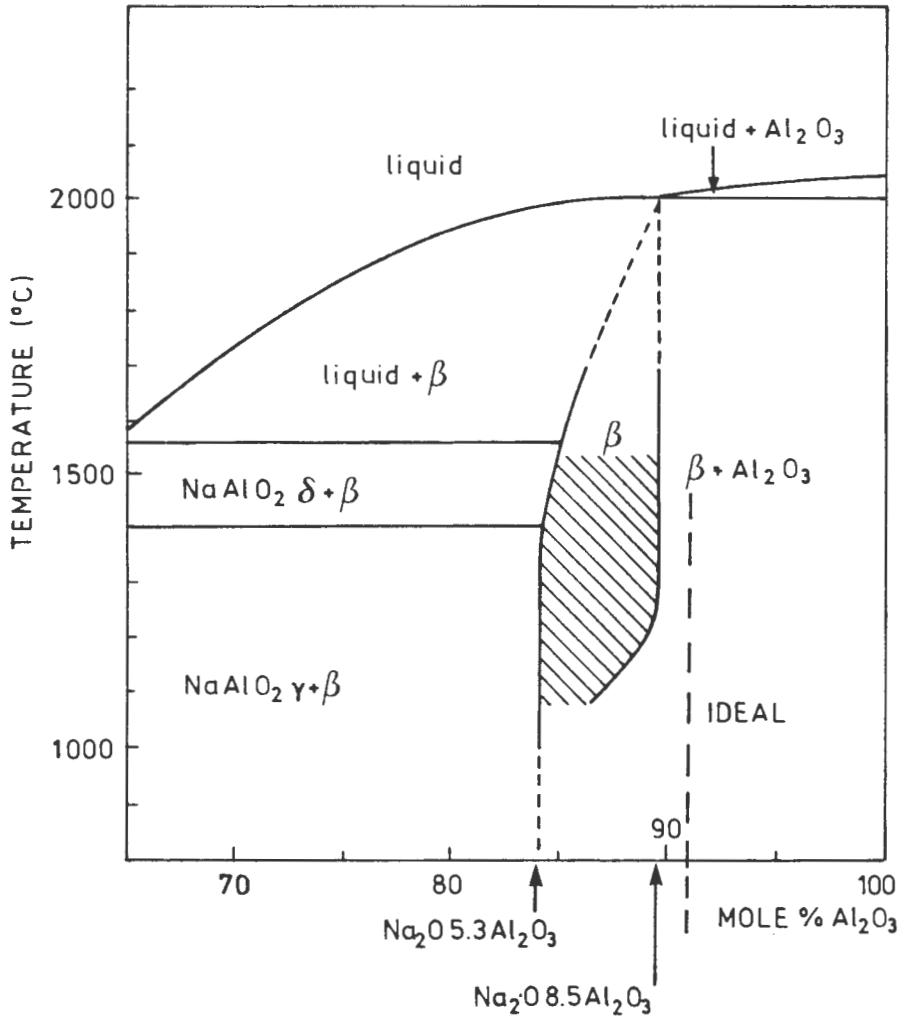

FIGURE 3.3. THE Na_2O/Al_2O_3 PHASE DIAGRAM.

An alternate mechanism for increasing the Na content of the β-alumina is by doping. Substitution of Al^{3+} with a cation of lower charge results in a deficiency of positive charge. Studies of the effect of Mg^{2+} doping on β-alumina showed that one extra Na^+ ion is incorporated in the conduction plane for every Mg^{2+} ion incorported in the spinel

The general formula for ß-alumina is thus

$$(Al_{11-y}Mg_y)(ONa_{1+x+y}O_{16+x/2}) \qquad (3.1.)$$

where x refers to interstitial oxygen in the conduction plane and y refers to Mg^{2+} ions substituted for Al^{3+} in the spinel.

In fact the Na^+ ions in β-alumina are slightly displaced from the BR positions, resulting in an in-plane order between the ionic displacements of the Na^+ ions (Boilot et al.;1980). This leads to the formation of a superstructure with a lattice constant of $a(3)^{0.5}$ in the conduction plane. The superstructure formed is shown in figure 3.4.

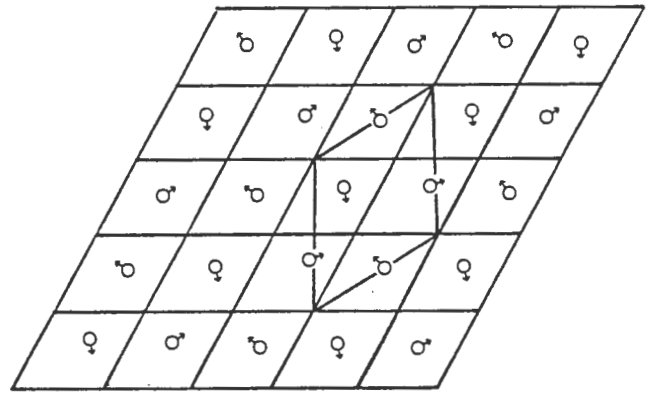

FIGURE 3.4. THE SUPERSTRUCTURE FORMED BY THE Na^+ IONS IN THE CONDUCTION PLANE OF β-ALUMINA.

The degree of ordering of cations and vacancies on a superlattice influences the activation energy for diffusion at low temperatures ie. larger correlation lengths are associated with higher activation energies. No long range order of the Na^+ ions has been observed in β-alumina; the disorder of the mobile ions results from competition between mobile ion/mobile ion repulsion and attraction to the randomly distributed charge compensating defects.

In 1979 Wolf proposed a conduction mechanism which fulfilled most of the known criteria. In Wolf's mechanism ions move in pairs; reference to figure 3.5.(a) shows that in his model Na^+ ions exist on the BR sites (marked 1) with an extra ion at the aBR site (marked 2). The interstitial ion, along with a BR ion then jumps to a mO-mO configuration shown in figure 3.5.(b) (marked in the figure as 3). The next step is a return to a BR-aBR configuration shown in figure 3.5.(c). The movement of Na^+ ions thus occurs by the

paired jumping of the ions using two equilibrium configurations and all three cation sites.

Kim et al. (1979) found that, at low temperatures, all excess Na^+ ions were found around oxygen interstitials. However, progressively increasing the temperature resulted in more and more Na^+ ions being freely mobile. This implies that the number of Na^+ ions available for conduction increases with increased temperature.

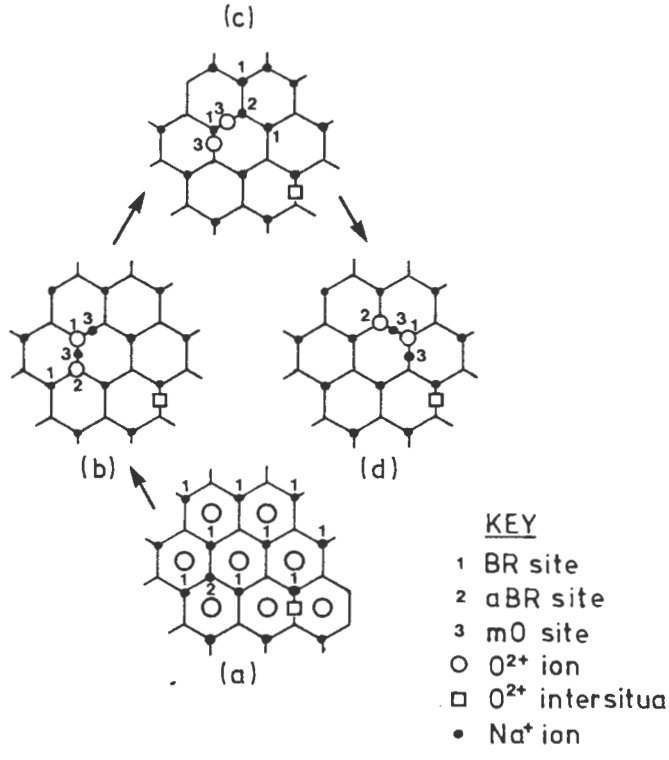

FIGURE 3.5. THE CONDUCTION MECHANISM IN β-ALUMINA.

The highest ionic conductivity found occurs approximately in the middle of the compositional range. At Na contents above this composition, the conductivity decreases due to the length of the c-axis decreasing as the conducting ion concentration increases. This compaction of the structure "freezes" the Na^+ ions in their sites in the conduction plane (Baffier et al.; 1979), rendering them non-conducting.

3.2. β"-ALUMINA

The crystal structure of β"-alumina was first determined by Yamaguchi et al. in 1968. The structure is a rhombohedral variant on the β structure, with a space group $R\bar{3}m$ and lattice parameters:

a= 5.592 $^{+}/_{-}$ 0.0004
c= 33.79 $^{+}/_{-}$ 0.001 (Schmid; 1986).

In β"-alumina the Na sites are staggered relative to one another ie. the conduction paths for the Na^{+} ions are no longer planar. The "conduction planes" in β"-alumina are thus referred to as conduction slabs. Each unit cell consists of three spinel blocks and three conduction slabs. The crystal structure of β"-alumina is shown in figure 3.6.(a).

The spinel blocks have the same configuration as β, but are stacked according to a three fold screw symmetry illustrated in figure 3.6.(b) (Yamaguchi et al.; 1968).

The oxygen atoms above and below the conduction slabs are staggered (recall that the oxygen atoms above and below the conduction plane in β-alumina were mirror images of one another). As a result the BR and aBR sites are crystallographically equivalent in β"-alumina. Each conduction slab contains two Na^{+} ions per unit cell.

Stoichiometric β"-alumina has a composition $Na_2O.\ 5.33Al_2O_3$. In practice the composition is in the range $Na_2O:Al_2O_3$ 1:5.2 to 1:8.3 implying that the general composition gives approximately 17% of the Na sites vacant. Mg^{2+} and/or Li^{+} ions (less commonly Co^{2+} or Zn^{2+} ions) are used to stabilise the β"-alumina by replacing an Al^{3+} in the centre of a spinel block. To maintain charge balance, additional Na^{+} ions are accommodated in the conduction plane. The Na^{+} content is thus proportional to the dopant concentration (Boilot et al.; 1980). The compensation mechanism in β"-alumina is exclusively the replacement of Al^{3+} by a lower valence ion. The general formula for Mg^{2+} stabilised β"-alumina is thus:

$$(Mg_y\ Al_{11-y})\ (O\ Na_{1+y}\ O_{16}) \qquad (3.2.)$$

where y refers to the concentration of Mg^{2+}.

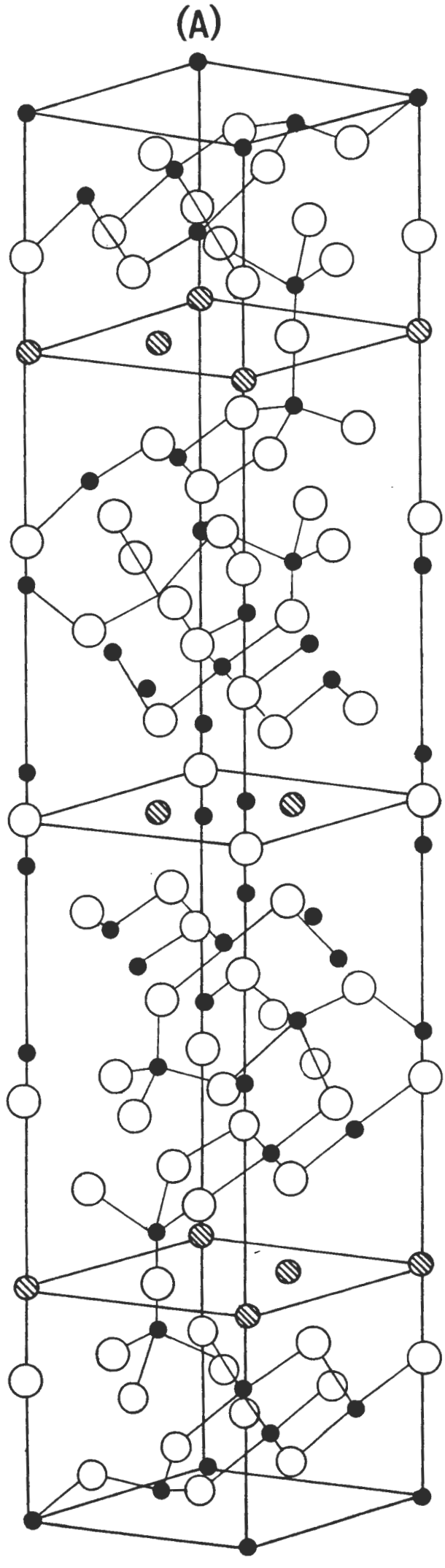

FIGURE 3.6.
(a) THE CRYSTAL STRUCTURE OF β"-ALUMINA.
(b) THE SPINEL BLOCK STACKING MODE IN β"-ALUMINA.

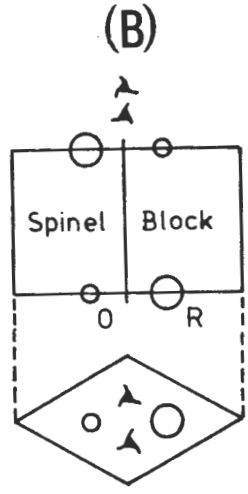

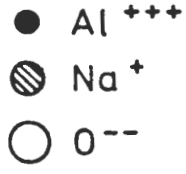

The Na^+ ions in β"-alumina are localised at sites equivalent to the BR and aBR sites in (the positions are crystallographically equivalent in β"). The average composition is approximately 1.7 Na^+ ions per unit cell. It follows that vacant sites exist in the conduction slab. Due to their high mobility the vacancies interact easily with one another, resulting in the formation of microdomains or clusters. The ordering of the distribution of Na^+ ions on a fraction of the total sites in the conduction plane results in the formation of a superlattice modelled by Boilot et al. (1980). This is shown in figure 3.7.

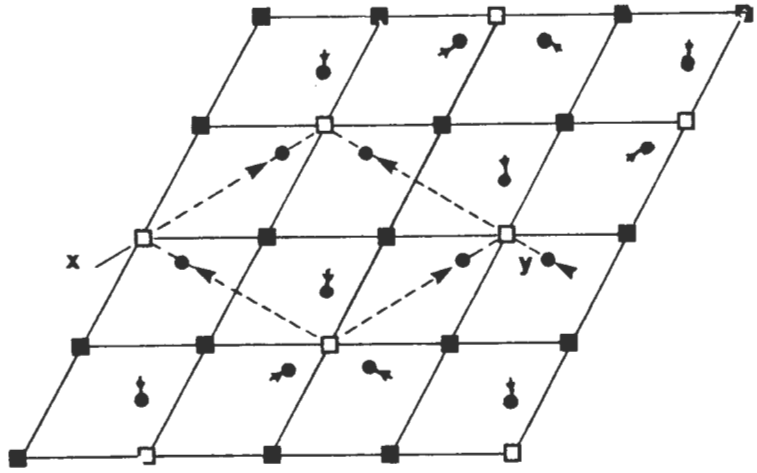

FIGURE 3.7. ORDERING OF THE VACANCIES IN THE CONDUCTION SLAB OF β"-ALUMINA

In this model Na^+ ions are missing from one third of the aBR sites, and the nearby Na^+ ions are shifted from their BR sites onto mO sites, toward the vacant aBR sites. It follows from this model that β"-alumina with a composition corresponding to $^1/_6$ of the cation sites vacant will have the longest correlation lengths and the largest activation energy. This was confirmed by Bates et. al in 1981.

The mathematically calculated activation energy for the motion of a single vacancy is an order of magnitude smaller than that found in practice. This effect is due to the ordering of interacting vacancies and interactions with the Mg^{2+} ions. The transport mechanism was thus attributed to the collective motion of vacancies (Wang et al.; 1980).

Non stoichiometric β"-alumina has a larger ionic conductivity than β-alumina. This is partially due to differences in composition and electrical compensation mechanisms which mask the effect of the lattice on the conductivity. However, ion-rich β-alumina has been synthesised with similar Na^+ compositions and ion compensation mechanisms to β". This allowed the effect of

the lattice on conduction to be examined. Boilot et al. (1980) pointed out that the conduction channel through the conduction path is narrower in β than in β"-alumina. Hence the Na^+ ions move through or close to an aBR site (d_{aBR-O} 2.31Å in β, compared to 2.50Å for β") accordingly diffusion of the Na^+ ions is slower in β than β"-alumina. In addition coherence lengths in β" are much shorter than in β (70Å for β", several hundred for β with the same Na^+ content). As a result β" has a larger conductivity than ion rich β.

3.3. POLYCRYSTALLINE β/β"- ALUMINA

The relative proportion of β and β"-alumina has a large influence on the conductivity of the polycrystalline electrolyte. An approximately linear relationship was found between the resistivity of the electrolyte and the β/β"-ratio (Youngblood et al. 1977,1978). Youngblood et al. (1978) also found that the resistivity increased from 2.84 to 4.45 Ohm cm as the grain size decreases from 100 to 2 microns. They attribute this effect to the fact that the grain boundaries are high resistance areas relative to the grains, and to the increased tortuosity effect with decreasing grain sizes.

The density (ie. porosity) of the sample was also found to have an important effect on conductivity (increased porosity severely reduced the conductivity)(Hooper 1977).

4. DEGRADATION OF THE BETA-ALUMINA ELECTROLYTE IN SODIUM/SULPHUR CELLS.

Degradation in Na/S cells has been studied extensively by other researchers. Degradation in these cells can be divided into three categories:
1) degradation of the electrolyte by Na
2) chemical contamination of the electrolyte
3) degradation of the electrolyte by S

4.1. DEGRADATION OF THE ELECTROLYTE BY NA.

4.1.1. CHEMICAL COLOURATION

Polycrystalline beta-alumina is discoloured when immersed in molten sodium. The discolouration proceeds as a discrete layer from the Na/electrolyte interface.

De Jonghe et al.(1981) attributed the discolouration to the reduction of beta-alumina by Na. They proposed that the reduction formed vacancies in the beta-alumina via the reaction:

$$2Na_E + (O_0)_{beta} \longrightarrow (Na_2O)_E + [(V_0)_{beta} + 2(e^-)_{beta}]$$

where beta refers to the beta-alumina, and E to the sodium electrode in which the oxygen dissolves.

Notice that the electrons remain loosely bound to the vacancy. The reduction of the beta-alumina results in an increased electronic conductivity of the order of $1x10^{-13}$ $Ohm^{-1}cm^{-1}$ (De Jonghe; 1986). The increased conductivity is thus too small to have a measurable effect on the Faradaic efficiency of the cell.

De Jonghe et al. (1982) found that the depth of the darkening at half maximum optical density is linearly dependent on the square root of the immersion time. The colouration-producing defects are transported more rapidly within the grain boundaries ($D_{lattice}/D_{GB}$ for β"-alumina is approximately 10^{-4}) than in the grains. Accordingly colouration proceeds substantially faster in small grain sized material. From this De Jonghe et al. calculated that complete homogenisation of the blackening of an electrolyte 2 mm thick at 350^0 C in oxygen free Na should take 0.5 years (De Jonghe et al; 1981). However, during cycling the oxygen fugacity increases on the Na entrance side and decreases on the Na exit side of the electrolyte. Accordingly only after prolonged one-way cycling is the electrolyte liable to be reduced to any great extent. Thus, under normal cycling

conditions of the cell, destructive reduction of the electrolyte is not expected (De Jonghe et al; 1986). The effect is illustrated in figure 4.1. from Yankulov et al. (1985).

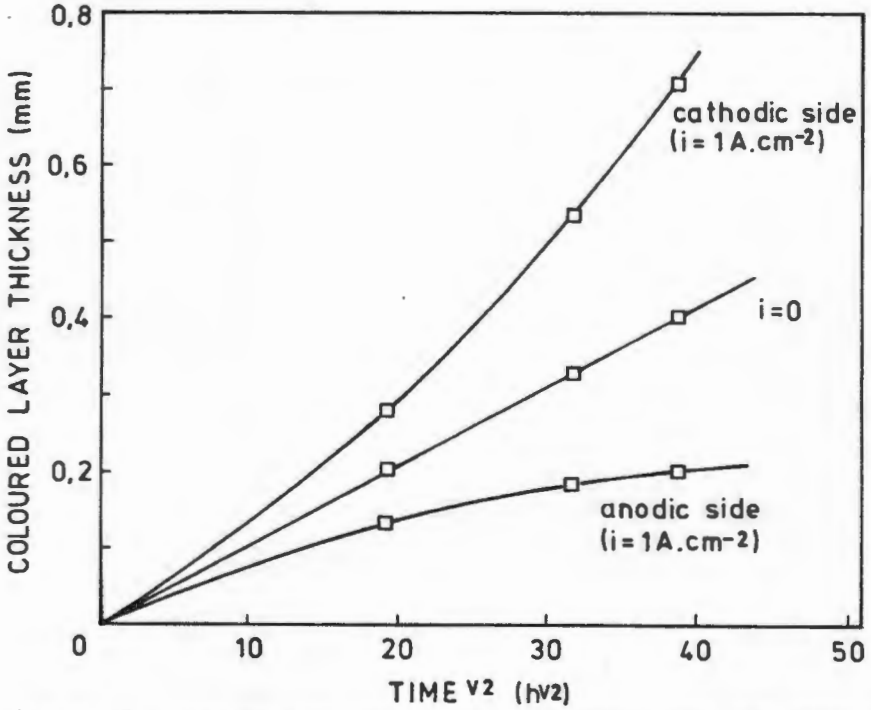

FIGURE 4.1. GRAPH OF THE TIME DEPENDENCE OF THE THICKNESS OF THE BLACKENED LAYER ON THE SQUARE ROOT OF TIME.

Notice that the discolouration does not result directly in failure of the electrolyte (De Jonghe et al.;1982)

4.1.2. DENDRITE FORMATION IN THE ELECTROLYTE

Beta-alumina electrolytes are susceptible to a type of degradation which manifests itself in the form of thin metallic Na filaments originating from the electrolyte/Na interface. The models for this type of electrolytic failure rely on the extension of existing surface microcracks during electrolysis. This is known as mode I degradation.

The surface of the electrolyte at the Na/beta-alumina interface contains Na-filled microcracks. Armstrong et al.(1974) proposed that, as the Na-filled cracks form low resistance paths for Na^+ ion current in the electrolyte during electrolysis, the Na^+ ionic flux is focused to the cracks. The flow of cathodically deposited Na from the tip of the crack during electrolysis results in Poiseuille pressure concentrated at the crack tip. If the Poiseuille pressure exceeds the critical pressure such that the

Griffith equation is satisfied, crack growth ensues. The Poiseuille pressure drops after crack extension. The crack is then refilled before extending again. The theory thus does not predict catastrophic crack growth.

In contrast Richman and Tennenhouse (1975) proposed that the driving force for crack propagation was subcritical crack growth by stress assisted dissolution of the solid electrolyte at the crack tip. This dissolution was determined by the stress due to the Poiseuille pressure, the Na current at the crack tip carrying solute away and the redeposition of electrolyte at the crack tip (due to the relative curvatures of the crack sides to the crack tip).

The fracture strength of a sample of electrolyte which was soaked (under constant load) in liquid Na, then cleaned and fractured was found to be independant on the time of soaking (Davidage et al.; 1979). The Richman and Tennenhouse theory, however predicts that the fracture strength of the electrolyte should be inversely proportional to the time of soaking. As a result of this discrepancy their theory has been largely discarded.

Both Armstrong et al. and Richman et al. assumed that the crack was of arbitrary thickness and that the equations of 2-D fracture mechanics were applicable. Shetty et al.(1977) refined the Armstrong model by attempting to incorporate the effect of crack width on the crack growth. They did so by assuming that a self-consistent crack shape could be calculated (using elasticity theory) such that the shape was consistent with the pressure due the viscous flow of Na within it. They further assumed that crack extension only occurred when the Poiseuille pressure in the crack exceeded the critical (Griffith) fracture strength. However, their theory predicted a critical current density of approximately 1500 $A.cm^{-2}$ for a 25 micron crack, whilst experimentally observed current densities were 1 to 2 $A.cm^{-2}$.

Virkar et al.(1983) examined the 3-D problem of filament extension. The flaw was assumed to be a ribbon shaped crack of length l, width 2c and a crack tip radius of c.

The maximum pressure at the crack tip was calculated to be

$$P_0 = \frac{(2\ n\ V_m\ E^3\ l^3)}{(1-v^2)\ F^4\ c^4}\ (i)^{0.25} \qquad \text{(Equation 4.1.)}$$

Where: i is the average current density in the electrolyte
F is the Faraday constant
K_{1c} is the critical stress intensity factor
n is the viscosity of Na
V_m is the molar volume of Na
v is the Poissons ratio of beta-alumina
E is the Youngs Modulus of the beta-alumina

ie.

$$P_0 = \frac{l^{3/4}\ (i)^{0.25}}{c} \times \text{const}$$

For fracture to occur P_0 must be larger than or equal to the critical pressure for crack propagation on the basis of the Griffith equation for a half-penny crack. Notice that as the pressure at the crack tip (refer to equation 4.1.) is dependent on the ionic current density in the electrolyte, it is possible to calculate a critical current density (for a given flaw size) at which the Griffith criteria is satisfied and crack propagation will occur. Mathematical manipulation yields the equation:

$$i_{crit} = \frac{D^2\ (1-\nu^2)^3\ F\ (K_{1c})^4}{256\ n\ V_m\ E^3} \times \frac{c^2}{l^3} \qquad \text{(equation 4.2.)}$$

For a flaw of length 100 microns, width 60 microns, at 300^0C the calculated i_{crit} from the Virkar model is approximately 150 A cm^{-2}. Previous calculations for the 2-d crack theories for cracks of this length gave i_{crit} values of about 3000 $A.cm^{-2}$. The experimental value is in the range 10 to 20 $A.cm^{-2}$.

Notice that equation 4.2. predicts that the critical current density is dependent on the viscosity of the Na. De Jong et al.(1981) found that cells operating at 300^0C had a critical current density of 300 $mA.cm^{-2}$ whilst cells operating near the melting point of Na had a critical current density of 40 $mA.cm^{-2}$. In addition, the critical current density was predicted to be strongly dependent on the the K_{1C} of the electrolyte. Recent studies on transformation-toughened beta-alumina indeed demonstrate that increasing K_{1C} increases the i_{crit}.

The influence of bad wetting by the sodium of the beta-alumina electrolyte on cracking was investigated by Virkar et al. (1981). They found that current enhancement occurred at the edges of unwetted areas, making these areas particularly susceptible to Mode I crack initiation and crack propagation.

Feldman et al (1982) disputed this by pointing out that once the crack had propagated out of the outer few microns the enhancement due to the bad wetting would decrease, and thus crack propagation would be arrested.

Viswanathan et al (1982) subsequently pointed out that, although the crack propagates out of the area where current enhancement occurs, in a 3-D crack the current enhancement due to increasing length is such that arrest of crack growth is unlikely.

The microstructure of the beta-alumina also has an influence on the critical current density. Beuchele et al. (1983) carried out an investigation into the effect of microstructure on mode I failures. They found that the average critical current density for crack propagation increased with decreasing average grain size.

Single crystal beta-alumina is a two dimensional Na^+ ion conductor. Beuchele et al. explained their experimental findings by pointing out that, as a result of this two-dimensional conduction, local ionic current densities near large grains are dependent on the grain orientation relative to the flow of the current. This implies that large grains which are oriented in such a way as to be blocking to the current result in a local increase in current in the immediately surrounding microstructure. If this occurs close to the Na/electrolyte interface this local current enhancement may result in a flaw, which would not be of critical length in the average current, becoming critical due to this local current enhancement.

The Virkar 3-D model for crack propagation suggests that, as crack propagation occurs very rapidly, electrolyte tubes with critical flaws should fail almost immediately on cycling. Thus the beta-alumina electrolyte tubes should fail by cracking of the beta-alumina in the first few cycles,or not at all. However, in 1986 Hitchcock and De Jonghe showed that time dependent electrochemically assisted crack growth may be active at subcritical current densities.

However, electrolytes had been successfully cycled for more than a year in spite of the proposed subcritical crack growth. Hitchcock et al. suggested that subcritical crack growth did not occur in these electrolytes due to a minimum flaw size limit on subcritical crack growth (ie. a flaw size below which subcritical crack growth would not occur). One such limit was supplied by Hitchcock et al.(1986).

They suggested that slow crack growth occurred by oxygen depletion at the crack tip. This depletion would result in the reduction of the electrolyte at the crack tip, producing slow crack propagation. Oxygen at the crack tip would be swept away by the new Na being deposited at the crack tip during electrolysis. This would be counteracted by the oxygen diffusing back to the crack tip in the liquid Na. The oxygen fugacity at the crack tip is thus dependent on the velocity of the liquid Na in the flaw and the diffusion rate of oxygen in molten Na.

The velocity of the Na, and hence the oxygen fugacity, at the crack tip is dependent on crack length and the current density. A critical oxygen fugacity exists above which reduction of the beta-alumina would not occur, and hence no subcritical crack growth should occur. The critical flaw

size for a Na^+ ion current density of 1000 $A.m^{-2}$ in the electrolyte was calculated to be between 50 and 100 microns.

4.1.3. INTERNAL SODIUM DEPOSITION (MODE II FAILURE)

In some cycled electrolytes evidence has been found of a progressive internal deposition of Na metal (De Jonghe et al.;1981). This is, however not a very common observation, and most failed cells are free of this form of degradation.

Mode II failure involves the progressive deposition of Na metal in the electrolyte at the Na/electrolyte interface during cell operation (De Jonghe et al.;1981). Feldman et al. (1982) proposed that the Na+ ions in the lattice are reduced by electron conduction from the Na/electrolyte interface.(De Jonghe et al.;1981).

If blocking conditions exist at either the Na source or Na sink during electrolysis, the ionic current will decay as a charge separation occurs at the blocking interface(s). The potential drop associated with the applied field will be opposed by the field of this charge-separated layer. As the charge separation at this interface is small, the field will be relatively large. Direct electronic breakdown of the beta-alumina by this field is, however, unlikely as a field of the order of 10^9 V m^{-1} is required for this to occur. A field of this size is unlikely in normal cell operation.

The electronic bandgap in beta-alumina is estimated at between 9 and 11 eV (Shen et al.;1977). Accordingly, the direct electron injection or thermal activation of electronic carriers is also unlikely to occur. However, the presence of defects or impurities in the electrolyte will create donor or acceptor states in the bandgap, and increase the electronic component of conductivity. If appropriate conditions for both ionic and electronic currents in the electrolyte are present, the electrons combine with Na^+ ions internally, resulting in the deposition of metallic Na under pressure in the electrolyte.

The effect thus becomes possible when there is a stationary gradient in the electronic/ionic transport number ratio (De Jonghe; 1982). For example, if an electrolyte contains an electronically conducting layer in contact with the negative electrode, then the electronic current will be controlled by an increase in chemical potential of the ion/electron combination product (metallic Na) when the current is maintained.

The deposition of Na under high pressure in the electrolyte could lead to the formation of microfractures in the electrolyte (De Jonghe; 1984). Notice that, though this is a degradation mechanism, it will not directly cause failure, but may result in mode I initiation.

4.2. CHEMICAL CONTAMINATION OF THE ELECTROLYTE.

4.2.1. POTASSIUM

K is a common impurity in commercial metallic Na, and often a constituent of the beta/alpha-alumina glass seal.

Lazennec et al. (1975) found that the presence of K in a Na/S cell caused rapid cell resistance rise and cell failure. The lifetime of the cell was found to be virtually independent of the amount of electrolysis that had taken place ie. failure occurred in both continuously cycled and intermittently cycled cells after a certain period.

Later Yasui et al.(1978) discovered that, in cycled cells, K slowly penetrated into the electrolyte. After a few cycles the distribution of K on the surface was non-uniform, but became more uniform after more cycles. This implies that, once the critical period of non-uniform K distribution is over, damage from the presence of K is unlikely. The addition of as little as 0.2% K to the molten Na was found to increase the cell resistance by a factor of two or three.

The resistance rise observed in the cells can be explained by the relative mobilities of Na^+ and K^+ in the beta-alumina. The K^+ ion exchanges with Na^+ in both Na-β and Na-β "alumina. Figure 4.2 illustrates the effect of partial K^+ ion exchange on the ionic conductivity of Na-β and Na-β" alumina. Notice that the conductivity of β-alumina decreases to a minimum at about 64 % exchange, but that the conductivity of β" remains largely unaffected by the K^+ ion exchange.

K-β alumina has a much lower ionic conductivity than Na-β alumina. This is due to the large size of the K^+ ion relative to the Na^+ ion (1.4Å for K^+ as opposed to 0.95Å for Na^+). The restricted size of the mO site in the conduction plane, through which the migrating cation passes during conduction results in an increase in the activation energy required for K^+ diffusion.

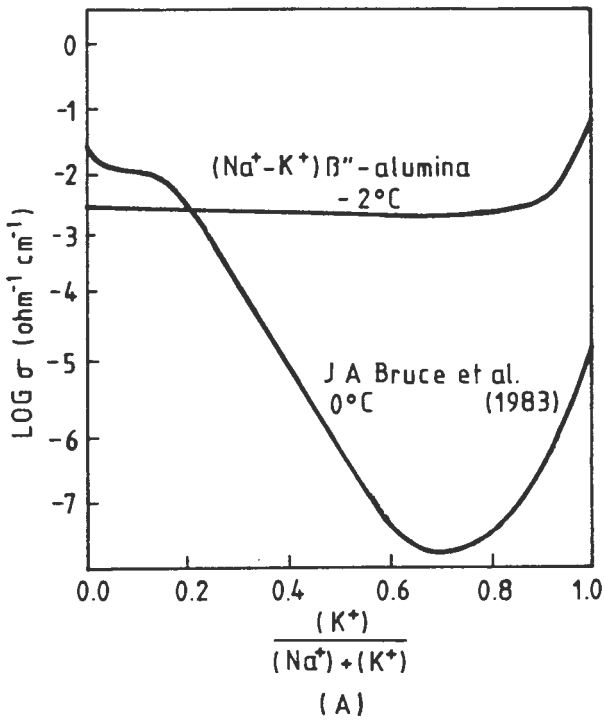

FIGURE 4.2. GRAPH OF THE IONIC CONDUCTIVITY OF Na/K-β ALUMINA AND Na/K-β" ALUMINA AS A FUNCTION OF THE AMOUNT OF Na^+ IN THE CONDUCTION "PLANE" ION EXCHANGED WITH K^+

The effect of partial K^+ ion exchange on ionic conductivity has been explained in terms of preferential site occupancy. Site energy calculations for β-alumina by Wang et al.(1979) showed that the larger K^+ ions prefer the BR sites, displacing the smaller Na^+ ions to the paired mO interstitial sites. Referring to the Wolf model for conduction in β-alumina, Bruce et al.(1986) suggested that when all the BR sites are occupied by K^+ all the pathways for Na^+ migration would be blocked. This will occur at 64% K^+ ion exchange. Accordingly they found a total absence of Na^+ ions on the aBR sites at 64% K^+ exchange. The exchange of more Na^+ results in an increase in the ionic conductivity of the β-alumina as the conductivity is then controlled by K^+ migration.

K-β" alumina has a higher conductivity than Na-β" alumina. Boilot et al. (1980) explained this by pointing out that K-β" alumina has a shorter coherence length than Na-β" alumina. They suggested that the difference in coherence length was a result of the thickness of the conduction channel in K-β" alumina being less than that of Na- " alumina (0.39Å in Na-β alumina as opposed to 0.28Å in K-β" alumina). This implies that the interionic repulsions between the K^+ ions in the conduction slab are reduced, shrinking the size of the ordered domains.

Tsurumi et al. (1987) used the Boilot et al. (1980) model of an ordered superstructure discussed in section 3.2.2., and the fact that in β"-alumina the alkali ions do not move independently to explain the behavior observed on K^+ ion exchange. They suggested that the mobility resulting from the cooperative motion of the alkali ions would be governed by the species with the lowest mobility ie. the Na^+ ions. The distance over which one Na^+ ion influences its K^+ neighbours would constitute the smallest unit of cooperative motion. They assumed that this distance was equal to the unit cell of the superstructure (refer to section 3.2.2.) ie. that $\sqrt{3}a$ is the smallest unit of cooperative motion. Once the unit cell of the superstructure contained less than one Na^+ ion, the conductivity would no longer be governed by the mobility of the Na^+ ion in β"-alumina and would thus increase rapidly. The model predicted that the inflection in the conductivity curve would occur at a composition of 93% K^+ ion-exchange. It did not predict the gentle decrease in conductivity observed for less than 93% K^+ exchange.

The mixed alkali effect in β"-alumina drops off rapidly with temperature (due to the breakdown of order in the conduction plane) and is not observed above 200^0 C (Boilot et al.; 1980).

From the previous section it would appear that the use of a single phase β"-alumina electrolyte would prevent any adverse effects due to the presence of K impurities.

Yasui et al. (1977) found that the pickup of K^+ ions by polycrystalline β/β"-alumina from a Na_2S_4 melt containing 1% $K_2S_{3.5}$ was governed by the grain boundary diffusion of the K^+ ion. Large grains in contact with the melt were found to contain the equilibrium amount of K, whilst the small grains did not. The observed diffusion of K^+ ions into the polycrystalline beta-alumina was 7 orders of magnitude slower than that for single crystals.

Bell et al. (1983) proposed a model (based on the effective percolation theory) that fitted the observed conductivity values of K^+ ion-exchanged polycrystalline beta-alumina. Their theory (called the mixed alkali percolation theory) showed that the conductivity measured was highly dependent on the proportion of the β-alumina phase present. This is due to the fact that, from Kummer et al. (1972), the K would preferentially segregate to the β-alumina phase. Thus even small amounts of the β phase would cause a drastic rise in electrolyte resistivity with K^+ ion exchange from the melt.

4.2.2. CALCIUM

Ca is a common impurity in ceramic powders. In addition Ca may be a contaminant in the S or Na electrodes.

Yasui et al.(1978) found Ca to be the most deleterious impurity in Na/S cells. 0.05 $^{w}/_{o}$ CaS in the S electrode was found to lead to large impedance rises of the beta-alumina electrolyte. Even in the absence of an electric field the Ca in the molten S was found to have concentrated at the grain boundaries and in the smaller grains of the electrolyte. On cycling the electrolyte was found to contain Ca-rich cracks parallel to the surface of the electrolyte. These cracks resulted in spalling of the electrolyte surface. Yasui et al. suggested that the Ca, concentrated in the grain boundaries of the β"-alumina may have caused the cracking of the ceramic.

Brieter et al. (1984) found that a Ca content of >200 ppm on the Na side of a cycled $Na/NaNO_3$ cell resulted in catastrophic pitting on the $NaNO_3$ side of the electrolyte. No damage was found on the Na/electrolyte interface. They suggested that the pitting was due to current channeling. The Na/electrolyte interface is thought to be covered with Ca, leaving only the small areas free of Ca and thus able to carry the Na^+ current. The local current density is therefore large, resulting in local heating. The temperature rise reduces the electrolyte resistance which in turn results in increased local current. The high local current density presumably results in the formation of pits, though the mechanism of pit formation is not known. Note that the Ca layer on the Na/electrolyte interface does not penetrate the surface.

Asymmetry of cell resistance (ie. a cell resistance which is larger on discharge than charge) has been associated with Ca impurities at the Na/electrolyte interface. A surface enrichment, relative to the bulk, of 100 times has been demonstrated in electrolytes showing resistance rise (Demott et. al.; 1985). The Ca was present in the form of a 400 nm thick surface coating of CaO and $Ca_3Al_2O_3$ on the Na/beta-alumina interface.

Demott et al. (1985) suggested that the Pb coating used to enhance wetting of the electrolyte by liquid Na disperses the CaO layer, thereby reducing resistance rise. In addition they added an oxygen getter to the Na electrode to prevent the formation of CaO. These two additions together were successful in eliminating resistance rise due to the presence of Ca in the molten Na.

Ion exchanging Na-β" alumina with Ca^{2+} ions from a $Ca(NO_3)_2/NaNO_3$ melt prior to cycling results in the

formation of Ca rich pockets in the electrolyte. After cycling visible cracking is found along the grain boundaries of the electrolyte. Longer ion exchange times results in the Ca being evenly distributed in the polycrystalline beta-alumina.

Research at British Rail confirmed that Ca^{2+} ions were mobile in the beta-alumina electrolyte. This was done by tracking the motion of Ca^{45} tracers from the S electrode through the electrolyte whilst the Na/S cell was being charged. In both cycled and uncycled cells the Ca^{45} tracers were found to have diffused through the electrolyte from the S electrode to the Na electrode (Demott et al, 1981). The Ca was found to be concentrated in the region close to the Na/beta-alumina interface.

Ion exchanging with Ca^{2+} in Na-β alumina results in a drastic reduction of the ionic conductivity (Ni et al.; 1981).

As conduction in β-alumina occurs via an interstitialcy mechanism (Wolf; 1979), a non-stoichiometric excess of Na^+ is essential ie. it is important to maintain the ratio of mobile ions to BR sites at values >1. If the ratio is μ1 the Na^+ ions become trapped in the potential energy wells at the BR sites. If this occurs the conduction mechanism changes from an interstitialcy mechanism to a high activation energy vacancy diffusion process (Farrington et al.; 1982).

Substitution of Na^+ by a divalent cation would result in a drastic reduction of the number of mobile Na^+ ions in the conduction plane. Therefore in partially ion exchanged Ca/Na-β alumina a large number of BR sites are vacant. The Na^+ ions are thus become trapped in deep potential wells at the BR sites with no ion pairs to enhance diffusivity. Accordingly the activation energy for conduction is high (Farrington et al.;1982).

Ion exchanging a single crystal of Na-β" alumina with Ca^{2+} ions results in a decrease in ionic conductivity similar to the mixed alkali effect seen in Na/K-β alumina (Ni et al.; 1981).

In contrast to β-alumina, conduction in β"-alumina occurs via a vacancy mechanism ie. the Na^+ content is usually less than the stoichiometric value. Accordingly some of the BR and aBR sites are vacant. Divalent substitution of Na^+ ions by Ca^{2+} in β"-alumina increases the vacancy population but does not change the conduction mechanism in β" as it does in β (Farrington et al.;1982).

Increasing the Ca content of the ceramic powders used to fabricate the beta-alumina electrolyte leads to an increase

in the resistivity of the electrolyte, and promotes grain growth (Buechele et al,; 1979) . A portion of the Ca is accommodated in the grains, resulting in β-alumina with the formula of approximately $3CaO.2Na_2O.5Al_2O_3$. The remainder of the Ca is situated in an intergranular phase with composition $CaO.6Al_2O_3$. The total dc resistivity has been found to be exponentially dependent on the Ca content.

In addition large amounts of CaO in the constituent powders decreases the amount of β"-alumina formed (Farrington et al.;1982).

4.2.3. WATER

Beta-alumina is moisture sensitive. Will et al. (1976) showed that water is rapidly taken up by the surface of the electrolyte, followed by a slow diffusion of H_3O^+ ions into the lattice. This leads to H_3O^+ ion exchange with Na^+.

Viswanathan et al. (1982) found that beta-alumina exposed to 100 % relative humidity for 24 hours was not wetted by liquid Na, even at 360^0 C, whilst beta-alumina which had not been exposed exhibited complete wetting at this temperature. They attributed this phenomenon to either the absorption of, or the ion exchange of H_3O^+ ions for Na^+ ions close to the surface of the beta-alumina. This would result in the formation of Na_2O or NaOH which would prevent wetting by the Na. Baking the electrolyte at 450^0C under vacuum was found to restore the original wetting characteristics.

They attributed the initial decrease in cell resistance sometimes seen during the first few cycles of a cell to the water, adhering to the electrolyte, being given off. They attributed the gradual increase of the cell resistance with further cycling seen in these cells to H_3O^+ ions diffusing down grain boundaries, effectively increasing the resistivity of the electrolyte. The resistivity of the electrolyte was found to decrease after heating the electrolyte to 700^0 C in air for 24 hours.

4.2.4. SILICA

Silicates are common impurities in commercial α-alumina powders and in the grinding media used in beta-alumina preparation.

Hsieh et al. (1978) demonstrated that beta-alumina prepared with more than 4 $^w/_0$ SiO_2 contained α-alumina as well as a glassy phase. The composition of the glassy phase was found to be either $Na_2O.Al_2O_3.2SiO_2$ or $Na_2O.Al_2O_3.4SiO_2$ depending

on the firing conditions. The silicate-containing polycrystalline β-alumina contained some grain boundaries covered by a very thin silicate layer. In addition it was found to contain a bulky aluminosilicate phase distributed inhomogeneously throughout the electrolyte, though with a preferred location at grain boundary triple points. The α-alumina grains present are expected to be evenly dispersed.

The ionic resistivity of the beta-alumina was found to increase with increasing SiO_2 content. This was probably due to an increase in the amount of α-alumina and aluminosilicates formed with increasing SiO_2 content in the β-Alumina precursors.

4.3. SULPHUR SIDE ATTACK

4.3.1. DEGRADATION BY THE SULPHUR

When a Na/S cell is cycled for extended periods degradation is sometimes seen on the sulphur side of the electrolyte (De Jonghe; 1986). The degradation occurs preferentially along grain boundaries and is more pronounced at the S rich compositions. The corrosion products have been tentatively identified as Al-sulphates and Na-sulphates. On static immersion a surface corrosion layer was found to form, which appeared to protect the electrolyte from any further damage. The cycling of the cell may, however, have resulted in a breakdown of the protection offered. The corrosion was found to proceed very slowly and no failures have been identified which could be directly attributed to attack by the S on the electrolyte.

4.3.2. DEGRADATION BY THE GRAPHITE FELT

The carbon felt in the S electrode has a much higher electronic conductivity than the S. Hence any non-uniform distribution of the felt would result in current concentrations at the interface. This will enhance mode I initiation (De Jonghe et al.;1981).

De Jonghe et al.(1981) found that, after extended cycling, the surface in contact with the S showed some degradation. The degradation was found to result from an imprinting effect: the light and dark areas on the electrolyte surface reflected the microstructure of the graphite filler in the S electrode. Close examination of the S/electrolyte interface revealed surface cracks.

Chouridy et al.(1986) showed that beta-alumina in contact with graphite produced an anodic current at 2.6 V. They attributed this to the reaction:

$$3(Na_2O)_{\beta\text{-alumina}} + C \longrightarrow Na_2CO_3 + 4Na^+ + 4e^-$$

and/or

$$(Na_2O)_{\beta\text{-alumina}} + C \longrightarrow CO + 2Na^+ + 2e^-$$

The reactions were partially reversible during the application of a cathodic current.

5. THE ZEBRA CELL.

In the Zebra cell, as in the Na/S cell, liquid Na acts as the cell anode, but the liquid S cathode is replaced by a novel solid electrode made up of NaCl and Fe.

The overall cell reaction during discharge of the cell is:

$$FeCl_2 + 2Na \xrightarrow[NaAlCl4]{\text{beta-alumina}} Fe + 2NaCl \quad (E_0=2.35\ V \text{ at } 250^0\ C)$$

The cell operates at temperatures between 200^0 and 300^0 C. Normal operation is at 250^0 C, compared to $>300^0$ C for Na/S cells. The beta-alumina tubes used to construct the cells are composed of essentially pure ß"-alumina to allow the highest conductivity possible. This is necessary due to the low operating temperatures of the Zebra cell.

A schematic layout of the cell is shown in figure 5.1.

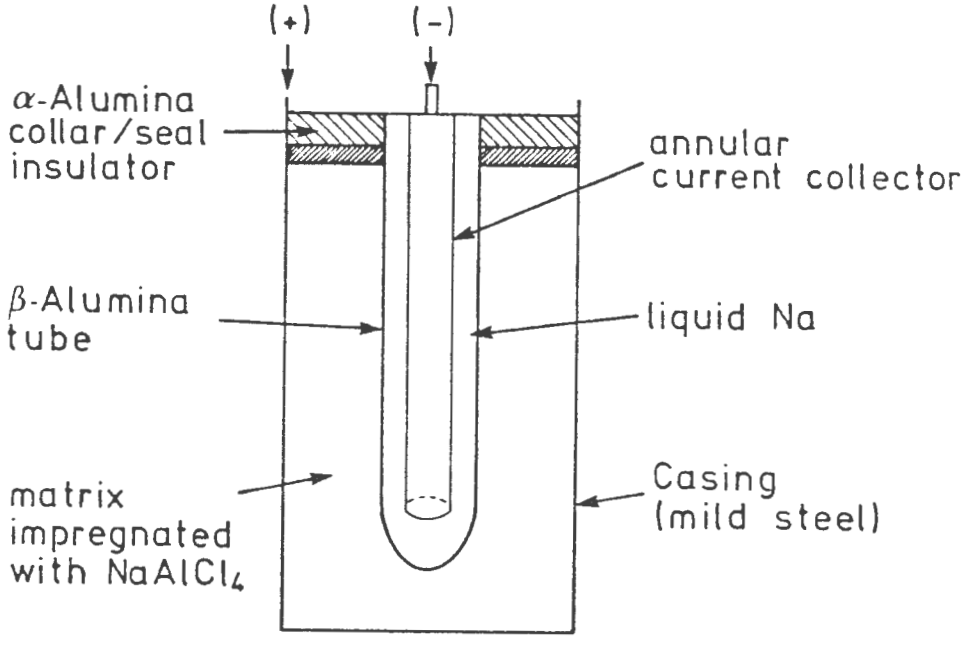

FIGURE 5.1. A SCHEMATIC ILLUSTRATION OF THE ZEBRA CELL

5.1. THE CATHODE

The cathode half cell reaction is:

$$Fe^{2+} \xrightarrow{NaAlCl4} Fe + 2e^{-}$$

In the charged state, the solid cathode electrode consists of a partially chlorinated, porous Fe matrix impregnated with molten $NaAlCl_4$.

The Fe matrix is electronically conducting. During charging of the cell some of the Fe metal is converted to $FeCl_2$. The detailed reaction of the Fe during discharge of the cell is not known.

The $NaAlCl_4$ is an electronic insulator. It acts as an extension of the electrolyte through the cathode by transporting Na^+ ions from the surface of the solid beta-alumina electrolyte to the electronically conducting Fe matrix. $NaAlCl_4$ wets beta-alumina and retains good contact during cycling. As a result the interfacial resistance on the cathode side is small (Bones et al.;1986).

Under normal cell operating conditions the $NaAlCl_4$ is not an electrochemically active species. The electrochemically active species (ie. Fe, $FeCl_2$, $Fe_xNa_yCl_{(2x+y)}$ and NaCl) are insoluble in $NaAlCl_4$. As a result the electrochemically active material is always associated with the electronically conducting Fe matrix (Coetzer; 1986).

The cathodes are produced by sintering mixtures of NaCl and Fe powder in a hydrogen furnace. They are constructed in a fully discharged state. This simplifies the assembly and sintering of the cathode as Fe powder and NaCl do not react vigorously with the atmosphere.

On charging NaCl is decomposed by the removal of Na from the cathode. This process creates porosity in the cathode. As a result, sufficient room is created in the cathode for expansion during the subsequent discharge cycle.

5.2. CYCLING OF THE CELL

The cell is cycled in the Fe^{2+} region (2.35 V).

If the cell is overcharged (ie. charged to a voltage of 2.75 V) Fe^{2+} is oxidised to Fe^{3+} via the overall cell reaction:

$$3NaCl + Fe \longrightarrow FeCl_3 + 3Na$$

Charging into this region results in a decrease in performance as $FeCl_3$ is soluble in $NaAlCl_4$. As a result, the Fe^{3+} may attack the beta-alumina.

If the cell is overdischarged (ie. discharged to a voltage of 1.60 V) the $AlCl_3$ from the melt is reduced to Al via the overall cell reaction:

$$AlCl_3 + 3Na \longrightarrow Al + 3NaCl$$

Severe overdischarge (ie. overdischarge for long periods) has been found to result in a loss of cell performance.

The three regimes of cell cycling are illustrated in figure 5.2. (Thackeray et al; 1987)

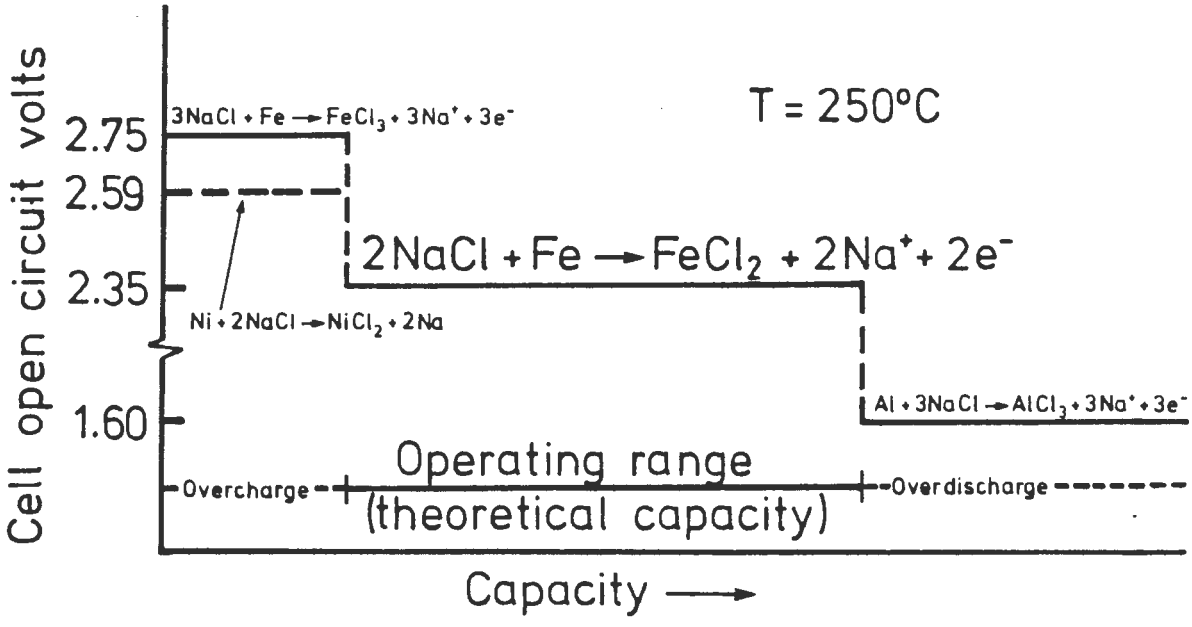

5.3. CATHODE ADDITIVES

To improve the cell performance and to protect the cell from abuse due to overcharging NaF and Ni have been included in the cathode

(a) Sodium Fluoride:
Cells incorporating Fe cathodes tend to undergo resistance rise during cycling. Small additions of NaF to the $NaAlCl_4$ melt were found to eliminate this problem (Coetzer; 1986).

(b) Nickel:
Ni is added to the cells to overcome the possibility of accidental overcharge (charging onto the Fe^{3+} plateau). The Ni is oxidised to $NiCl_2$ prior to the $FeCl_2$ being oxidised to $FeCl_3$ (see figure 5.2.). The Ni reaction is:

$NiCl_2 + 2Na \rightarrow Ni + 2NaCl \qquad E_0=2.59$ V at 250^0 C

Overcharging onto the Ni plateau does not result in a loss of cell performance. A further advantage of adding Ni to the cathode is that, after a few cycles, the metallic matrix assumes an advantageous morphology due to electrochemically induced Fe/Ni alloy formation (Coetzer; 1986).

5.4. Failure of the Zebra Cell

When the beta-alumina cracks, the liquid Na enters the cathode where it reacts with the $NaAlCl_4$ via the reaction:

$$NaAlCl_4\ (liq) + Na(liq) \rightarrow 4NaCl(s) + Al(s)$$

The mixture formed blocks off the crack and tends to block off further reaction (Dell et al.;1987). Moreover if the cell does fail catastrophically by cracking, the Al formed by the above reaction should ensure that the cell fails in the short-circuit mode.

In practice the cells are in series in the battery. Failing in a conducting mode ensures that if one cell fails catastrophically the rest of the string will continue to operate.

Another advantage of the new cathode is that, on failing, the reaction of Na and $NaAlCl_4$ results in the formation of NaCl and Al. This means that none of the reaction products are inherently dangerous and the reaction is self-inhibiting (Dell et al.;1987).

6.MICROSTRUCTURAL AND PHASE CHARACTERIZATION OF THE SUPPLIED ELECTROLYTE.

To determine the microstructural characteristics of the supplied electrolyte prior to the examination of failed cells, the average grain size and phase composition of the electrolyte were determined.

6.1.EXPERIMENTAL PROCEDURE

To determine the microstructure of the supplied beta-alumina electrolyte, a polished sample of the electrolyte was thermally etched by placing it in a furnace in air at 1400^{0} C for 30 minutes (G.Evans, 1987). The specimen was gold/palladium coated prior to examination in the SEM.

To determine the phases present in the electrolyte a sample of the supplied electrolyte tube was ground to a fine powder using an agate mortar and pestle and then studied using X-ray diffraction. The diffraction pattern was obtained using Cu K_{α} radiation.

To determine whether any amorphous phases were present in the electrolyte an approximately 10 micron thick section of electrolyte was examined under a petrographic microscope. The sample was prepared by mounting a section of the electrolyte on a glass slide and then grinding it down using an oil lubricant. The petrographic microscope was set up such that the sample was viewed through crossed polarizers: ie. the incident light on the sample was polarised, whilst the sample was viewed through a second polarizer at right angles to the first. A mica slide was placed between the sample and the second polarizer. Amorphous material is not birefringent. This implies that the light passing through it should be dictated by the mica slide, in this case red/magneta, irrespective of the orientation of the sample to the polarised light. Thus, by rotating the electrolyte sample, the amount of amorphous material in the electrolyte can be determined.

6.2 RESULTS AND DISCUSSION

The thermally etched microstructure of the supplied electrolyte is shown in figure 6.1.

Notice that the average grain size is approximately 5 μm. A distinct bimodal grain structure is seen with large grains and small grains, but few intermediate sized grains. The largest grain found (not shown) was 100 μm.

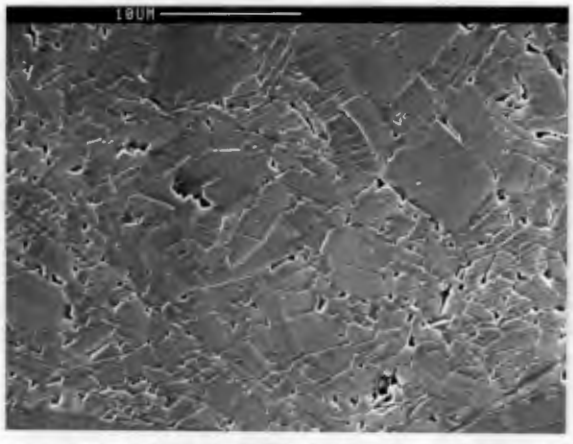

FIGURE 6.1. THE THERMALLY ETCHED MICROSTRUCTURE OF THE SUPPLIED BETA-ALUMINA CERAMIC.

An X-ray diffraction pattern of the electrolyte is shown in figure 6.2. Notice that the only phases identified were β and β"-alumina.

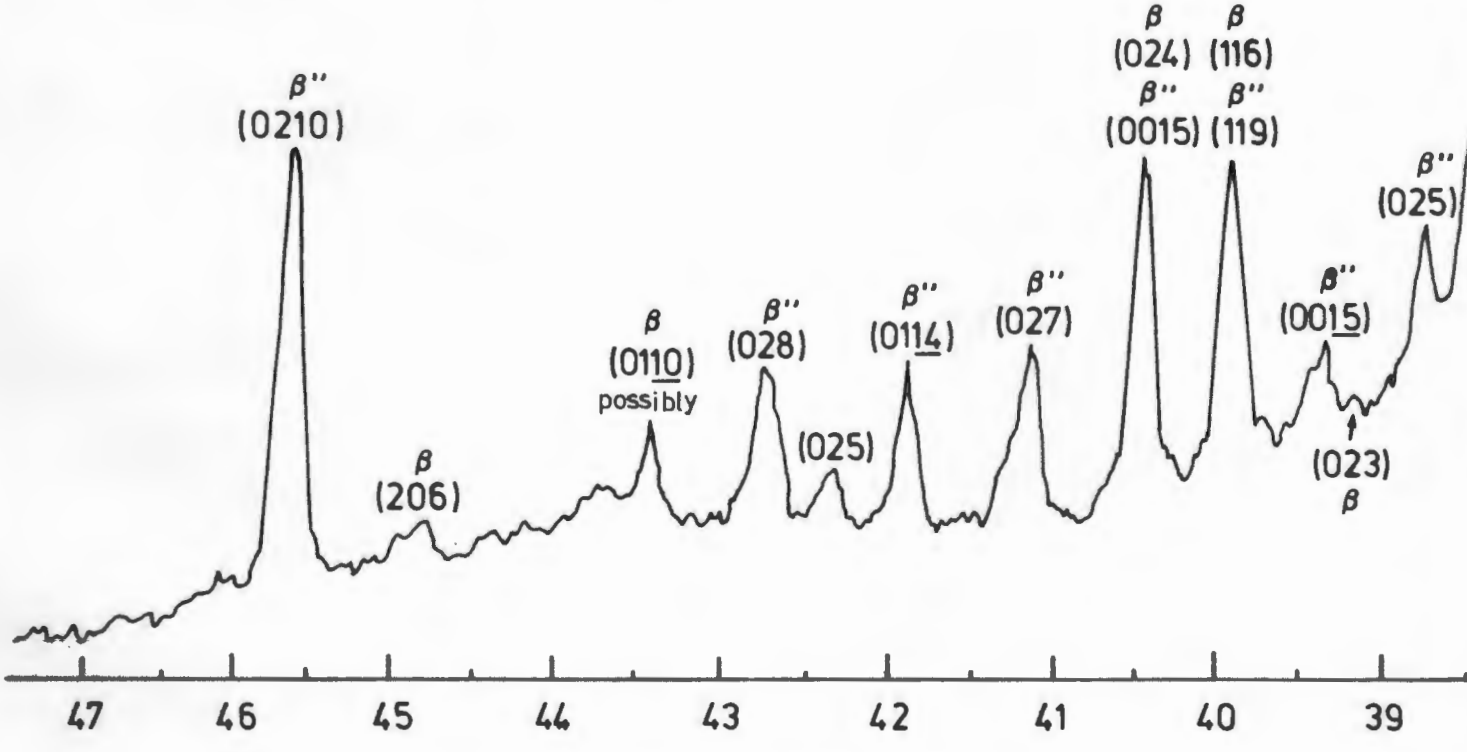

FIGURE 6.2. AN X-RAY DIFFRACTION PATTERN OF THE SUPPLIED BETA-ALUMINA CERAMIC.

The edge of the thin section was found to be thin enough to study under a petrographic microscope. Figure 6.3. shows the sample at 90^0 and 180^0 rotation of the stage. Notice that all the grains in the electrolyte are birefringent. The changes in colour with rotation were due to thickness and orientation variations in the sample.

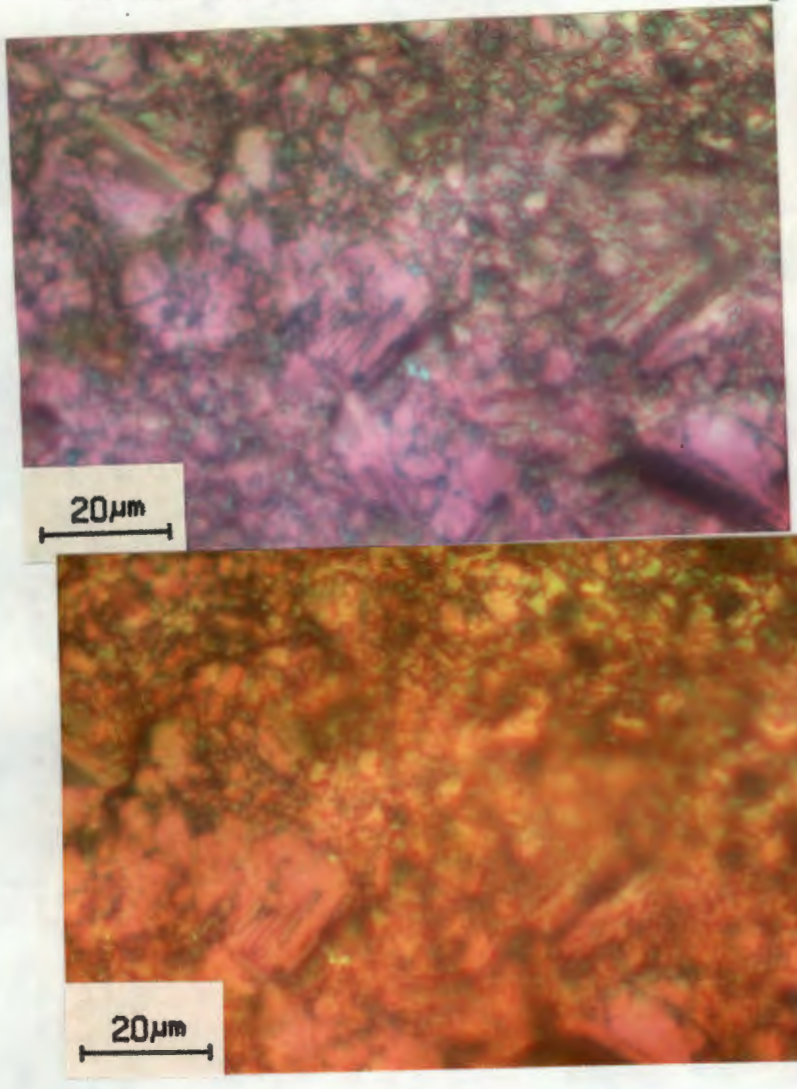

(a) Sample viewed at 90°

(b) Sample viewed at 180°

FIGURE 6.3. MICROGRAPHS OF THE BETA-ALUMINA ELECTROLYTE UNDER THE PETROGRAPHIC MICROSCOPE (Note that the angles mentioned refer to the rotation of the stage on which the sample is resting).

The electrolyte is thus a purely β/β"-alumina electrolyte with an average (in terms of volume) grain size of approximately 5 μm and a few extremely large grains, and no significant amount of glassy phase.

7.ELECTROLYTES FROM FAILED CELLS.

Under normal cycling conditions the Zebra cell does not undergo any form of degradation, even after more than 1000 cycles (Coetzer; 1986) at 250 ^{0} C. However, occasionally a cell does exhibit a performance degradation after relatively few cycles. This chapter is devoted to an investigation by the author into the possibility that degradation of the electrolyte was the cause of the cell degradation.

The cells were all cycled by Zebra Power Systems (PTY) Limited. The cycling of the cells was automatically controlled. Both the charging and discharging of the cell was done at a preset constant current. The switching from charge to discharge was done when the applied voltage was larger than a preset value. The cells were all run on the Fe^{2+} plateau. As the cell nears the end of its charge cycle (ie. just prior to moving onto the Ni^{2+} plateau) the internal resistance of the cell increases slightly. To keep the current constant the voltage applied to the cell rises accordingly. By monitoring the cell charge voltage and setting the trip voltage in such a position that the charging of the cell is terminated prior to the cell being charged onto the Ni^{2+} plateau.

Discharge of the cell is kept at the preset current level by automatically varying the load through which the cell is discharging. The cell voltage is monitored, and when it drops below a preset value the discharge is terminated. The termination of the cell discharge is set at a voltage above that of the Al plateau ie. both charge and discharge occur in the Fe^{2+} plateau.

The current used for charging is smaller than the discharge current. The first cycle of the cell is done at a low current charge and discharge to allow the cell to "run in".

The cells were removed from cycling at the discretion of the operator; thus for several of the cells no record existed as to the criteria used by the operator for removing the cell from cycling. After being removed from cycling, the cells were stored in a sealed state at room temperature in air for periods ranging from several weeks to several months.

In this section the chemical and physical characteristics of solid beta-alumina electrolytes from cells which had exhibited specific types of degradation will be discussed.

The electrolytes to be discussed are :
1) an electrolyte from a cell which showed no degradation of cell performance on cycling.
2) an electrolyte from a cell which had failed by a total loss of capacity after only a few cycles.
3) an electrolyte from a cell which had shown a capacity loss after accidental overdischarge onto the Al plateau.
4) an electrolyte from a cell which had shown a progressive capacity loss with cycling.
5) an electrolyte from a cell which had shown a drastic increase in cell resistance after being stored at operating temperature, but not cycled, for a period of one year.

Each of the above cells will be discussed in terms of:
1) optical and SEM appearance of the electrolyte (cracking, discolouration, etc.)
3) chemical composition of a polished cross-section of the electrolyte wall relative to that of an uncycled electrolyte.
2) chemical composition of the Na/electrolyte and cathode/electrolyte interfaces

The bulk chemical composition of the electrolytes from the degraded cells will be compared to that of an electrolyte as supplied by the manufacturer to determine whether or not any chemical "poisoning" of the electrolyte had occurred. In addition, the chemical compositions of the cells which had shown degradation will be compared to those of the "good" cell to determine whether the chemical composition of the electrolyte can be related to the degradation mode observed.

The chemical compositions of the sodium/electrolyte and cathode/electrolyte interfaces of each beta-alumina electrolytes were studied to determine whether any surface films could be detected ie. to determine whether the degradation of cell performance could be related to an interfacial effect.

7.1.EXPERIMENTAL PROCEDURE

The cells were dissected in a glove-box which had been purged with N_2 for several hours. The N_2 atmosphere was used to avoid reaction of the beta-alumina electrolyte, the Na, and the cathode salts of the cell reacting with air.

The electrolytes were removed from the cells by cutting through the outer casing of the cell and then heating the cell, using a heating tape, to 200^0 C. This melted the $NaAlCl_4$ electrolyte (melting point approximately 150^0 C) making it possible to pull the electrolyte tube from the cell.

The process was not always successful as those tubes which had cracked during cycling generally broke during removal from the cell. When this occurred the remainder of the tube was cut from the cell container. Cutting the electrolyte from the cell invariably resulted in the tube being mechanically damaged.

The tubes were placed in sealed plastic bags (filled with N_2 gas) prior to removal from the glovebox to prevent reaction with air during storage.

The tubes were examined optically under a low power optical microscope to determine whether any adhering surface layer was present. They were then cleaned by placing them in an ultrasound bath in ethanol for approximately 10 minutes. Though the cleaning of the electrolyte may have disturbed any adhering surface layers, not cleaning the electrolytes was not viable as any adhering $NaAlCl_4$ reacted with moisture in the air (forming HCl) making "as is" examination difficult.

The cleaned beta-alumina electrolytes were again examined under a low power optical microscope. This time attention was paid to discolouration of the tube and the extent and directionality of any cracking present.

To determine the depth of any discolouration or damage of the tube wall, cross-sections of the electrolyte were cut from the tube using a diamond saw. Each cross-section was hot mounted in Beuhler Transoptic Powder. The mounted samples were ground on 800 grit silicon carbide water paper to remove surface damage caused by the diamond saw. They were then polished for 3 hours with 15 micron, 7 micron, 2.5 micron and 0.25 micron diamond paste. Contact with water was inevitable during the grinding but was avoided during polishing.

Due to the relatively small surface area and hardness of the electrolyte relative to the mount some beveling of the edges of the sample was seen. As a result, the edges were generally more damaged by polishing than the bulk.

The polished cross-sections were chemically decorated by placing them for approximately 15 minutes in a 1 molar aqueous solution of silver nitrate (De Jonghe et al.; 1980). This process resulted in metallic silver being deposited on degraded regions and cracks, rendering them dark against a light background when viewed in reflection through crossed polarizers.

Samples from the cycled beta-alumina tubes were studied under an SEM. The samples were prepared by cleaning in isopropanol prior to being examined in a Cambridge Sterioscan 200 SEM. It was found that, though beta-alumina

is an electronic insulator, no conductive coating of the sample was necessary provided that low magnifications were used. Generally, images at magnifications less than 1000X were not plagued by charging problems.

Interaction of the electron beam of the SEM with the mobile Na in the conducting planes of the beta-alumina resulted in the formation of globules of Na metal on the surface being studied. Globule formation was minimised by working at low magnifications and by limiting the time that any one area was viewed.

EDS analyses were done in conjunction with the SEM examination using a Tracor Northern 5400 x-ray analyser. Semi-quantitative analyses were obtained from the spectra using the Tracor 5400 SSQ package. Details of the conditions used, the accuracy of the analyses and the problems associated with the analyses are discussed in Appendix 1.

In addition, standard polished cross-sections of the beta-alumina electrolyte tube wall were analysed to determine whether the bulk composition of the electrolyte was dependant on the type of degradation observed. The cross-sections of the tube wall were prepared by cutting a sample from a position midway down the length of the tube. The samples were hot-mounted, then polished to a finish of 0.25 microns by means of the same polishing procedure as discussed earlier. After polishing, the samples were carbon-coated. They were then analysed under the standard conditions given in appendix 1 at a magnification of 1000 X. Twelve analyses were generally done per electrolyte, three analyses at each of four positions across the wall thickness: three analyses were done on the portion of the tube wall closest to the Na/electrolyte interface, three on the portion of the tube wall closest to the cathode/electrolyte interface, and then three each at two positions between the two wall extremes. All the results were examined relative to a polished cross-section of an uncycled tube. Notice that these analyses were not necessarily representative of the whole tube but, as all the samples examined came from more or less the same area in each of the tubes, it is probably valid to compare the chemical compositions at that position for each of the cells.

After the analyses had been completed, the polishing oil (Struers DP Lubricant: Blue) was found to contain K. As this only emerged subsequent to the examinations, it was not possible to change the polishing oil and repeat the analyses. Accordingly the analyses obtained for K from the sections were regarded as being unreliable and will be ignored in the following sections. In addition, as the SSQ package only computed normalised weight percent, the

analyses obtained for all of the elements would be affected by the K contamination from the polishing oil. To prevent any incorrect conclusions being drawn from the results it was thus decided to use the analyses as only a qualitative guide to the elements present.

7.2. RESULTS:

All the cycled tubes examined had a black band on the cathode surface of the tube in the region close to the a-alumina ring. During the dissection of the cells it became apparent that this area was not submerged in the molten $NaAlCl_4$ electrolyte and was thus not current carrying. At no time was any cracking found in this region, and the outer blackening did not extend beyond the outer few microns of the surface. The black band was seen in all of the electrolyes from the cycled cells and will not be mentioned for each cell in turn.

The Na/electrolyte interface was invariably found to be blackened. The detailed investigation carried out into the blackening mechanism with respect to the Pb coating will be discussed in chapter 8. However, unless the blackening was significantly different to that normally seen in cycled cells, the blackening will not be mentioned in the following sections.

The analyses of the Na/electrolyte, cathode/electrolyte and polished cross-sections are given in tables 7.1., 7.2. and 7.3. respectively. These analyses will be discussed under the relevant cells.

7.2.1. The Uncycled Electrolyte

The uncycled electrolyte tube was white along its entire length.

SEM examination of the surface which, in a cycled cell, would make up the Na/electrolyte interface, showed it to have a bimodal grain structure ie. it was made up of small grains interspersed with a few large grains (> 50 μm). The structure of the surface is shown in figure 7.1.

The "cathode/electrolyte interface" was found to consist of approximately 20 μm spheres made up of fine grains. Several coarse grains (>20 μm) were also found on the surface. The microstructure is shown in figure 7.2.

TABLE 7.1.: EDS ANALYSES OF CATHODE/ELECTROLYTE INTERFACES OF THE CYCLED BETA-ALUMINA ELECTROLYTES

Description	Na_2O	Al_2O_3	CaO	K_2O	FeO	Cl	SiO_2	Pb
Uncycled	5.92±0.42	92.58±1.06	0.00±0.00	0.01±0.01	0.06±0.03	1.03±0.45	0.28±0.06	0.00±0.00
Good	5.13±0.23	93.18±1.56	0.00±0.00	0.01±0.01	0.10±0.03	1.23±0.58	0.30±0.03	0.00±0.00
Overdischarged	4.35±0.30	93.92±0.24	0.01±0.01	0.18±0.06	0.43±0.09	0.64±0.30	0.38±0.01	0.00±0.00
Capacity loss	3.91±0.01	95.34±0.03	0.12±0.01	0.10±0.07	0.13±0.03	0.67±0.01	0.25±0.00	0.00±0.00
1 year	5.15±0.36	93.31±0.59	0.00±0.00	0.00±0.00	0.93±0.61	0.22±0.07	0.35±0.11	0.00±0.00

TABLE 7.2.: EDS ANALYSES OF THE SODIUM/ELECTROLYTE INTERFACES OF THE CYCLED BETA-ALUMINA ELECTROLYTES

Description	Na_2O	Al_2O_3	CaO	K_2O	FeO	Cl	SiO_2	Pb
Uncycled	2.97±0.18	84.21±1.45	0.00±0.00	0.01±0.00	0.30±0.06	1.56±0.39	0.00±0.00	10.97±0.99
Good	6.48±0.23	92.60±0.38	0.11±0.05	0.01±0.01	0.25±0.06	0.00±0.00	0.52±0.10	0.04±0.05
Early Failure	6.35±0.14	87.44±1.14	0.56±0.20	0.00±0.00	0.37±0.01	4.45±0.48	0.61±0.27	0.34±0.34
Overdischarged	3.29±0.08	91.47±0.78	0.82±0.44	0.23±0.01	0.19±0.14	0.49±0.18	0.31±0.18	3.13±.14
Capacity loss	5.36±0.02	92.83±0.18	0.20±0.01	0.01±0.01	0.11±0.07	0.02±0.02	0.29±0.01	1.27±0.20
1 year	5.25±1.03	88.82±5.09	0.13±0.17	0.25±0.55	0.24±0.11	0.09±0.14	0.97±1.26	2.05±0.99

TABLE 7.3.: EDS ANALYSES* OF POLISHED CROSS-SECTIONS OF CYCLED BETA-ALUMINA TUBES

Description	Na_2O	Al_2O_3	CaO	K_2O	FeO	Cl	SiO_2	Pb
Uncycled:								
1)Anode	6.38±0.56	92.29±0.85	0.00±0.00	0.96±0.18	0.00±0.00	0.08±0.03	0.29±0.09	0.00±0.00
2)Mid Anode	6.34±0.36	92.85±0.30	0.00±0.00	0.48±0.24	0.00±0.00	0.05±0.04	0.25±0.12	0.00±0.00
3)Mid Cathode	6.36±0.21	92.60±0.23	0.00±0.00	0.61±0.35	0.00±0.00	0.10±0.06	0.26±0.05	0.00±0.00
4)Cathode	6.29±0.35	92.42±0.42	0.00±0.00	0.77±0.32	0.00±0.00	0.12±0.08	0.27±0.09	0.00±0.00
Good:								
1)Anode	2.40±0.17	89.23±0.48	0.09±0.01	7.49±0.45	0.40±0.15	0.05±0.03	0.08±0.01	0.17±0.10
2)Mid Anode	4.64±0.19	92.04±0.06	0.02±0.01	3.23±0.29	0.06±0.02	0.09±0.02	0.10±0.03	0.00±0.00
3)Mid Cathode	4.68±0.07	92.43±0.05	0.03±0.02	2.53±0.02	0.04±0.04	0.05±0.04	0.12±0.06	0.00±0.00
4)Cathode	2.66±0.51	90.98±0.63	0.02±0.02	6.11±1.06	0.11±0.02	0.04±0.02	0.04±0.02	0.00±0.00
Early Failure:								
1)Anode	6.00±0.29	93.14±0.01	0.01±0.01	0.62±0.26	0.10±0.01	0.01±0.01	0.14±0.13	0.00±0.00
2)Mid Anode	6.05±0.54	92.94±0.33	0.00±0.01	0.68±0.27	0.07±0.08	0.00±0.00	0.22±0.09	0.00±0.00
3)Mid Cathode	6.19±0.37	92.77±0.19	0.07±0.05	0.63±0.34	0.63±0.34	0.00±0.00	0.26±0.03	0.00±0.00
4)Cathode	5.92±0.06	90.90±0.30	0.02±0.03	0.67±0.37	0.67±0.37	0.00±0.00	0.16±0.10	0.00±0.00
Overdischarge:								
1)Anode	5.35±0.40	93.29±0.51	0.25±0.03	0.67±0.28	0.25±0.11	0.00±0.00	0.14±0.03	0.00±0.00
2)Mid Anode	5.86±0.38	93.46±0.43	0.00±0.00	0.60±0.31	0.00±0.00	0.00±0.00	0.16±0.09	0.00±0.00
3)Mid Cathode	5.52±0.24	93.56±0.18	0.67±0.14	0.69±0.24	0.00±0.00	0.00±0.00	0.23±0.13	0.00±0.00
4)Cathode	5.08±0.10	92.85±0.25	0.25±0.10	1.63±0.58	0.23±0.10	0.02±0.01	0.25±0.09	0.00±0.00
Capacity Loss:								
1)Anode	3.54±0.08	91.31±0.18	0.01±0.01	5.04±0.29	0.08±0.03	0.07±0.01	0.01±0.01	0.00±0.02
2)Mid Anode	4.61±0.24	92.39±0.11	0.02±0.01	2.68±0.33	0.06±0.01	0.04±0.01	0.14±0.12	0.00±0.00
3)Mid Cathode	5.06±0.20	92.75±0.29	0.04±0.02	1.89±0.41	0.04±0.01	0.04±0.01	0.19±0.19	0.00±0.00
4)Cathode	3.00±0.65	91.33±0.87	0.01±0.01	5.33±1.52	0.08±0.02	0.04±0.03	0.11±0.11	0.00±0.00
Stood 1 Year:								
1)Anode	4.97±0.21	92.11±0.19	0.07±0.03	2.35±0.40	0.03±0.01	0.01±0.00	0.25±0.11	0.01±0.02
2)Mid Anode	5.66±0.31	92.65±0.19	0.01±0.01	1.39±0.42	0.02±0.01	0.01±0.00	0.16±0.01	0.00±0.00
3)Mid Cathode	5.89±0.26	92.39±0.37	0.01±0.01	1.13±0.65	0.03±0.02	0.00±0.00	0.23±0.05	0.00±0.00
4)Cathode	5.67±0.19	92.70±0.20	0.00±0.00	1.20±0.39	0.11±0.05	0.00±0.00	0.25±0.10	0.00±0.00

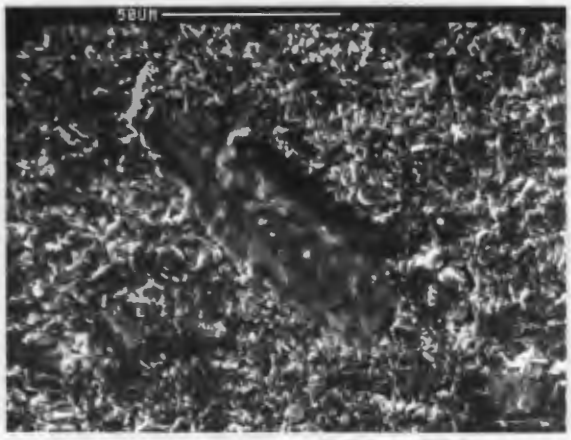

FIGURE 7.1. AN SEM MICROGRAPH OF THE Na/ELECTROLYTE INTERFACE OF AN UNCYCLED BETA-ALUMINA ELECTROLYTE.

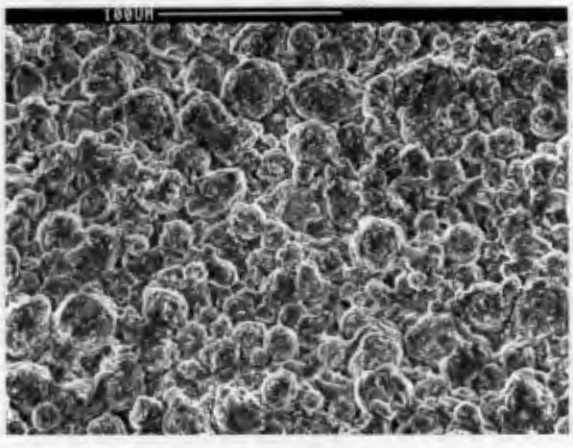

FIGURE 7.2. AN SEM MICROGRAPH OF THE CATHODE/ELECTROLYTE INTERFACE OF AN UNCYCLED BETA-ALUMINA ELECTROLYTE

(a) The Na/Electrolyte Interface:
Extremely large amounts of Pb (10.97 $^{+}/_{-}$ 0.99 $^{w}/_{o}$) were detected on the interface. 2.97 $^{+}/_{-}$ 0.18 $^{w}/_{o}$ Na and 84.21 $^{+}/_{-}$ 1.45 $^{w}/_{o}$ Al were detected. No other elements were detected.

(b) The cathode/electrolyte interface:
5.92 +/- 0.42 w/o Na and 92.58 +/- 1.56 w/o Al were detected. Surprisingly 1.03 +/- 0.45 w/o Cl was detected on the surface. This was presumably caused by contamination of the electrolyte during storage.

(c) Polished Cross-section:
No major impurity was detected in the analysis of the polished cross-section other than K from the polishing oil.

7.2.2. A Good Cell

The cell was subjected to seven cycles of charging and discharging. At the end of the cycling the cell was found to have roughly half the theoretical capacity of the cell, and was maintaining a very high Faradaic efficiency.

On removal of the electrolyte from the cell it was apparent that no cracking nor discolouration of the tube was present.

A silver decorated polished cross-section of the electrolyte showed only a thin black layer on the Na/electrolyte interface. In one region traces of internal damage were seen (see figure 7.3).

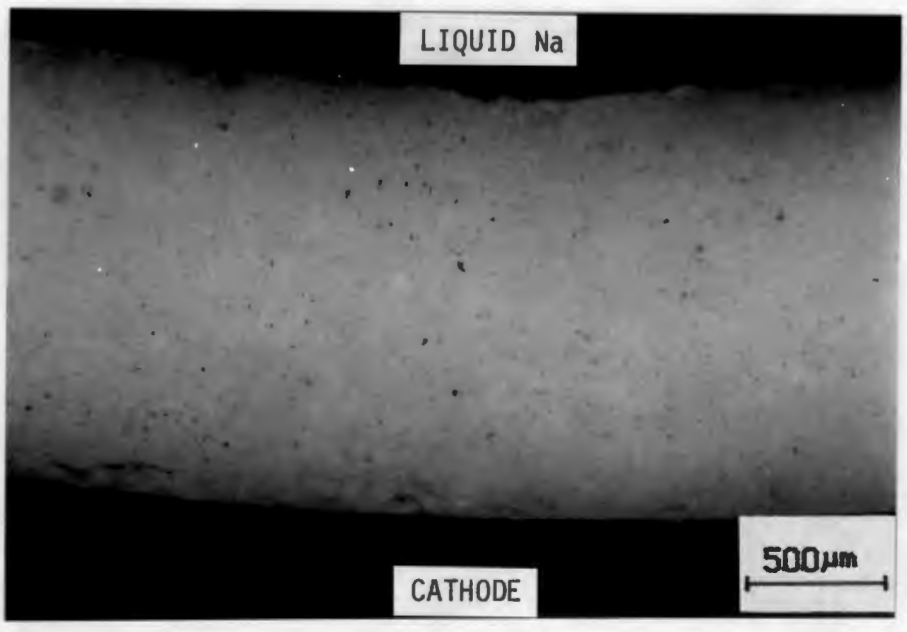

FIGURE 7.3. AN OPTICAL MICROGRAPH OF AN Ag DECORATED POLISHED CROSS-SECTION OF A GOOD CELL

The grain structure of the Na/electrolyte and cathode/electrolyte interfaces was found to be similar in appearance to that of the uncycled electrolyte.

(a)

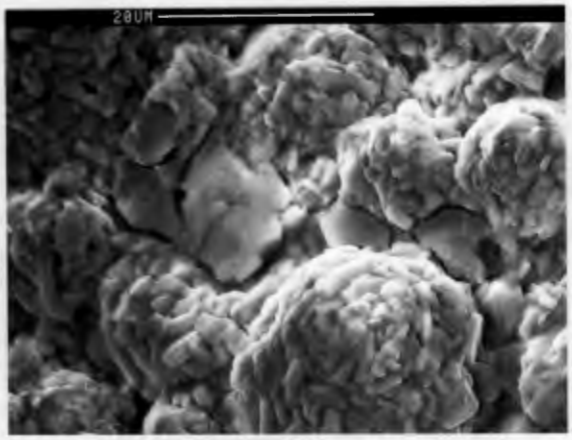

(b)

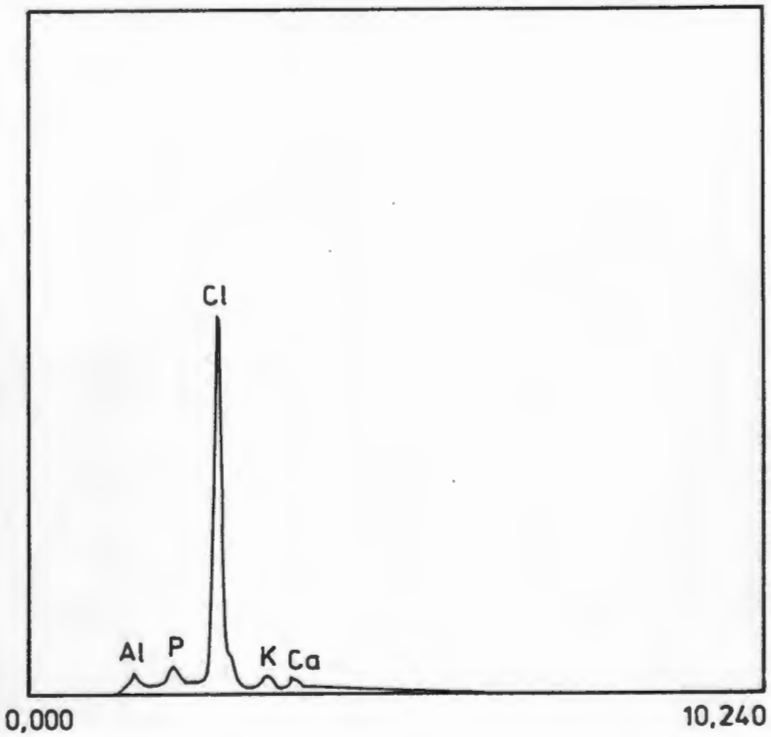

FIGURE 7.4. (a) AN SEM MICROGRAPH OF THE CATHODE ELECTROLYTE INTERFACE OF A GOOD CELL SHOWING ADHERENT GRAINS.
(b) THE EDS SPECTRUM FORMED BY SUBTRACTING THE BACKGROUND BETA-ALUMINA SPECTRUM FROM THAT OF THE ADHERENT GRAINS (WHICH INCLUDE SOME COUNTS FROM THE BACKGROUND). THE SPECTRA ARE NORMALISED WITH RESPECT TO Al PEAK INTENSITY.

The outer surface was found to have adherent deposits (see figure 7.4)

Notice that the analyses of the deposits showed them to be rich in Cl,with traces of Al, K, Ca and P.

(a) Cathode/electrolyte Interface:
Chemical analyses of the surface of the tube yeilded a Na content relative to Al which was similar to the uncycled electrolyte (5.13 $^{+}/_{-}$ 0.23 $^{w}/_{0}$ Na relative to 93.18 $^{+}/_{-}$ 1.56 $^{w}/_{0}$ Al) of the tube. 1.23 $^{+}/_{-}$ 0.58 $^{w}/_{0}$ Cl was found on the interface.

(b) Na/Electrolyte Interface:
The interface was found to contain small amounts of Pb (0.04 $^{+}/_{-}$ 0.05 $^{w}/_{0}$). The ratio of Na (6.48 $^{+}/_{-}$ 0.23 $^{w}/_{0}$) to Al (92.60 $^{+}/_{-}$ 0.38 $^{w}/_{0}$) was similar to that of the uncycled tube.

(c) Polished Cross-section:
Analyses taken on a polished cross-section of the tube showed that no major impurity pickup had occurred. The slightly higher Fe was found to be caused by adhering Fe from the cathode and did not penetrate into the beta-alumina electrolyte.

7.2.3. Early Failure

The cell was cycled for only one and a half cycles, and then failed on discharge. The full cycle performed showed almost complete Faradaic efficiency and was close to theoretical capacity.

In this cell the cathode was contained within the beta-alumina electrolyte tube, with the Na situated between the outer casing of the cell and the electrolyte.

On removal from the cell large amounts of cracking of the beta-alumina tube was found to have occurred.
Unfortunately, severe mechanical damage occurred during the removal of the electrolyte from the cell. It was thus difficult to distinguish between cracking which had occurred during cell operation, and cracking caused by removal of the electrolyte from the cell. It was, however, possible to remove the dome of the tube relatively intact from the cell. The dome of the tube, prior to cleaning in ethanol, is shown in figure 7.5.

FIGURE 7.5. AN OPTICAL PHOTOGRAPH OF THE DOME OF AN ELECTROLYTE TUBE FROM A CELL WHICH FAILED AFTER ONLY TWO CYCLES.

The dome of the electrolyte was cleaned and then pieced together. The base of the dome was found to be too smashed to be reconstructed. The direction of cracking was determined by tracing the direction of cracking back from the bifurcations of the crack. The suggested direction of cracking is shown in figure 7.6. There was one obvious initiation point as indicated in the diagram. The surfaces of the crack in this region were examined under the SEM.

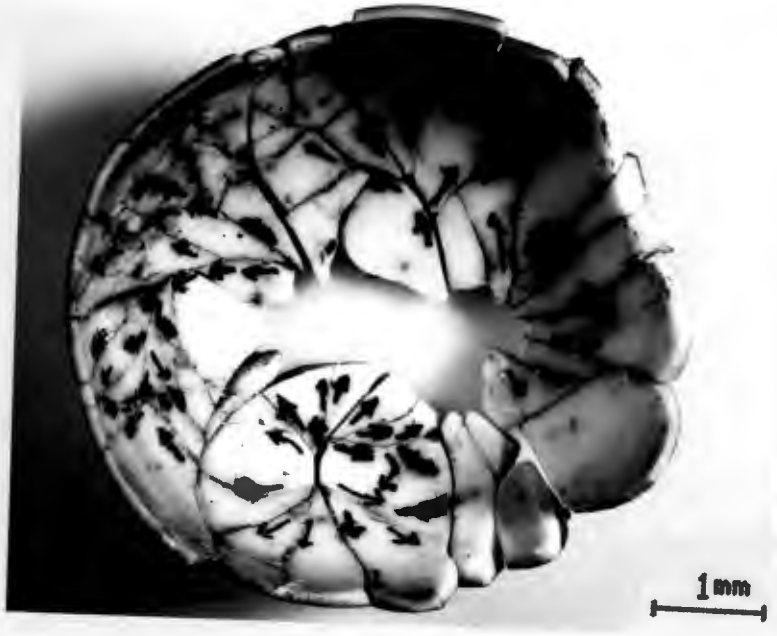

FIGURE 7.6. AN OPTICAL PHOTOGRAPH OF THE DOME OF THE ELECTROLYTE TUBE SHOWN IN FIGURE 7.6. AFTER CLEANING AND RECONSTRUCTION. THE ARROWS SHOW THE SUGGESTED DIRECTION OF CRACK PROPAGATION

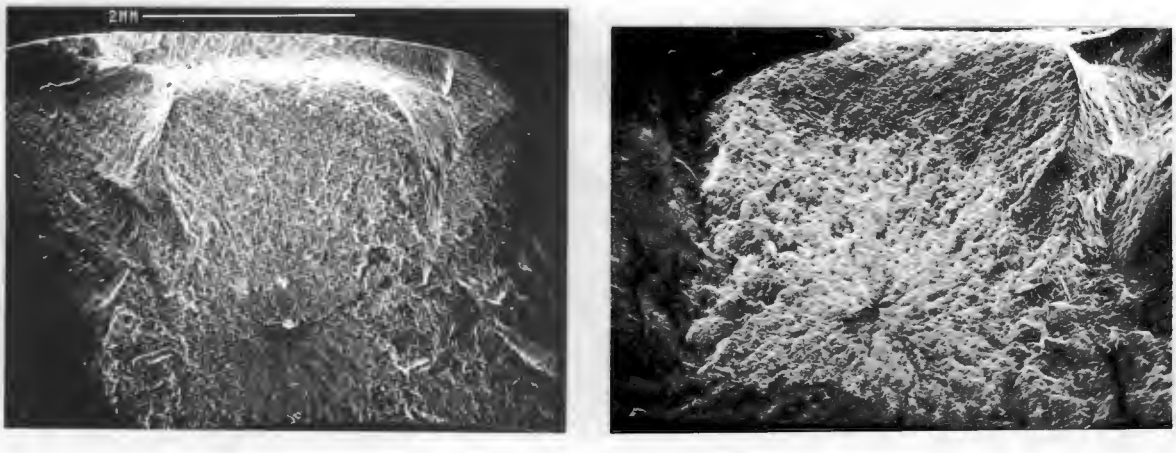

FIGURE 7.7. SEM MICROGRAPHS OF THE TWO MIRROR FRACTURE SURFACES OF A CRACK SHOWING THE PORE WHICH APPEARED TO BE ONE OF THE INITIATION POINTS OF THE CRACKING.

Examination of the fracture surface at the proposed initiation site (figure 7.7.) revealed a large pore close to the cathode side of the electrolyte. The fracture surface was consistent with a brittle fracture of the electrolyte with the crack initiating at the internal pore. No blackening of the electrolyte within the pore was found. The inner surface of the pore was similar to that seen on the as-sintered outer surface of the electrolyte. The pore is shown in figure 7.8.

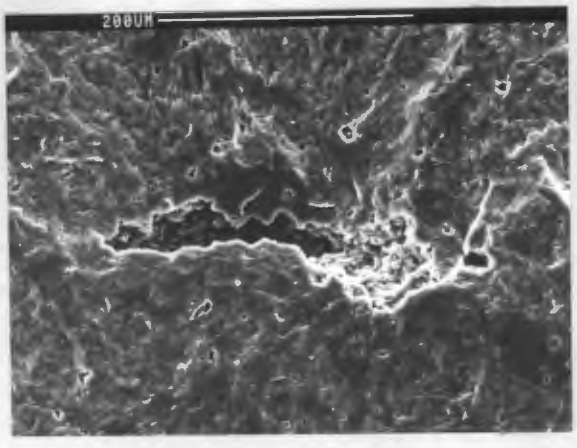

FIGURE 7.8. AN SEM MICROGRAPH SHOWING THE INTERIOR OF THE PORE WHICH INITIATED THE CRACKING.

The cathode/electrolyte interface of the tube was found to contain several black spots (see figure 7.7.). A polished, silver-decorated section of one of the spots is shown in figure 7.9. As can be seen the black layer giving the spot its colour is limited to the cathode/electrolyte interface.

Some of the spots were found to have a black layer on both the cathode and anode surfaces. However, once again the blackening did not extend into the bulk of the electrolyte. No discernible difference in chemical composition was found to exist between the black spot and the surrounding electrolyte.

Analyses of standard cross-sections of the tube showed that no major impurity pickup had occurred during cycling ie. there was no obvious general chemical pickup which could have resulted in failure.

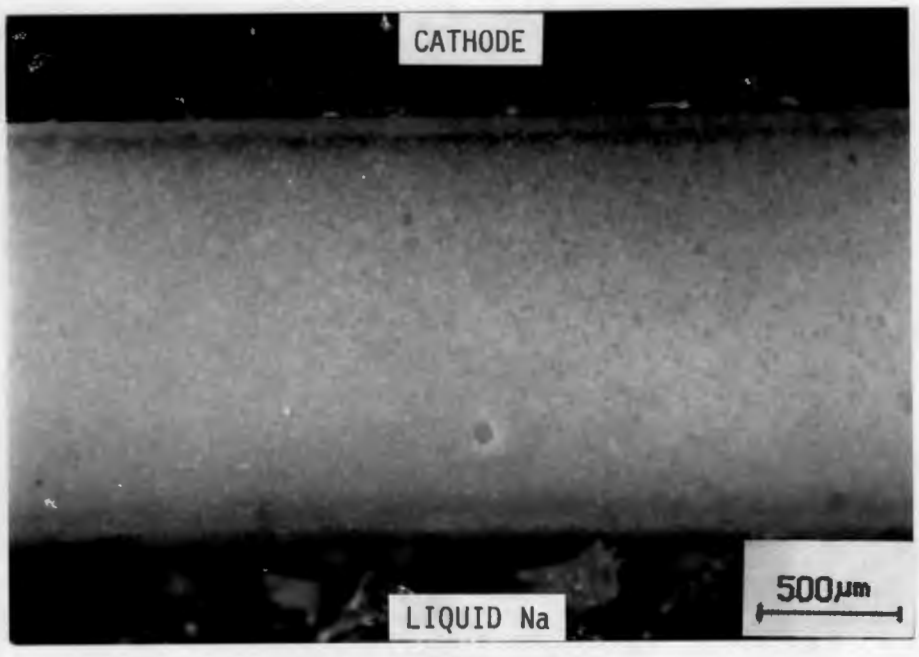

FIGURE 7.9. AN OPTICAL MICROGRAPH OF AN Ag DECORATED POLISHED CROSS-SECTION OF A "BLACK SPOT" ON THE ELECTROLYTE.

The Na/electrolyte interface of the tube was found to be Na rich with an average of 6.35 $^{+}/_{-}$ 0.14 $^{w}/_{o}$ Na and 87.44 $^{+}/_{-}$ 1.14 $^{w}/_{o}$ Al. 0.34 $^{+}/_{-}$ 0.34 $^{w}/_{o}$ Pb was detected.

7.2.4. An Overdischarged Cell

The cell did approximately 42 cycles. The cell capacity was good for most of the cycles, but the cell showed a drastic capacity loss after being accidentally overdischarged. Several more cycles were done, but the cell capacity remained low.

On removal of the beta-alumina electrolyte from the cell, cracks up to 100 mm in length were found running the length of the tube. Most of the cracking had occurred in the dome of the electrolyte.

Approximately midway down the length of the tube severe pitting of the cathode/electrolyte interface of the tube was seen. Severe discolouration of the tube occurred in this

region. However the remainder of the cathode/electrolyte interface did not show any discolouration.
The grain structure of the Na/electrolyte interface of this tube was found to be similar to that of the uncycled tube. However, some breakdown of the large grains appeared to have occurred. The grain structure of the interface is shown in figure 7.10.

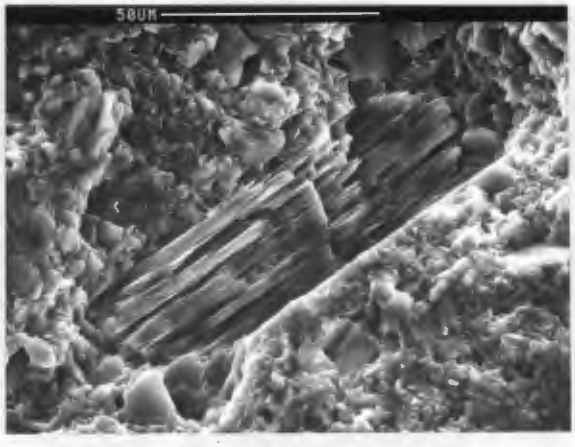

FIGURE 7.10. AN SEM MICROGRAPH OF THE STRUCTURE OF THE Na/ELECTROLYTE INTERFACE OF AN OVERDISCHARGED CELL.

A silver decorated polished cross-section of the tube wall showed only a very thin black layer on the Na/electrolyte interface, with no discolouration or damage at the cathode/electrolyte interface. This is shown in figure 7.11.

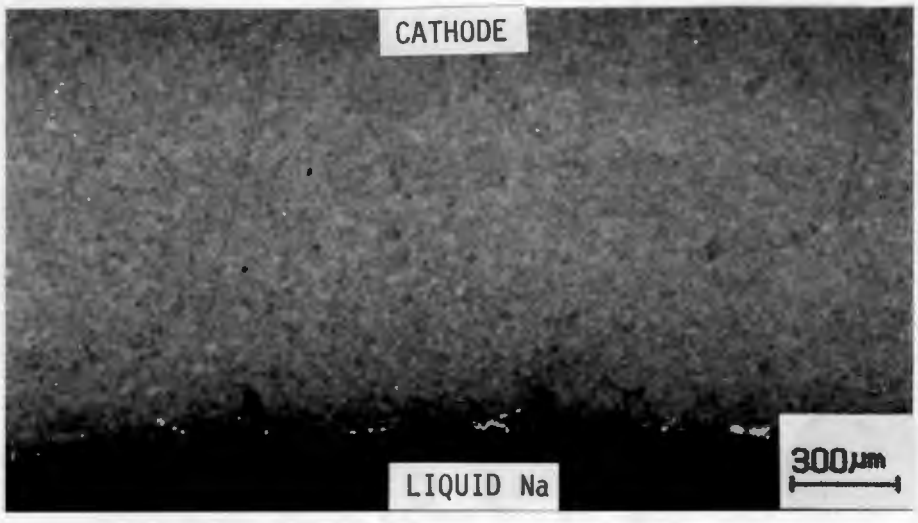

FIGURE 7.11. AN OPTICAL MICROGRAPH OF AN Ag DECORATED POLISHED CROSS-SECTION OF THE ELECTROLYTE WALL FROM AN OVERDISCHARGED CELL.

(a) Na/Electrolyte Interface:
Relatively large amounts of Pb were detected on the interface ($3.13^{+}/_{-}$ 0.14 $^{w}/_{o}$). In addition a large amount of K ($0.23^{+}/_{-}0.01$ $^{w}/_{o}$) was detected on the interface. The amount of Na detected relative to the Al ($3.29^{+}/_{-}0.08$ $^{w}/_{o}$ Na to 91.47 $^{+}/_{-}2.24$ $^{w}/_{o}$ Al) was slightly smaller than that found in the other cells.

(b) Cathode/Electrolyte Interface:
The interface was found to be slightly Na-depleted relative to the uncycled tube (4.35 $^{+}/_{-}$ 0.30 $^{w}/_{o}$ Na to 93.92 $^{+}/_{-}$ 0.24 $^{w}/_{o}$ Al). Traces of Fe (0.43 $^{+}/_{-}$ 0.09 $^{w}/_{o}$), K (0.18 $^{+}/_{-}$ 0.06 $^{w}/_{o}$) and Cl (0.64 $^{+}/_{-}$ 0.30 $^{w}/_{o}$) were detected on the interface.

(c) Standard Cross-section:
Analyses of standard cross-sections showed that a small amount of Ca was distributed throughout the electrolyte. No other impurity pickup was detected.

7.2.5. Capacity Loss

The cell performed seven cycles. The cell capacity gradually decreased until, after three cycles, the cell capacity was less than a third of the theoretical capacity. The cell capacity thereafter remained roughly constant.

On removal of the electrolyte tube from the cell, no macroscopic damage of the electrolyte tube was observed. In addition, no discolouration of the cathode/electrolyte interface was present.

However, it was apparent that the Na/electrolyte interface was not totally black, but contained grey areas (see figure 7.12)

A study of a silver-decorated polished cross-section of the electrolyte showed a thick black discolouration of the Na/electrolyte interface, but otherwise no signs of internal degradation of the electrolyte were found. The silver decorated cross-section is shown in figure 7.13.

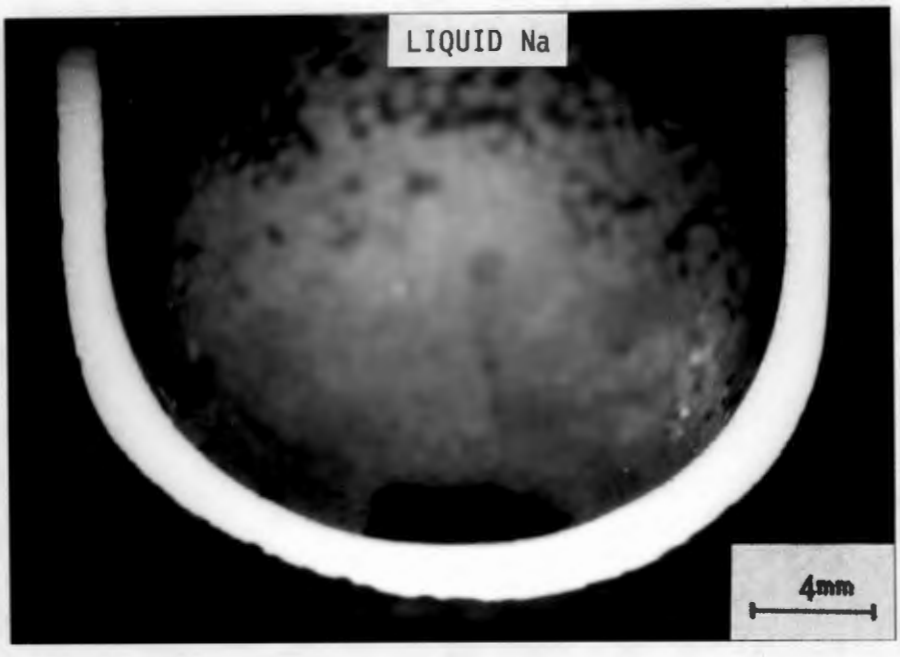

FIGURE 7.12. AN OPTICAL PHOTOGRAPH OF A CROSS-SECTION OF THE DOME OF AN ELECTROLYTE FROM A CELL WHICH HAD EXPERIENCED CAPACITY LOSS DURING CYCLING.

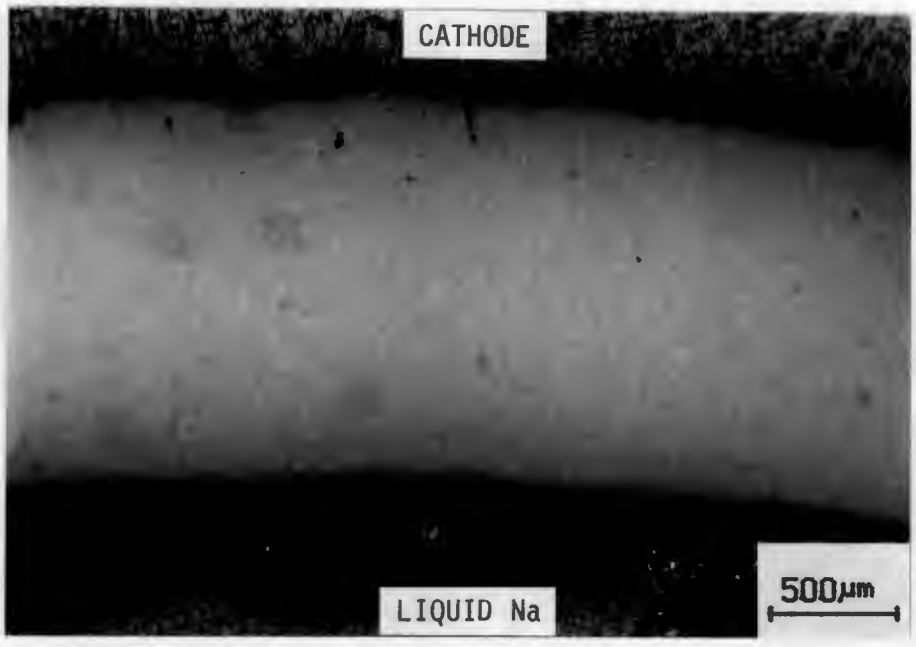

FIGURE 7.13. AN OPTICAL MICROGRAPH OF AN Ag DECORATED POLISHED CROSS-SECTION OF AN ELECTROLYTE FROM A CELL WHICH HAD EXPERIENCED CAPACITY LOSS DURING CYCLING.

SEM examination of the Na/electrolyte interface of the tube showed a severe degradation of the inner wall, with a very rugged surface finish. This is illustrated in figure 7.14.

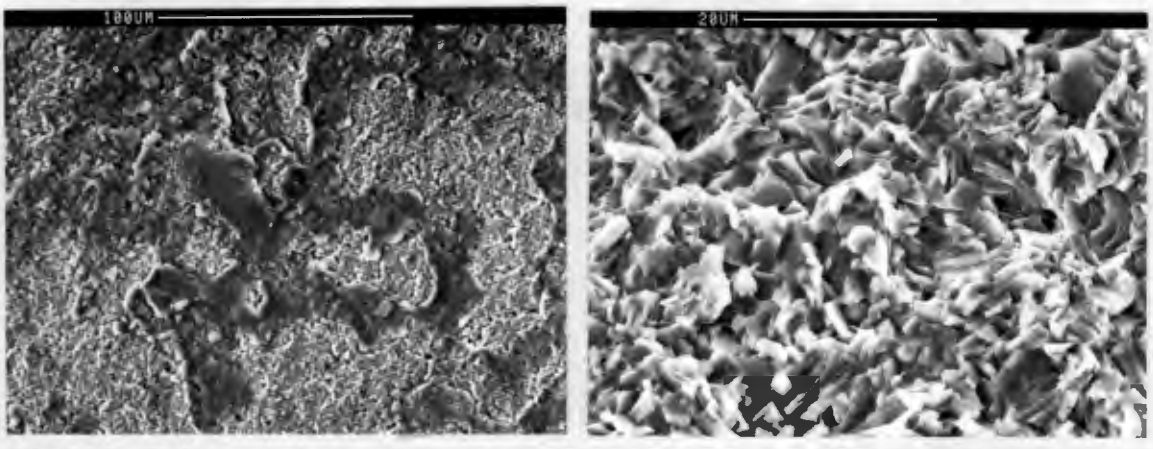

FIGURE 7.14. (a) AN OPTICAL PHOTOGRAPH OF THE Na/ELECTROLYTE INTERFACE OF A CELL EXHIBITING CAPACITY LOSS.
(b) THE GRAIN STRUCTURE OF THE Na/ELECTROLYTE INTERFACE SHOWN IN (a).

The cathode/electrolyte interface was found to be covered by a film of debris (shown in figure 7.15). Notice, though, that the grain structure of the interface closely resembled that of the uncycled tube.

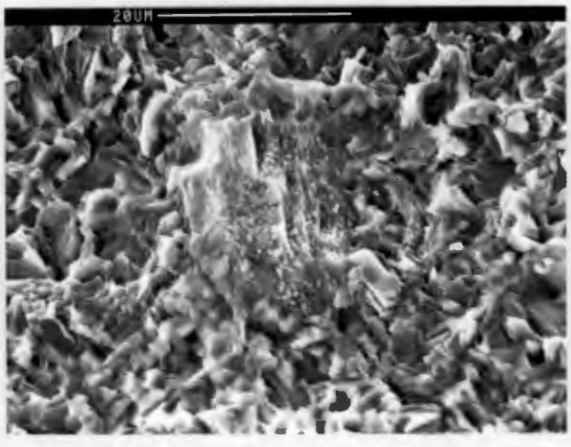

FIGURE 7.15. AN SEM MICROGRAPH OF THE GRAIN STRUCTURE OF THE CATHODE/ELECTROLYTE INTERFACE OF A CELL WHICH SHOWED CAPACITY LOSS WITH CYCLING.

(a) Na/Electrolyte Interface:
Chemical analyses of the interface showed that the Pb was evenly distributed over the surface (1.27 ± 0.20 $^{w}/_{0}$). The ratio of Na to Al (5.26 ± 1.03 $^{w}/_{0}$ to 92.83 ± 0.18 $^{w}/_{0}$ respectively) was found to be similar to that of the uncycled electrolyte. The areas showing macroscopic breakdown (see figure 7.14 (b)) showed a marginal difference to the uncycled Na and Al compositions (4.69 and 92.60 $^{w}/_{0}$ respectively).

(b) Cathode/Electrolyte Interface:
The surface showed a depletion of Na on the surface (3.91 ± 0.01 $^{w}/_{0}$) relative to the Al (95.34 ± 0.03 $^{w}/_{0}$). Small amounts of K (0.18 ± 0.06 $^{w}/_{0}$) were also detected.

(c) Polished Cross-section:
The polished cross-section did not show any major deviations of chemical composition relative to the uncycled tube.

7.2.6. A Cell Which Stood Uncycled for 1 Year

The cell was subjected to seven complete cycles, then left for 1 year at normal operating temperature (250^{0} C) in a discharged state. After a year 2 cycles were done with the cell prior to removal from the battery.

The cell resistance was originally 12 m Ω, after 1 year it was found to be 48 m Ω. The capacity of the cell in the first cycle was low originally, decreased steadily during the original cycling schedule to roughly 50% of the theoretical capacity. The cell capacity was found to have remained roughly constant after the one year storage at operating temperature.

On removal from the cell severe cracking was found in the base of the beta-alumina tube. The cathode/electrolyte interface was slightly grey (see figure 7.16).

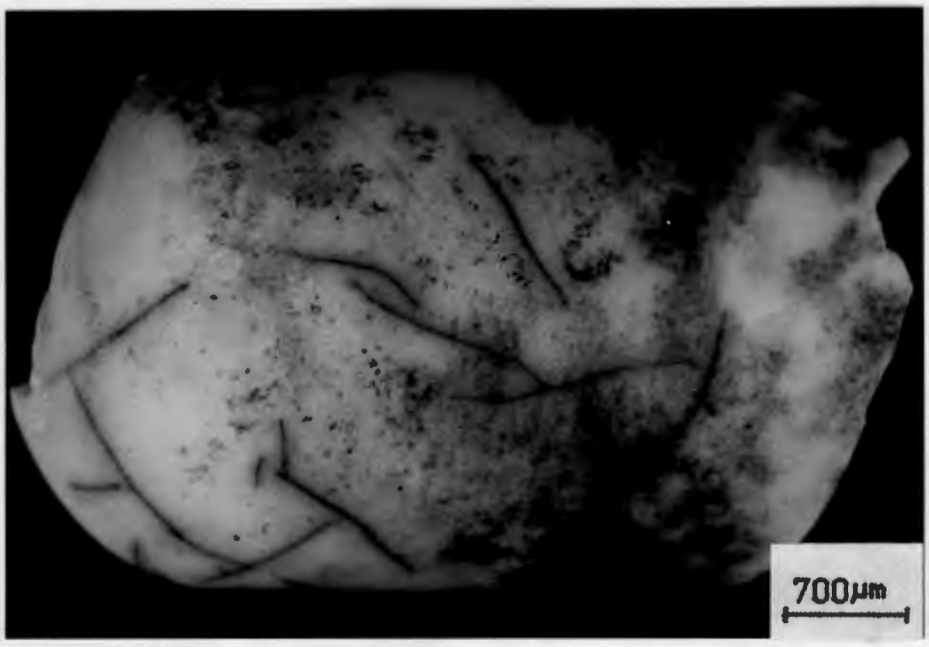

FIGURE 7.16. AN OPTICAL PHOTOGRAPH OF THE DOME OF AN ELECTROLYTE TUBE FROM A CELL WHICH HAD STOOD UNCYCLED FOR 1 YEAR.

A study of a silver decorated polished cross-section of the beta-alumina electrolyte (see figure 7.17.(a)) showed that little blackening of the Na/electrolyte surface had occurred.

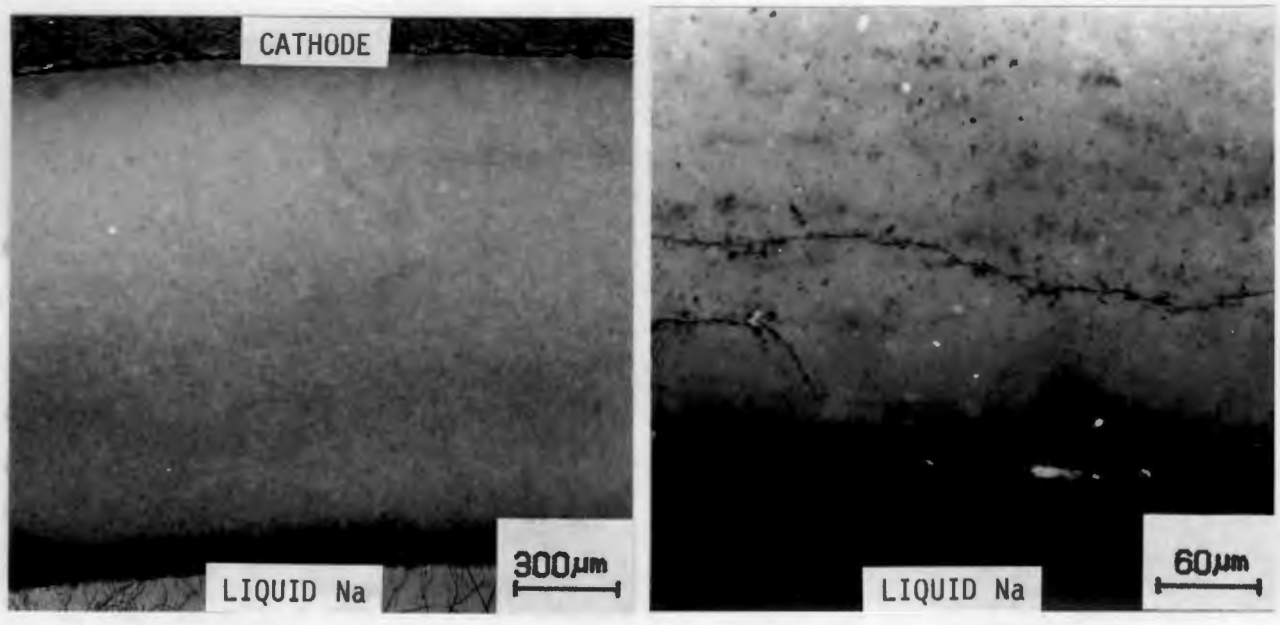

FIGURE 7.17. OPTICAL MICROGRAPHS OF AN Ag DECORATED POLISHED CROSS-SECTION FROM A CELL WHICH HAD STOOD UNCYCLED FOR 1 YEAR:
(a) AN UNDAMAGED AREA
(b) AN AREA SHOWING INTERNAL DAMAGE.

However, in another portion of the cross-section a large amount of internal damage of the tube was found (refer to figure 7.17.(b)).

The grain structure of the Na/electrolyte and cathode/electrolyte interfaces were similar to those of the uncycled electrolyte.

Higher up on the tube Fe rich deposits were found (again possibly residual cathode material). These deposits are shown in figure 7.18. In addition, some crystals were found which were very rich in Al (see figure 7.19). Their significance was unclear, though their very low numerical density made their significance questionable.

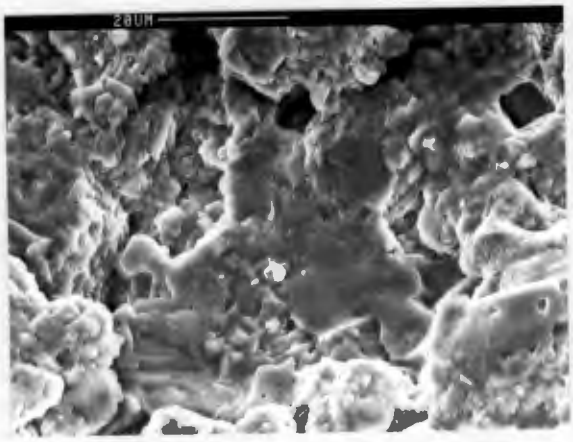

FIGURE 7.18. SEM MICROGRAPH OF AN Fe RICH GRAINS ON THE CATHODE/ELECTROLYTE INTERFACE.

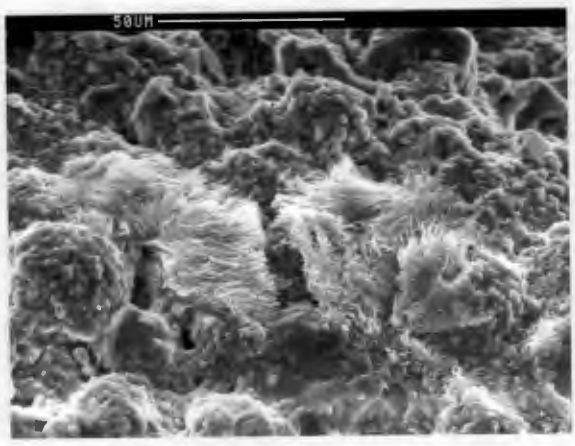

FIGURE 7.19. AN SEM MICROGRAPH OF Al RICH GRAINS FOUND ON THE CATHODE/ELECTROLYTE INTERFACE.

(a) Na/Electrolyte Interface:
Analyses of the interface showed a amount of Na (5.25 ± 1.03 w/o) relative to Al (88.82 ± 5.09 w/o). 2.05 ± 0.99 w/o Pb was detected on the interface.

(b) Cathode/Electrolyte Interface:
Analyses of the interface showed large amounts of Fe (0.93 ± 0.61 w/o). This was probably due to adhering cathode material.

The amount of Na detected was similar to that of the uncycled tube (5.15 $^{+}/_{-}$ 0.36 $^{w}/_{0}$) relative to Al (93.31 $^{+}/_{-}$ 0.59 $^{w}/_{0}$).

(c) Polished Section:
Analysis of a silver decorated polished cross-section of the tube revealed no discernible change in composition relative to the uncycled tube.

7.3.DISCUSSION

7.3.1. The Good Cell

The electrolyte from this cell showed no macroscopic damage after cycling. In addition no major impurity pickup occurred.

Close examination of the adhering grains seen on the cathode/electrolye interface (figure 7.2.) shows that they are distinct from the beta-alumina electrolyte. The grains contained a large amount of Cl, but the form in which the Cl is present is not apparent as there was no corresponding cation concentration detected. The lack of discolouration of the surface of the tube, and the high Cl content of the grains suggests that the grains may be adhering $NaAlCl_4$. Notice that this surface had not been cleaned with alcohol an hence unreacted $NaAlCl_4$ may indeed have been present.

The fact that the Na content of the cathode/electrolyte interface was lower than that of the uncycled cell may be misleading in that adhering $NaAlCl_4$ would react with moisture in the air during storage to form $Al(OH)_3$, NaCl and HCl. The HCl would have been removed by the alcohol, as would the NaCl as both are slightly soluble in alcohol. The $Al(OH)_3$ is insoluble in alcohol and would thus remain on the surface. Adhering $Al(OH)_3$ on the surface would have increased the amount of Al detected.

It is apparent from the analysis of the beta-alumina electrolyte that the iron cathode and molten $NaAlCl_4$ electrolyte of the Zebra cell are not necessarily deleterious to the beta-alumina electrolyte during normal cycling conditions.

7.3.2. Early Failure

The cell failed by a sudden, irreversible loss of electrical capacity ie. some form of internal short-circuiting had taken place. Internal shorts are generally caused by either rupture of the beta-alumina electrolyte or by seal failure.

Severe cracking of the electrolyte was observed on examination of the electrolyte. The majority of the cracks found in the electrolyte were darkened on the cathode/electrolyte interface. As it was known that mechanical cracking of the tube had occurred during extraction from the cell, it was assumed that the cracks which did not show blackening on the cathode/electrolyte interface were caused by mechanical damage during the removal of the electrolyte from the cell and were thus not present at the time of cell failure.

The fracture surface at the "initiation point" was not consistent with the cracking having been caused by Na-dendrite formation in the electrolyte. The dendrite could only have initiated at the pore if the electronic conductivity of the beta-alumina was sufficient to warrant Na metal formation inside the pore. The only known way of increasing the electronic conductivity of beta-alumina significantly is by ionic substitution of the Na^+ by impurities. As no major impurity pickup in the electrolyte was detected it seems unlikely that the cracking was caused by Na metal being deposited in the pore, initiating mode 1 cracking.

A possible explanation for the cracking observed is that the electrolyte did not crack during the cycling but rather during the rapid cooling of the cell on removal from the battery. The history of the cell, as regards handling, is unfortunately not known. However, it is possible that when the cell failed, it was immediately removed from the hot-box and allowed to cool in air. Beta-alumina is prone to cracking by thermal shock, and as a result the electrolyte may have cracked due to thermal shock subsequent to cycling.

Although no tests have been done on the effect of rapid cooling of the cell, the thermal conductivity of beta-alumina would be expected to be considerably less than that of the liquid Na. The beta-alumina would thus insulate the cathode causing a large thermal gradient across the beta-alumina electrolyte. As a result, a compressive stress would be set up on the Na/electrolyte surface and a tensile stress on the cathode/electrolyte surface. If the stress was large enough, cracking would be expected to occur from the cathode/electrolyte surface. The pore which appeared to be the initiation point of at least some of the cracking was indeed in the proximity of the cathode/electrolyte interface. In addition, the fast fracture region around the

pore is asymmetrical and extended toward this surface. Whether the cooling rate would be sufficient to cause this type of failure is not known.

If the failure of the cell was not caused by cracking of the electrolyte, then the internal shorting which resulted in the early failure was probably caused by a mechanical failure of the seals, or failure of one of the electrical insulators in the cell.

A further possible explanation for the cracking observed in the electrolyte is that the cathode expanded during cell operation. The stress caused by the cathode expansion may thus have been sufficient to cause mechanical failure of the electrolyte at its weakest points, one of which would have been the internal pore.

The obvious way that the cathode could have expanded was that it may have absorbed moisture from the air during assembly. The major effect of moisture absorption would be the formation of HCl and Al from $NaAlCl_4$ as well as the oxidation of the Fe skeleton in the cathode. Both of these processes would be expected to cause the cathode to expand when the cell is heated to operating temperature.

The significance of the black spots found on the cathode/electrolyte is not clear. It was noteworthy though that the black spots only appeared to occur in the vicinity of the blackened cracks. Nevertheless at no stage was a crack found which ran through a black spot. They were not accompanied by any local chemical composition change in the electrolyte.

A possible explanation for the presence of the black spots is local high electric field blocking conditions at the interface. If the Fe cathode is not in intimate contact with the electrolyte over the entire surface, but touches the surface at a few discrete points the local electric field in the electrolyte will be very high during cycling. This would result in a high local Na current, but with a blocking electrode at the cathode/electrolyte interface. As a result Na metal may be deposited within the electrolyte, possibly resulting in the formation of these black spots. The fact that the spots tend to become more and more intense closer to their centers tends to support this theory. However, this does not explain how occasionally spots are found on the Na/electrolyte interface opposite the spot on the cathode interface.

The extremely thin black layer seen on the Na/electrolyte interface was not surprising as the cell was operational for only a short period. The lack of internal damage is consistent with the suspicion that the cracking was not caused by Na current through the electrolyte.

Furthermore, the lack of impurity pickup by the electrolyte during its relatively few charge and discharge cycles tends to confirm that the failure was not related to contamination of the electrolyte.

7.3.3. Overdischarge

The degradation of the cathode/electrolyte interface of the tube from the overdischarged cell was surprising as no major impurity pickup was detected, and the Na content of the interface was fairly similar to that of the uncycled electrolyte.

The breakdown of the cathode/electrolyte interface observed in this cell was not found in other beta-alumina electrolytes from other overdischarged cells. It thus seems more likely that the feature was due to exposure to the atmosphere, or moisture pickup by the electrolyte during storage after removal of the beta-alumina electrolyte from the cell.

The pitting observed on the cathode/electrolyte interface appeared to be similar to that observed by other researchers when Ca additions were made to the liquid Na anode of cells, and the cells discharged the cells. A close study of the surface in the region of the pitting did not reveal any traces of adherent cathode material, nor any features which may have been associated with local cathode effects. It therefore seems likely that the pitting was caused by Ca impurities in the liquid Na and was not directly associated with the loss of cell capacity during overdischarge. The Ca detected in the polished cross-section tends to confirm this.

The cracking observed in the electrolyte was extensive, yet no internal shorting of the electrolyte was reported. Other cells which had also exhibited capacity loss on overdischarge did not contain cracking. It thus seems likely that the cracking was subsidiary to the cell degradation. The cracking, and sealing of the cracks will be discussed in a later chapter

Studying the reaction at the Al plateau:

$$NaAlCl_4 + 3Na^+ + 3e^- \longrightarrow Al + 4NaCl$$

it will be noticed that four electrons per $NaAlCl_4$ unit must be added to form the Al metal. As $NaAlCl_4$ is an electronic insulator, the electron must be supplied by the electronically conducting Fe backbone in the cathode. As the Al formed is not soluble in the $NaAlCl_4$, the Al will probably form by plating onto the Fe matrix. On charging of the cell the Al metal would be expected to convert to $AlCl_3$,

which is a Lewis acid and would be expected to attack the electrolyte by removing Na from the conduction planes. No evidence of this process was found. The only obvious way that the observations can be explained is that the proposed Al coating somehow affects the electrochemical properties of the Fe matrix (possibly by some form of alloying affect) forming a relatively stable compound for which the kinetics of Al dissolution during charge are much slower than those for $FeCl_2$. The argument is purely speculative though and no evidence is known to exist for such a compound.

7.3.4. Capacity Loss

Capacity loss is generally associated with some form of electrochemical decrease of either a cathode or anode constituent of the cell, an increase in the internal resistance of the cell, or some form of degradation of the cathode.

The degradation of the Na/electrolyte interface of the tube is consistent with the uptake of some ion with a larger ionic radius than Na^+. This form of surface degradation has been associated before with substitution of the Na^+ ion in the conduction plane with a larger ion (Kummer et al.;1972).

The Pb was evenly spread between the unspalled and spalled areas. It is thus unlikely that the spalling was caused by ion-exchange of the Na^+ by Pb^{2+} as this would be expected to result in the spalled-off areas being lower in Pb than the remaining areas. In addition, if the electrolyte reacted with moisture subsequent to removal from the cell (ie. during storage) with the resultant spalling of the surface, the Pb concentration would be higher in the areas where no spalling had occurred than in the spalled areas.

It is thus more likely that the tube was stored for a protracted period prior to use in the cell. The surfaces of the beta-alumina tube would have degraded with time by ion exchange of the Na^+ with H_3O^+. The presence of the H_3O^+ ions in the conduction planes would result in a decrease in the ionic conductivity of the electrolyte with a resulting high internal resistance of the cell.

If the current of the discharging cell was large, the large internal resistance of the cell would result in a relatively large internal voltage drop in the cell. This would result in the trip voltage at which the discharge would be automatically stopped and the charging of the cell resumed. As the charging of the cell takes place at a lower current than discharging, the effect of the high cell resistance due to the beta-alumina would not be as pronounced.
Nevertheless the high internal resistance would result in

the cell receiving fewer ampere hours charge than required to give it full capacity. This would imply that the next discharge of the cell would result in an even lower cell capacity. The effect would thus be cumulative: resulting in a progressive loss of capacity.

The apparent layer on the cathode/electrolyte interface is probably a result of the degradation of the electrolyte by the moisture. The Cl on the surface may have simply have been due to adhering $NaAlCl_4$ on the surface.

It is interesting to note that this cell had the thickest black layer on the Na/electrolyte interface of any of the electrolytes examined. The only explanation which presents itself is that, in this cell, the oxygen fugacity is the lowest of any of the the cells examined (ie. the reduction reaction proceeded to a larger extent than for any of the other cells). Blackening of the electrolyte is not generally recognised as a destructive mechanism in terms of cell capacity, so the blackening would not explain the cell capacity loss.

7.3.5. Cell Which Stood Fully Discharged for 1 Year

The cracking of the electrolyte and the internal resistance rise should be distinguished.

The point during cycling at which the cracking of the electrolyte occurred is not apparent. There was no suggestion that the cell had undergone internal shorting or total capacity loss during cycling. However, internal shorting in the electrolyte would be expected to decrease the internal resistance, rather than the increase observed in the cell. Accordingly, it does not seem likely that the cracking of the electrolyte occurred during the final two cycles after being stored at temperature for a year. In addition the final two cycles were relatively good capacity cycles for this particular cell. It is therefore unlikely that the resistance rise observed was related to the cracking of the electrolyte.

In spite of standing in contact with liquid Na for a year the blackening of the Na/electrolyte interface was extremely limited. This is consistent with the liquid Na having been saturated with oxygen during cell assembly, and hence very little reduction of the beta-alumina ceramic taking place.

The fact that the electrolyte tube was slightly grey along its entire length appeared to be associated with adhering cathode material. This appears to be confirmed by SEM examination, which showed that the layer was not continuous. Yet it is surprising that, though all the tubes were extracted from the cells in an identical manner, only this

tube showed any discolouration on the cathode/electrolyte interface. Though the evidence is tentative, this may be an indication that some form of surface layer was present during cycling. If this was the case, the high internal resistance of the cell would not be unexpected due to the hinderance of Na^+ ion current through the electrolyte. The layer, if it was indeed present, was too diffuse for any tentative hypothesis to be meaningful as to its composition, or possible cause.

7.3.6. General Discussion

In spite of the limitations imposed by K contamination of the electrolyte during polishing, it is apparent that the polished sections did not reveal any large scale contamination of the electrolyte in any of the degradation modes studied. Thus no evidence was found that any of the failures were caused by poisoning of the electrolyte.

The study of the cathode/electrolyte interface was obviously complicated by the fact that the surface was expected to have residual cathode material attached. However, it is noteworthy that, except in the case of the cell which had shown steady capacity loss, the grain structures of the surfaces were intact.

A surface of the electrolyte which was ion-exchanged with a larger ion is generally found to be severely degraded (Kummer ;1972). The relatively unblemished surface of the electrolyte after cycling of the Zebra cell suggests that little, if any, contamination of the beta-alumina had occurred during the cycling of the Zebra cells. It thus seems likely that, in the Zebra cell, the electrolyte is not generally severely degraded by impurities during cycling, even under extreme cycling conditions.

The capacity loss of the Zebra cells at 250^0 C may have been caused by exposure of the beta-alumina tube to moisture prior to cycling. The evidence seen does not implicate the cathode or any inherent property of the cathode with capacity loss at this temperature.

Generally no evidence was found of any layer present on the cathode/electrolyte interface, though some traces of layer formation may have been present on the cell which was left at operating temperature for a year.

Cracking was seen in several of the cells, several of which had not failed via internal shorting. It would thus appear that cracking is not necessarily deleterious to the performance of the Zebra cell. The cracking of the beta-alumina electrolyte in the Zebra cell will be discussed in greater depth in a later chapter.

As the failures do not generally (excluding capacity loss) appear to have been caused by bulk chemical contamination of the electrolyte, nor by any obvious physical contamination of the electrolyte, it seems likely that the failures were caused by some cathode or cathode/electrolyte interfacial effect. From the research done it thus appears that a study of these areas of the cell, rather than the electrolyte, will have to be undertaken to determine the source of the cell degradation.

8.The Effect of Pb Coating the Na/Electrolyte Interface

Several different wetting agents are used in the Zebra cell to enhance wetting of the beta-alumina by the liquid sodium. For this thesis only one of these wetting agents was studied, namely Pb.

Pb enhances the wetting of beta-alumina by liquid Na (Demott et al.; 1985), thereby reducing the Na/electrolyte interfacial resistance in Na/S cells. The effect of the coating on the continued wetting of the electrolyte during cycling, and its effect on cell degradation are not known.

The Na/electrolyte interfaces of cycled and uncycled electrolytes were studied. This was done to determine whether, after wetting had been affected, the adherence of the Pb to the Na/electrolyte interface was necessary for continued wetting of the surface. In addition the effect of the Pb coating on the cracking mechanisms of the electrolyte was studied.

8.1.INTRODUCTION

The phase diagram of Na/Pb (see figure 8.1) shows that none of the Pb alloys formed with Na are soluble in liquid Na at cell operating temperatures (200^0 to 300^0 C).

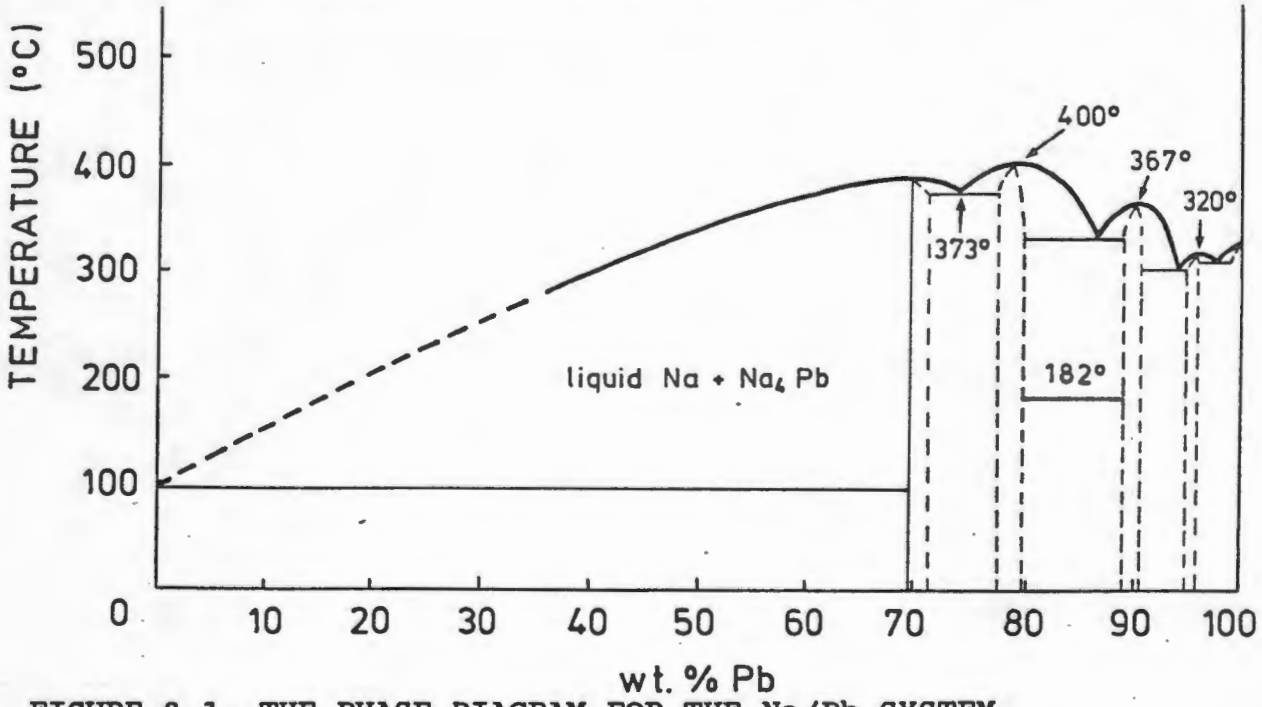

FIGURE 8.1. THE PHASE DIAGRAM FOR THE Na/Pb SYSTEM.

There is far more liquid Na in the cell than Pb in the coating, the Pb may thus be expected to slowly dissolve into the liquid Na.

Na-β alumina can be ion exchanged with $PbCl_2$ at 600^0 C. The ionic conductivity of the ion exchanged electrolyte decreased with increased Pb^{2+} content. This was ascribed to a reduction in the number of interstitial Na^+ ions in the conduction planes/slabs with increased Pb^{2+} ion exchange (cf. section 4.2.2.1.).

Farrington et al. (1982) found that single crystals of Na-β" alumina could be fully converted to Pb-β" alumina by heating in molten $PbCl_2$ at 600^0 C. They found that the ionic conductivity of fully ion exchanged Pb-β" alumina was similar to that of Na-β" alumina ($\sigma_{Na-\beta"}= 9.13x10^{-1}$ Ohm^{-1} cm^{-1}, $\sigma_{Pb-\beta"}= 1.5x10^{-1}$ Ohm^{-1} cm^{-1}). They attributed the high ionic conductivity of Pb-β" alumina to the fact that the Pb^{2+} interacts weakly with the vacancies in the conduction slab. The vacancies are thus very mobile. Accordingly diffusion in the conduction slab of the β"-alumina is relatively easy.

No literature was found on the effect of the Pb coating on Na-beta alumina electrolyte during cycling. However, Brieter et al. studied cells which used Hg as an anode with a Na cathode. Though Hg is liquid at cell operating temperatures and Pb would probably be solid the sizes and chemical properties of Pb and Hg are similar.

Brieter et al. found an increase in anodic current at voltages above 2.8 V at 350^0 C. They attributed this current to the reaction

$$Na_2O \text{ (solid electrolyte)} + Hg \text{ ---> } 2Na^+ + HgO + 2e^-$$

The reaction was found to be partially reversible during the cathodic sweep. After cycling red HgO was found on the Hg/beta-alumina interface.

The oxidation of Hg to Hg^{2+} occurs at a standard electrode potential of -0.051 V whilst the oxidation of Pb to Pb^{2+} occurs at 0.126 V. Thus electrochemically the oxidation of Pb is more favorable than that of Hg.

Cracking of the electrolyte was observed in the Na/Hg cells. This was attributed to preferential oxidation of the electrolyte at the grain boundaries. Grain boundary attack would increase the effective surface area of the grain boundaries and would thus enhance the attack.

The Hg was found, after cycling, to have penetrated to a depth of approximately 50 μm. The area containing the Hg was found to be black.

8.2.EXPERIMENTAL METHODS AND RESULTS.

8.2.1. THE DISTRIBUTION OF PB ON THE INTERFACE

To determine the concentration and distribution of the Pb coating on the electrolyte prior to cycling, the surface of an uncycled electrolyte was studied.

The surface of an uncycled tube was coated with a Pb acetate solution and then heated to 250^{0} C. The surface was examined using EDS to determine the concentration and distribution of Pb on the surface.

The averaged Pb concentration (an average of 28 spectra at 5 KeV and 1000 X magnification) was 54.79 $^{+}/_{-}$ 8.12 $^{w}/_{0}$. Note that the standard deviation for the results was relatively small, implying that the Pb was evenly distributed over the surface. The analyses were all done at 5 KeV to make the technique more sensitive to local surface variations in Pb content.

A series of 15 analyses were done at 5 KeV (1000 X magnification) on a tube after it had performed one cycle. The averaged Pb concentration was found to be 1.33 $^{+}/_{-}$ 1.00 $^{w}/_{0}$. If the Pb content of the two interfaces is assumed to have been similar prior to cycling, the decrease in Pb content of the interface after 1 cycle was substantial.

Some of the cycled electrolyte tubes discussed in chapter 7. were examined to determine the amount of residual Pb coating after different numbers of cycles. Each standard deviation represents the average of 4 analyses obtained from at least 2 samples. All the analyses were done at 5 KeV. The average Pb concentration verses the number of cycles is shown in figure 8.2.

No correlation appears to exist between the number of cycles performed and the amount of Pb detected on the Na/electrolyte interface. Notice that in each case the Pb analyses were similar to those of the electrolyte which had done one cycle.

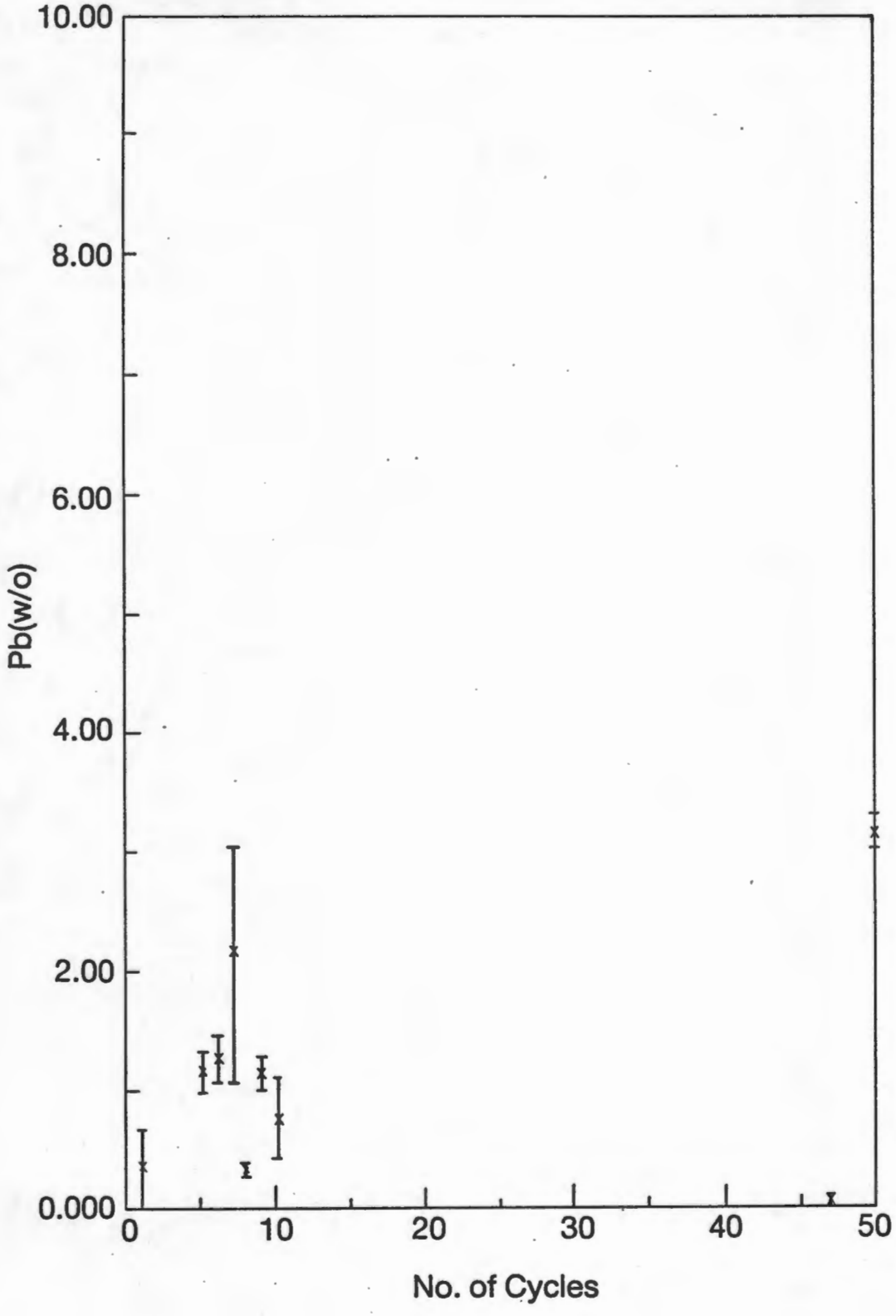

FIGURE 8.2. GRAPH OF THE ANALYSED Pb CONCENTRATION (at 5 KeV) ON THE Na/ELECTROLYTE INTERFACE VERSES THE NUMBER OF CYCLES PERFORMED.

SEM examination of the Pb coated Na/electrolyte interface of both cycled and uncycled electrolytes did not generally reveal any grains or features which could be attributed to the Pb.

However, examination of an area from a tube which had carried very little current revealed Pb grains adhering to the interface. The grains are shown in figure 8.3. The surface was in contact with liquid Na throughout the cycling of the cell. The Pb concentrations in this entire area were larger than most of the other tubes (3.16 $^{w}/_{o}$), but less than those of the uncycled interface. The grains demonstrate that the Pb is not totally dissolved in the liquid Na, even though the phase diagram shows that Pb is generally soluble in liquid Na at this composition.

It isthus reasonable to assume that the initial removal of Pb from the Na/electrolyte interface connected to the passage of Na through the electrolyte. If this was true the Pb concentration on the surface should be dependent on the orientation of the various grains on the interface eg. blocking grains would be expected to have more Pb than conducting grains.

To determine the dependence of the Pb concentration on the local microstructure, analyses were done on grains on the Na/electrolyte interface of a cycled cell. The results are shown in figure 8.4.

(a)

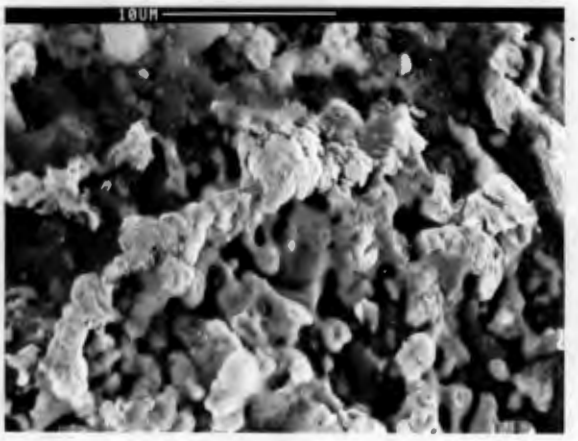

(b)

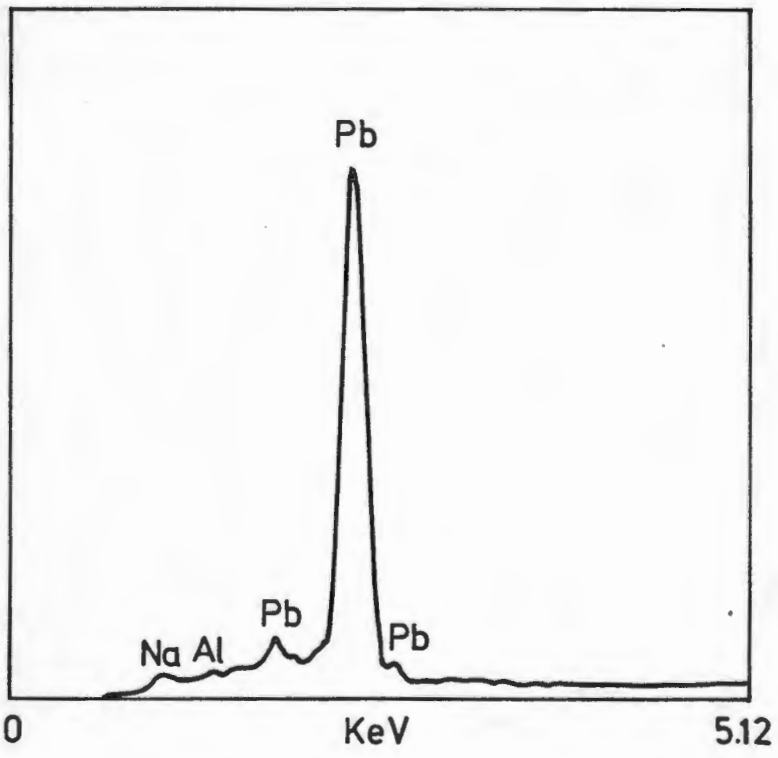

FIGURE 8.3. (a) SEM MICROGRAPH OF Pb RICH GRAINS FOUND ON THE Na/ELECTROLYTE INTERFACE OF A CYCLED CELL.
(b) EDS SPECTRUM OF (a) WITH THE BACKGROUND (due to the beta-alumina) SUBTRACTED. THE SPECTRA WERE NORMALISED TO Al PEAK INTENSITY.

TABLE 8.1. EDS ANALYSES OF THE Na/ELECTROLYTE INTERFACE SHOWN IN FIGURE 8.4. ALL THE ANALYSES WERE DONE AT 20 KeV.

	Na_2O	Al_2O_3	CaO	K_2O	FeO	SiO_2	Cl	Pb
(1)	14.90	80.75	0.00	0.00	0.04	0.06	0.01	0.20
(2)	26.69	70.39	0.18	0.00	0.28	0.34	0.04	2.17
(3)	48.04	48.10	0.54	0.12	0.19	0.69	0.08	2.30
(4)	46.66	51.89	0.14	0.00	0.00	0.18	0.02	1.03
(5)	46.45	50.69	0.15	0.00	0.39	0.11	0.00	2.23
(6)	17.55	79.59	0.06	0.03	0.19	0.18	0.16	2.18
(7)	47.11	49.33	0.20	0.07	0.26	0.09	0.05	2.87

All the analyses are in weight percent

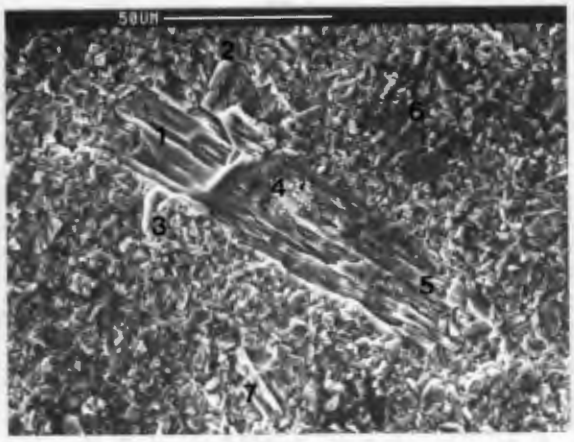

FIGURE 8.4. AN SEM MICROGRAPH OF AN Na/ELECTROLYTE INTERFACE. THE FIGURES ON THE MICROGRAPH CORRESPOND TO THOSE IN TABLE 8.1.

Notice that the amount of Pb detected was similar irrespective of the grain being analysed. The small differences seen were attributed to the effect of the orientation of the different grains relative to the X-ray detector. The local Pb concentrations do thus not appear to be dependent on the microstructure.

To determine the distribution of the Pb with respect to depth from the surface of the electrolyte, a number of analyses at different maximum excitation depths were done.

The maximum depth to which X-rays for a particular element are detected is a complex function ofseveral varyables, incluеding:

1) SEM acceleration voltage;
2) Excitation energy for the particular element;
3) The characteristic absorption coefficient of the particular material;
4) The ionization cross-section for the particular element.

By varying the SEM acceleration voltage it is possible to change the maximum depth to which a particular element can be detected. Thus, by acquiring EDS spectra at different SEM acceleration voltages it is possible to assess the relative distribution of the particular element as a function of depth from the surface.

Russ[1] (1984) pointed out that it is possible to determine whether an element is present in the form of a surface layer using EDS. If the ratio of the intensities of two peaks (one from the substrate and the other from the layer) is plotted as a function of SEM acceleration voltage (KeV), then the point at which an inflection is seen is the point at which the sampling depth equals the thickness of the layer.

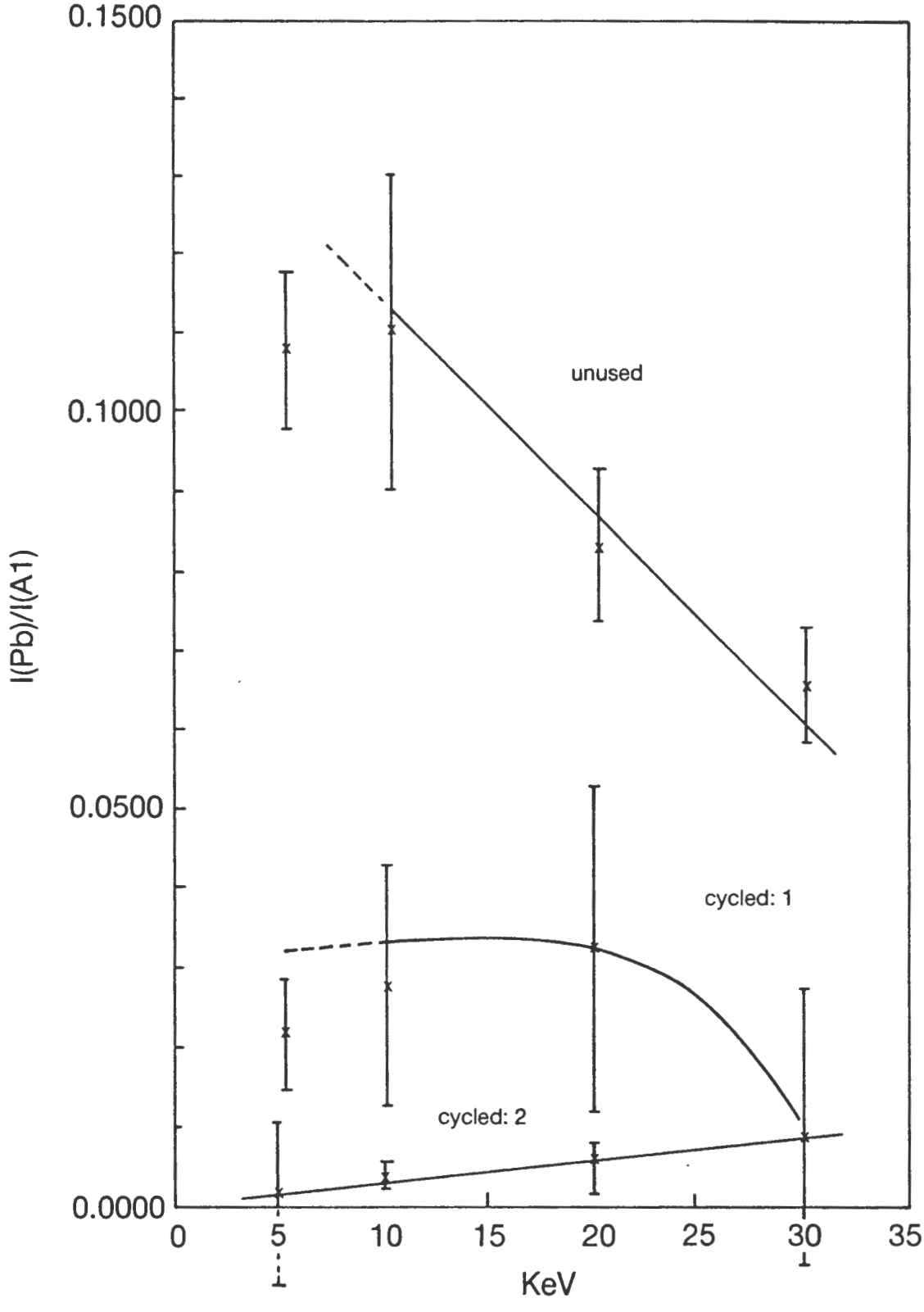

FIGURE 8.5. GRAPH OF THE RATIO OF THE INTENSITY OF THE Pb PEAK (I_{Pb}) TO THAT OF THE Al PEAK (I_{Al}) DETECTED ON THE Na/ELECTROLYTE INTERFACES FOR DIFFERENT CYCLING HISTORIES AT DIFFERENT SEM ACCELERATION VOLTAGES. UNUSED REFERS TO AN UNCYCLED ELECTROLYTE, CYCLED 1 AND CYCLED 2 REFER TO TWO DIFFERENT CYCLED ELECTROLYTES.

To assess the distribution of the Pb as a function of depth, the ratio of the intensities (areas) of the Pb (coating) and Al (substrate) peaks were obtained at 30, 20, 10 and 5 KeV SEM acceleration voltages. The average of 5 spectra at each KeV (magnification 1000 X) was taken. The analyses were carried out on one uncycled and two cycled tubes. A plot of I_{Pb}/I_{Al} versus KeV is shown in figure 8.5.

Notice that for the uncycled cell the intensity of the Pb peak relative to that of Al generally increased with decreasing KeV. The fact that the I_{Pb}/I_{Al} ratio at 5 KeV was less than expected was probably due to the energy of the beam being close to the critical excitation energy for Pb. Thus a large proportion of the electrons of the beam were not of sufficient energy to excite Pb.

The analyses for the cycled cells did not generally show an increase in I_{Pb}/I_{Al} with decreasing KeV. In fact, in "cycle 2" a decrease of I_{Pb}/I_{Al} was found with decreasing KeV. The Pb distribution thus appears to have changed with cycling.

Examination of a polished cross-section of a tube showed that the Pb was limited to the outer few microns of the tube. Figure 8.6. shows a line scan of one such area. Notice that most of the peaks closely follow the microstructure of the electrolyte, and are thus probably due to an increase in background counts. This implies that the peaks seen were caused by the geometry of the surface, rather than the presence of Pb.

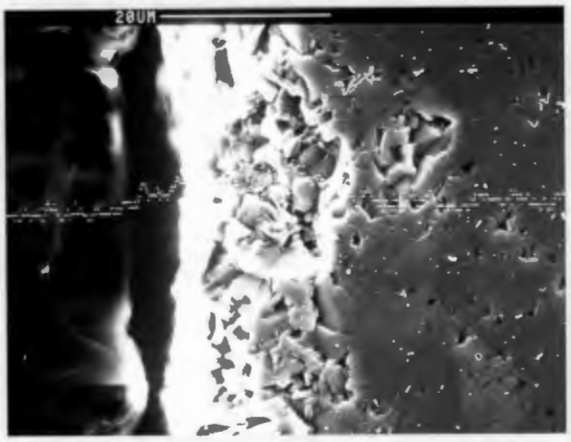

FIGURE 8.6. SEM MICROGRAPH WITH A SUPERIMPOSED Pb LINE SCAN OF A CROSS-SECTION OF A CYCLED BETA-ALUMINA ELECTROLYTE.

In addition, grains and pores in the polished cross-section of an electrolyte tube which were directly connected to the

Na/electrolyte interface were examined using EDS, the results of these analyses are given in table 8.2.

TABLE 8.2. EDS ANALYSIS ON THE Na/ELECTROLYTÉ INTERFACE OF A POLISHED CROSS-SECTION OF A CYCLED CELL.

	Isolated Pore	Pore Connected to the Interface	Nearby Grain
Na_2O	5.18	0.87	6.37
Al_2O_3	93.07	97.46	93.05
CaO	0.00	0.00	0.00
K_2O	0.94	0.75	0.00
FeO	0.07	0.08	0.11
SiO_2	0.24	0.00	0.44
Cl	0.00	0.07	0.12
Pb	0.00	0.68	0.00

The Pb coated uncycled electrolyte is black. After cycling the black layer seen on the electrolyte interface has two possible sources:

1) The Pb "coating"
2) Blackening due to the reduction of the electrolyte by Na (cf. section 4.1.1.).

To assess the amount of blackening due to the Pb coating, the blackening due to reduction of the electrolyte by Na was removed. This was done by heating the electrolyte in air to 250^0 C for 24 hrs. This "bleaches" the black areas by reintroducing oxygen into the conduction layers of the beta-alumina (De Jonghe et al;1982).

All the blackening of the Na/electrolyte interface was found to have been removed by the bleaching. An EDS examination of the Pb content both before and after heating showed that no Pb was lost from the interface. No sign of red PbO was found.

8.2.2. THE INFLUENCE OF THE Pb COATING ON CRACKING

If the cracking of the electrolyte was caused by bad wetting of the beta-alumina by the Na, the Pb content in the region of the cracks would be expected to be different to that of the rest of the interface.

A series of analyses done on the Na/electrolyte interface in the region of a crack showed no detectable change of Pb concentrations in the region of the cracks.

Examination of the fracture surface of a crack showed that the Pb was limited exclusively to the few microns of the crack close to the Na/electrolyte interface (see figure 3). Careful examination of the crack revealed that fine debris (see figure 8.7.) was present on the fracture surface.

Though confirmation was not possible (due to the size of the debris relative to the sampling depth), the Pb was believed to be located in this debris.

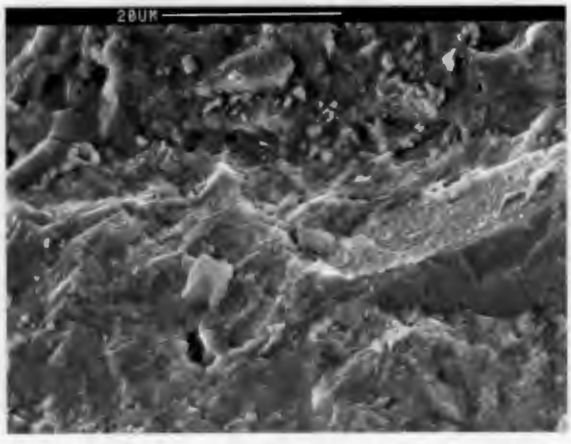

FIGURE 8.7. SEM MICROGRAPH OF Pb RICH DEBRIS ON THE FRACTURE SURFACE OF A CRACK EXTENDING THROUGH THE BETA-ALUMINA ELECTROLYTE.

However, in one crack examined, a Pb layer was found on the fracture surface midway between the cathode and anode surfaces. The layer and its position are shown in figure 8.8.

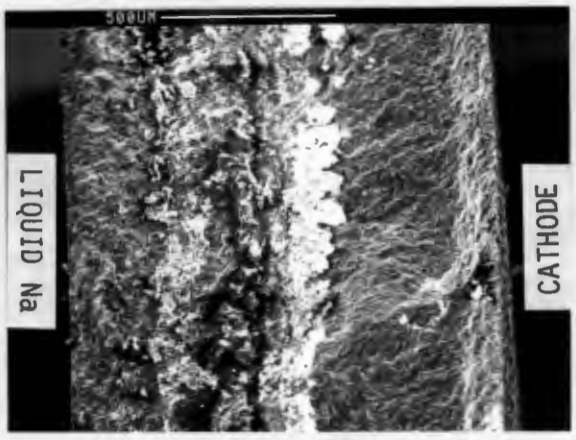

FIGURE 8.8. SEM MICROGRAPH OF THE FRACTURE SURFACE OF AN ELECTROLYTE SHOWING A CENTRAL (white) Pb RICH LAYER.

The layer was assumed to have been caused by a pre-existing flaw in the electrolyte being filled with lead acetate prior to activation.

8.3.DISCUSSION

8.3.1. The Effect Of Cycling on the Pb Coating

On cycling the Pb concentration at the Na/electrolyte interface decreased dramatically. The concentration loss appears to occur predominantly within the first cycle of the cell, with no subsequent loss in the remaining cycles. This implies that the Pb could have either diffused into the beta-alumina electrolyte or gone into solution in the molten Na.

If the Pb coating ion-exchanges totally within the electrolyte it is possible, due to the relatively small amount of Pb in the coating, that it would be below the detection limit for Pb of the EDS system.

Referring to figure 8.5. it is apparent that, if there is an inflection point in the graph it would have to be below 10 KeV. At the inflection point the sampling depth for Pb is approximately equal to the thickness of the coating. If it is assumed that the inflection point of the I_{Pb}/I_{Al} graph is below 10KeV SEM acceleration voltage we can calculate the thickness of the coating. Using a nonogram from Russ (1984) the thickness of the coating is estimated to be less than 0.2 İm. The nonogram is given in appendix 2.

Assuming that:

Pb layer thickness:	:	0.2 μm
Length of tube covered by Pb:		22 mm
Wall thickness	:	1.5 mm
Inner tube Radius	:	27 mm
Density of Pb:	:	11344 kg m^{-3}
Density of beta-alumina	:	3240 kg m^{-3}

Providing that the Pb was uniformly distributed in the electrolyte the amount of Pb detected in the electrolyte would be approximately 0.11 $^{w}/_{0}$. This would be close to the detection limit of the EDS system for Pb. It is thus possible, if all the Pb diffused into the electrolyte, that the Pb concentration would be too small to be detected using the EDS system.

In the Hg/Na cells of Brieter et al. the Hg was found to have diffused to a depth of 50 μm from the Hg/electrolyte interface. If all the Pb in the original coating diffused to this depth, the Pb detected would be 3.30 $^{w}/_{0}$. The analyses of polished cross-sections (cf. Table 7.3.) did not reveal Pb concentrations in the region of the Na/electrolyte interface which were consistent with this. In the majority of the analyses of the polished cross-sections no Pb was detected in the region of the Na/electrolyte interface.

High magnification analyses of grains in the polished cross-section in the region of the interface did not reveal any Pb in the grains.

It is thus unlikely that the large decrease of the Pb on cycling at the interface was caused by the Pb diffusing into the electrolyte. However it is possible that some of the Pb did diffuse into the beta-alumina.

Figure 8.1. shows that Pb is soluble in Na. Using the dimensions given in section 8.3.1. the Pb would form a 2.1×10^{-4} $^{w}/_{0}$ solution in the molten Na. From the phase diagram 20 to 30 $^{w}/_{0}$ Pb is soluble in molten Na at 200^{0} to 300^{0} C. The Pb in the coating may thus have been expected to dissolve in the Na.

However the Pb does not appear to simply dissolve in the liquid Na. In figure 8.3. Pb grains were found that had been in contact with molten Na for a considerable period.

Furthermore the Na/electrolyte interface which had been in contact with liquid Na for 1 year (table 7.2.) still contained Pb. The Pb thus does not slowly dissolve off with time into the liquid Na. After the initial loss the Pb concentration over the surface appears to remain approximately constant irrespective of the number of cycles done.

The Pb rich grains were only found on areas where the Na^{+} current was known to be low. The removal of Pb from the interface therefore appeared to be current dependent. However, the microscopic distribution of the Pb is approximately evenly distributed over the surface. The Pb grains seen on the surface may have been due to inhomogeneities of the Pb distribution in the original coating.

One possible reason for the Pb not dissolving as predicted in the phase diagram is that the diffusion of Pb in liquid sodium may be very slow. The Pb grains would then establish a local equilibrium concentration of Pb in the immediate surrounding Na. When the cell was charged the local equilibrium would be disturbed by the Na flow from the

electrolyte carrying the dissolved Pb with it. This would result in the grains progressively dissolving.

However most of the Pb in the original coating is not in the form of large grains but in the form of a very thin coating of an estimated thickness less than 0.2 Ìm. Thus establishing a local equilibrium would probably severely thin the coating. This implies that the coating may have been severely thinned prior to application of the Na current.

The depth analyses of the Pb suggests that the residual Pb after cycling is fairly evenly distributed with respect to depth. However grains from the cross-section of the tube wall which were in contact with the interface did not contain any detectable Pb. One possible explanation for this is that the residual Pb was trapped in pores which were joined to the interface. If the Pb was situated in these pores it would dissolve at a much slower rate than the coating due to its large volume relative to its area exposed to the liquid Na. This appeared to be consistent with analyses done on pores connected to the Na/electrolyte interface and pores which were not.

However, Pb was detected on the Na/electrolyte surfaces of the beta-alumina grains. This suggests that either some of the Pb has diffused into the conduction layers of the grains or that a very thin layer of Pb covered the surface. Analyses of grains joining the Na/electrolyte interface did not reveal any Pb.

Removing the blackening due to contact with liquid Na by bleaching did not reveal any black residue due to the Pb nor any PbO (red). This suggests that the Pb is not present as a thin layer on cycled electrolyte.

If the Pb does enter into the conduction planes of the beta-alumina it should do so preferentially into the β-alumina (Kummer ;1972). This would result in the conductivity β-alumina being reduced (ie. increase the local resistivity). Entering into the β"-alumina would not drastically affect their ionic resistivity. Thus, since the electrolyte is made up of mainly β"-alumina and providing that the Pb did not diffuse to any great depth, diffusion of Pb^{2+} ions would not be expected to dramatically reduce the ionic conductivity of the Na/electrolyte interface.'k

The degree of wetting of Na/Pb beta-alumina by liquid Na and hence the interfacial resistance is not known. A SIMS profile of the interface to assess the Pb distribution with respect to depth and microstructure should be done to obtain the true distribution of the Pb on the interface.

8.3.2. The Influence of the Pb Coating on Cracking.

Very little difference in Pb content on the interface was seen between the cracked and uncracked areas. Though not conclusive, this suggests that the area should have been wetted by the liquid Na.

The Pb did not penetrate to any great depth into cracks in the electrolyte. In addition, no cracks were found extending only a short distance from the Na/electrolyte interface. This suggests that the cracks are due to Na-dendrite formation rather than cracking from the reduction of the beta-alumina by Pb.

However, if the Pb was causing cracking of the electrolyte the cracks would eventually reach a length where they would become critical for the passage of Na (approximately 100 μm) and then the crack would propagate by dendrite formation.

No red PbO was found on the surface of the electrolyte, it is thus unlikely that the electrolyte was being reduced by the Pb. It therefore does not appear likely that the Pb promoted initiation of the cracks.

It is obvious from the Pb layer found in the pre-existing flaw of the the "55" that Pb does not prevent the formation of Na dendrites through the electrolyte. A flaw filled with Pb would be electronically conducting and accordingly would remain a Na^+ current concentrator in the electrolyte. The Na would be deposited directly in the electrolyte causing cracking of the electrolyte.

From this study it would thus appear that the Pb is not likely to have caused cracking in the electrolyte.

9.CRACKING OF THE ELECTROLYTE.

Dell et al (1987) noted that some of the cracks in the electrolyte of the Zebra cell sealed, thus not allowing internal shorting to occur. As a result, cracking in the Zebra cell is not necessarily catastrophic to the cell performance. They attributed the sealing mechanism to the reaction:

$$3Na + NaAlCl_4 \longrightarrow 4NaCl + Al$$

The NaCl and Al formed by the above reaction are insoluble in the liquid Na and the $NaAlCl_4$ They thus presumably formed a plug in the cracks, rendering them non-conducting.

In addition if the cracking was so extensive that the sealing mechanism could not eliminate the short, the cell failed in a conducting mode. They attributed this the Al formed in the above reaction would effectively join the Fe in the cathode to the current collector of the anode rendering the cell conducting. Thus catastrophic failure of one cell due to shorting does not necessarily eliminate the capacity of an entire string of cells. The detailed mechanism of the sealing of the cracks is not known.

In addition the direction of cracking, anode to cathode or vice-versa, was not known, nor were the details of the sealing mechanism. These problems will be examined in this section.

9.1.EXPERIMENTAL PROCEDURE

To determine the direction of cracking, the blackening of the electrolyte by Na of several cracks was examined. The depth of blackening proportional to the time the electrolyte has been in contact with liquid Na. Na dendrite formation should result in the blackening progressively decreasing with distance from the Na/electrolyte interface. Cracking from the cathode would not be expected to produce any significant trend.

The square of the depth of half of the optical density of the maximum blackening is dependent on the time of exposure of the electrolyte to Na ie.

$$x^2 = 0.92\ D\ t \qquad \text{(Beuchele; 1979)}$$

Where D is the diffusion coefficient of the blackening
x is the distance from the fracture surface to the point where the optical density is half that of the maximum blackening
t is the time of exposure of the electrolyte to Na.

A polished cross-section of a crack was Ag decorated (see section 8.1. for details of process). The depth of the half-maximum of the blackening as a function of distance from the Na/electrolyte surface was optically estimated.

In addition, the cracks from a variety of cycled cells were examined using a low power optical microscope, the SEM and EDS to determine the chemical composition of the fracture surface as a function of distance from the Na/electrolyte interface.

9.2.RESULTS

9.2.1. The Direction of Cracking

The square of the depth of the half-maximum darkening versus the distance from the Na/electrolyte interface for one of the cracks examined is shown in figure 9.1.

Notice that the blackening gradually decreases with distance from the Na/electrolyte interface. This implies that the electrolyte had been exposed for progressively shorter periods of time to liquid Na as the distance from the fracture surface increases.

9.2.2.Examination of Cracks from Cycled Cells.

Several cells were received which had failed by shorting through the electrolyte. However, several cells were examined with no reported failure due to internal shorting, but the electrolytes were found to contain cracks.

From an optical examination of cracks from several cycled beta-alumina electrolyte tubes, the obvious difference between cracks which had caused cell failure by shorting and cracks which had not (ie. presumably sealed and unsealed

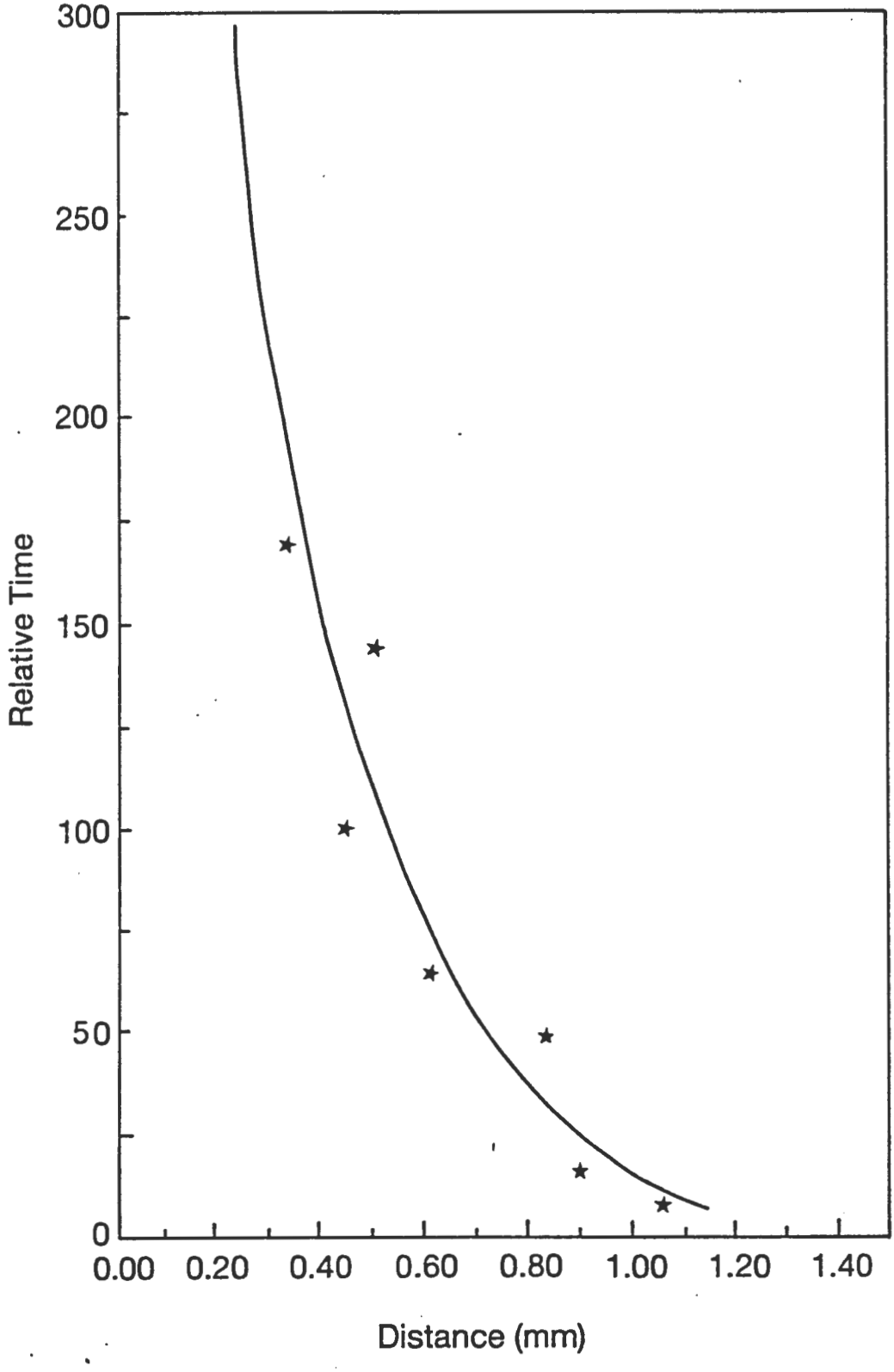

FIGURE 9.1. GRAPH OF RELATIVE TIME (THE SQUARE OF THE DEPTH FROM THE FRACTURE SURFACE OF HALF THE MAXIMUM OPTICAL DENSITY) VERSES TIME FOR A CRACK THROUGH THE BETA-ALUMINA TUBE.

FIGURE 9.2. A COMPOSITE OF SEM MICROGRAPHS OF THE UNCLEANED FRACTURE SURFACE OF A SEALED CRACK. ACCOMPANYING EDS ANALYSES ARE GIVEN IN TABLE 9.1.

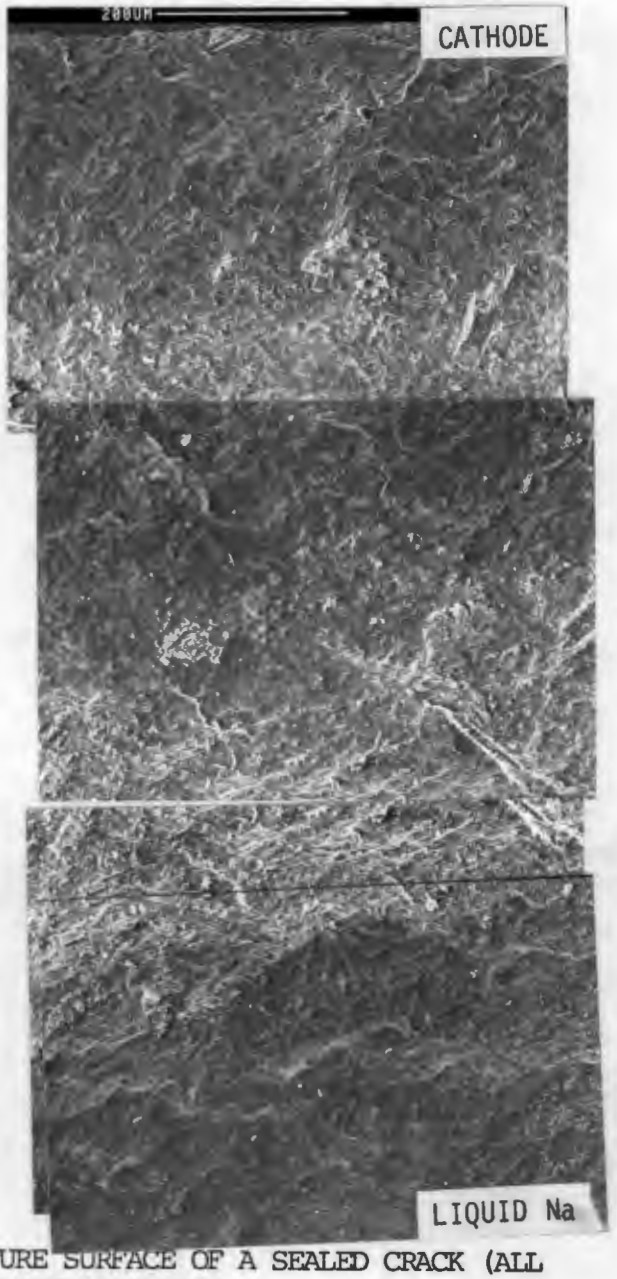

TABLE 9.1. EDS ANALYSES OF A FRACTURE SURFACE OF A SEALED CRACK (ALL ANALYSES ARE GIVEN IN WEIGHT PERCENT).

	A	B	C
Na_2O	10.05	22.32	6.99
Al_2O_3	81.21	51.69	81.95
CaO	0.00	0.00	0.00
K_2O	0.00	0.00	0.00
FeO	0.10	7.99	10.45
SiO_2	0.48	0.00	0.25
Cl	1.85	17.75	0.21
Pb	6.29	0.27	0.00

cracks) was that the "sealed" cracks were invariably much longer (approximately 100mm) than the "unsealed" cracks (approximately 10mm). SEM examination of the cracks revealed that the "sealed" cracks were much broader than the unsealed cracks.

A composite SEM micrograph of a crack which had apparently sealed is shown in figure 9.2. along with the appropriate EDS analyses.

The Pb scan of the fracture surface of a sealed crack is shown in figure 9.3.(a). Notice that the Pb was limited to a few microns of the fracture surface in the region of the Na/electrolyte interface. The Cl and Fe scans are shown in figures 9.3.(b) and (c). Note that the areas with the largest amounts of Fe did not correspond to the areas containing the largest amounts of Cl.

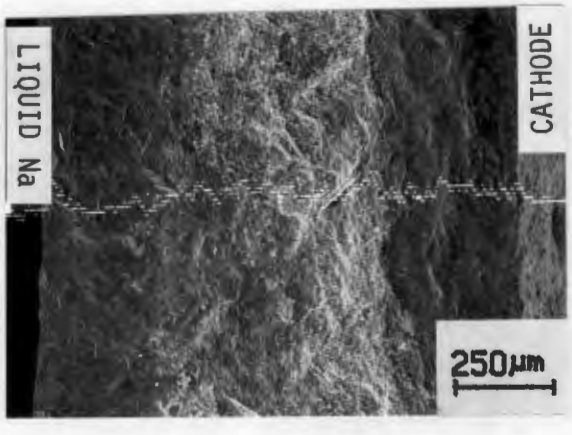

FIGURE 9.3.(a) AN SEM MICROGRAPH OF THE FRACTURE SURFACE OF A SEALED CRACK WITH A Pb LINE SCAN OF THE SURFACE SUPERIMPOSED.

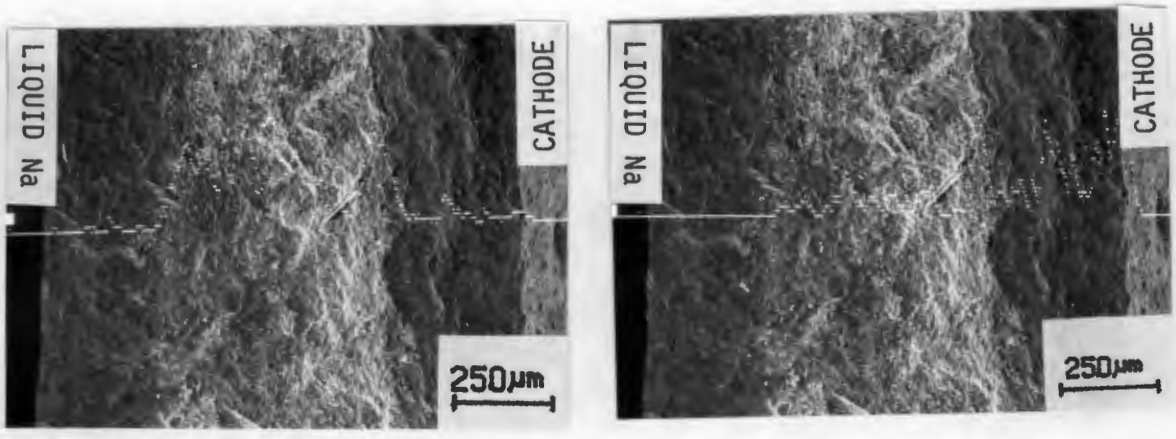

(b) (c)

FIGURE 9.3.(b) AN SEM MICROGRAPH OF THE FRACTURE SURFACE OF A SEALED CRACK WITH A Cl LINE SCAN OF THE SURFACE SUPERIMPOSED.
(b) AN SEM MICROGRAPH OF THE FRACTURE SURFACE OF A SEALED CRACK WITH A Fe LINE SCAN OF THE SURFACE SUPERIMPOSED.

The Na and Al scans were not done as they were complicated by the effect of the sampling depth relative to the size of the contaminant.

9.3. Discussion.

9.3.1.Direction of cracking

The study of an Ag exchanged cross-section of the crack showed that the depth of blackening decreased with distance from the Na/electrolyte interface. This is consistent with cracks which had been formed by Na dendrite formation.

The fracture surfaces of all the cracks studied contained abnormally large (relative to the interface) Pb concentrations close to the Na/electrolyte interface. From the discussion in chapter 8 this suggests that the Pb was present due to accumulation of Pb in pre-existing flaws during the coating of the electrolyte. If this was the case then these flaws were probably the initiation sites for the cracks. The tubes, though, are dye penetrant tested by the

manufacturers. Nevertheless the flaws are on the inside of the tube (where the flaws are most difficult to detect) and presumably very thin. The sensitivity of the dye penetrant test is not known, and it may thus be possible that the flaws were too fine to be detected by this technique.

The cracks found extending from the S/beta-alumina interface in Na/S cells (re.section 4.3.) and the cracks extending from the Hg/beta-alumina interface in Na/Hg cells (Brieter et al.; 1976) were both identified as being caused by "stress corrosion cracking" (SCC). In both cases the cracks were found to be branched and many were found to extend only a portion of the way through the electrolyte. No branched cracks were found in the Zebra cells. This is consistent with Na dendrite formation but inconsistent with a SCC mechanism.

Examination of a variety of polished cross-sections of the electrolyte tube wall did not reveal evidence of cracking extending a limited distance into the electrolyte from the cathode/electrolyte interface. However internal damage was found in the region of the the Na/electrolyte interface which appeared to be associated with crack initiation. An example of such damage is shown in figure 9.4.

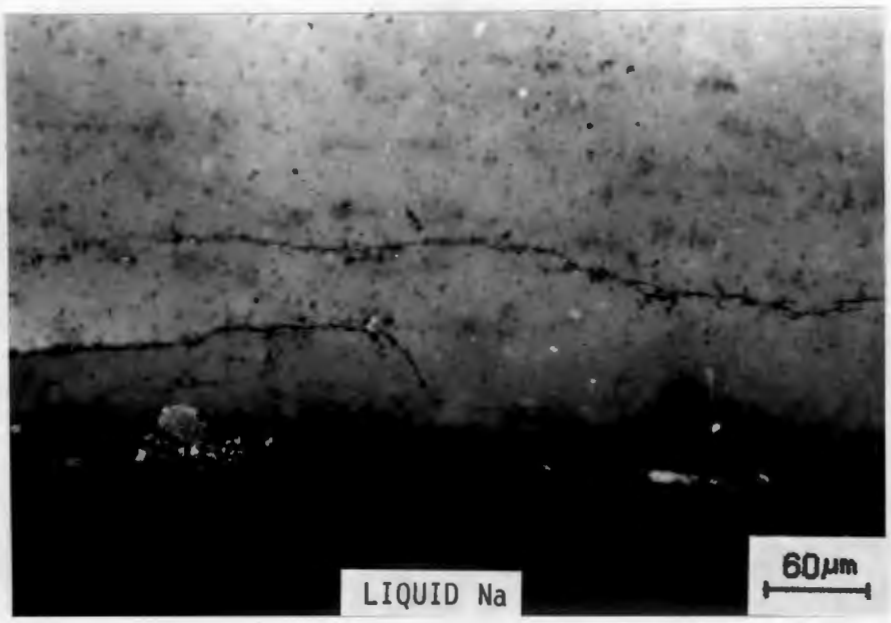

FIGURE 9.4. AN OPTICAL MICROGRAPH OF INTERNAL DAMAGE IN THE REGION OF THE Na/ELECTROLYTE INTERFACE OF A CYCLED BETA-ALUMINA ELECTROLYTE,

Fractography of the fracture surface was inconclusive as no sign of degradation of the beta-alumina (ie. breakdown or dissolution of grains), nor evidence of shear planes (normally associated with mechanical failure) was found. Even a backscatter image of the surface (see figure 9.5.) failed to show any evidence of directionality in the cracking direction.

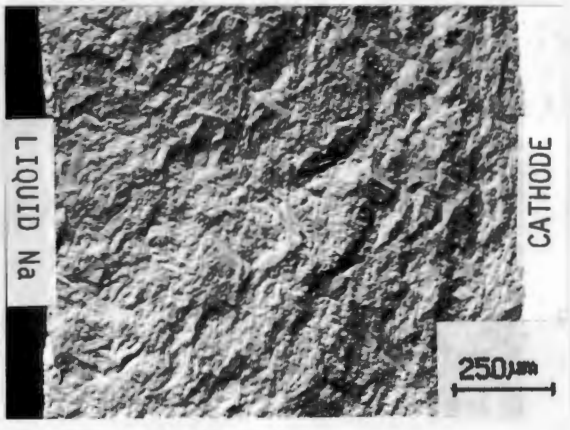

FIGURE 9.5. A BACKSCATTER MICROGRAPH OF THE FRACTURE SURFACE OF A SEALED CRACK.

As the $NaAlCl_4$ is not an electronic conductor no current concentration will occur in interfacial flaws in beta-alumina on the cathode side. Hence a mechanism for dendrite formation analogous to Na-dendrite formation is not possible.

It is thus likely that the cracking of the electrolyte was caused by Na dendrite formation. However the possibility that cracking initiated from the cathode/electrolyte interface cannot be excluded.

10.3.2. Possible Sealing Mechanisms

From table 9.1. it is apparent that the cracks contain large concentrations of Na and Cl. Thus the sealing suggested by Dell et.al (1987) seems reasonable. The seal appears to consist predominantly of NaCl.

The distribution of Al in the crack is not known. Nevertheless the deposits within the crack contained surprisingly little Al. However the cracks were all black on the cathode/electrolyte interface. The blackening may have been caused by a thin layer of deposited Al. This was observed previously when the beta-alumina electrolyte was mechanically broken in a cell.

The presence of Fe in the crack was surprising as the Fe is insoluble in molten $NaAlCl_4$. The Fe matrix is in contact with the electrolyte. It is thus possible that the Fe moved in with the $NaAlCl_4$ during sealing. Alternatively, the Fe may have been picked up as an impurity by the crack during removal of the electrolyte from the cell.

The penetration of a Na dendrite through the electrolyte wall would occur on charging of the cell ie. when the Na^+ ions are diffusing in the electrolyte from the cathode to the anode. As all the evidence found suggests that the cracking in the Zebra cell occurs via Na dendrite formation, it will be assumed that the sealing of the cracks occurs during the charge cycle of the cell.

One possible mechanism for the sealing of the cracks is simply the diffusion of $NaAlCl_4$ into the cracks on penetration of the electrolyte wall by the Na dendrite. The liquid Na at the crack tip is under high pressure. On crack penetration of the electrolyte wall into the cathode the liquid Na at the crack tip would burst out into the cathode reacting violently with the $NaAlCl_4$ to form NaCl and Al at the $Na/NaAlCl_4$ interface.

The reaction should, however be self-inhibiting as both NaCl and Al are insoluble in Na and $NaAlCl_4$. The true extent of this self-inhibition is not known, but the interfacial surface area between the Na and the $NaAlCl_4$ is very small. Even though the reaction is extremely exothermic (which should tend to cause the diffusion more rapidly) the reaction would be expected to terminate rapidly and thus sealing by this mechanism seems unlikely.

For a seal to be effective the reaction product must eliminate the current enhancing effect of the crack. If this did not occur the Na pressure at the Na/seal interface would again rise from Na being fed in from the sides of the crack and "break" the seal. Thus the depth to which the $NaAlCl_4$ penetrates the crack would determine whether the seal is effective.

A possible mechanism whereby the $NaAlCl_4$ can penetrate to a greater depth than may be expected from normal diffusion is the opening up of the crack to relieve internal stresses.

The green beta-alumina tubes are generally produced by isostatically pressing the beta-alumina powder onto a magnesia former. The green tubes are then removed from the former and fired. Though the tube wall thickness is relatively small, it is possible that internal stresses are set up in the tube at this stage. Internal stresses may be caused by differential cooling between the inner and outer surfaces of the tube. If there are internal stresses the electrolyte would be expected to have a tensile hoop stress on the outer surface, and a compressive hoop stress on the inner surface. The stress distribution in the dome would be more complex.

Internal stresses would result in the crack, on penetrating the tube wall, being split open to relieve the internal stresses.

The local potential difference through the electrolyte would be instantaneously eliminated on Na penetration, hence the Na will no longer be fed into the crack. The volume created would thus be predominantly filled by $NaAlCl_4$. This would explain the depth of penetration of NaCl into the cracks. The effect is illustrated schematically in figure 9.6.

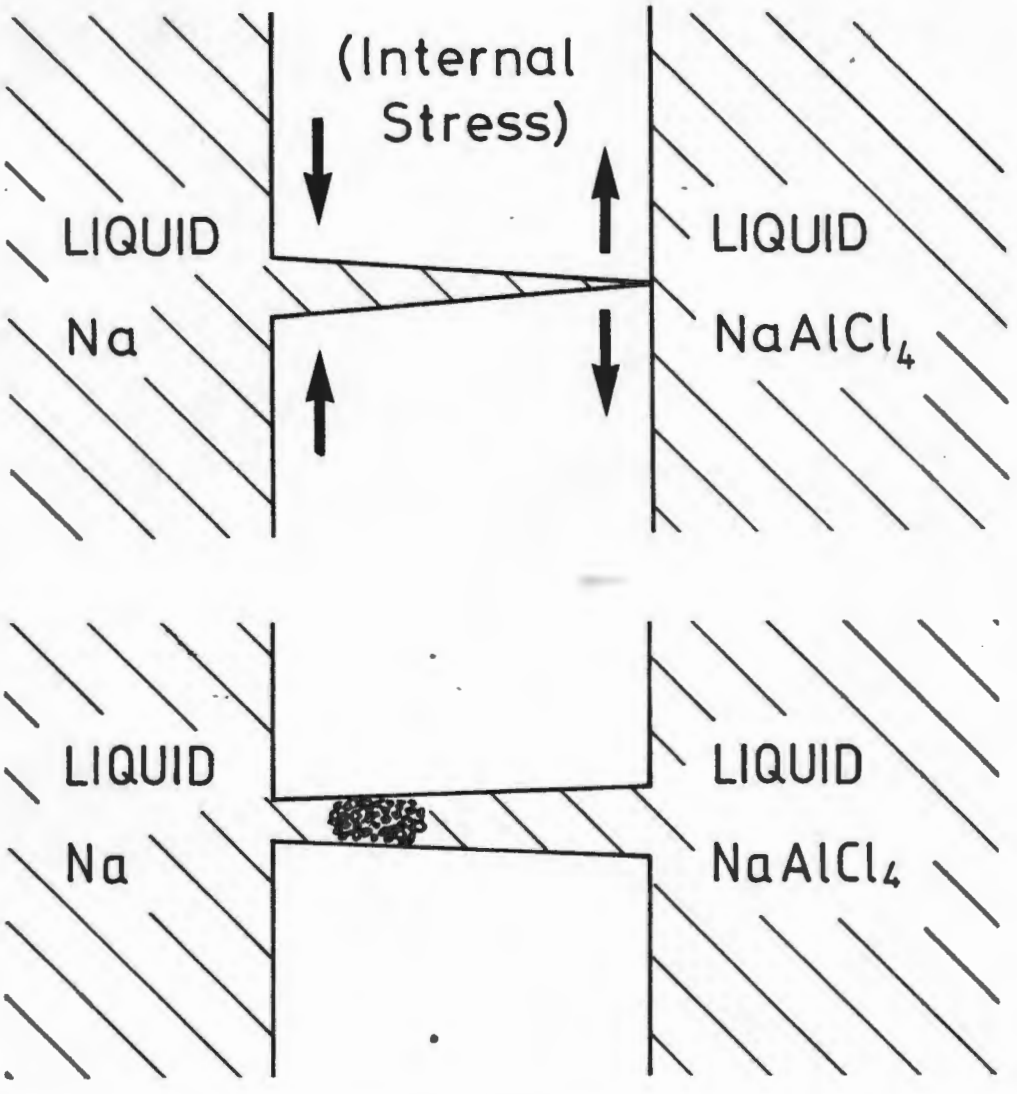

FIGURE 9.6. A SCHEMATIC REPRESENTATION OF A POSSIBLE SEALING MECHANISM OF CRACKS IN THE ELECTROLYTE OF THE ZEBRA CELL:

(a) ON RUPTURING THE ELECTROLYTE WALL THE Na AT THE CRACK TIP IS UNDER PRESSURE AND BURSTS OUT INTO THE $NaAlCl_4$ IN THE CATHODE.

(b) THE INTERNAL STRESSES IN THE BETA-ALUMINA ELECTROLYTE ARE RELIEVED BY THE CRACK WIDENING ON THE CATHODE SIDE: CREATING A NEW VOLUME WHICH SUCKS THE LIQUID $NaAlCl_4$ INTO THE CRACK. THE $NaAlCl_4$ REACTS WITH THE Na IN THE CRACK TO FORM A PLUG.

Evidence for this mechanism was found in a few of the tubes. In a few of the cracks the cathode/electrolyte side of the crack was much wider than the Na/electrolyte side (see figure 9.7.).

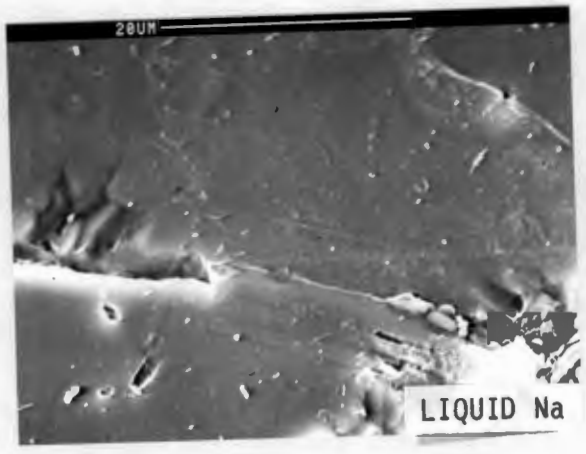

FIGURE 9.7. AN SEM MICROGRAPH OF A POLISHED CROSS-SECTION OF A CRACK SHOWING THE CRACK TO BE THICKER AT A DISTANCE FROM THE Na/ELECTROLYTE INTERFACE THAN AT THE INTERFACE.

A third possible mechanism is the suction of electrolyte into the crack by a venturi effect caused by the high velocity of the sodium at the crack tip.

The theories for crack propagation assume that the crack is considerably shorter than the wall thickness ie. the cracks were modeled assuming that initiation was far more crucial than the actual propagation. The current enhancement increases with increasing crack length ie. the pressure at the crack tip remains critical for fracture once the crack has initiated. However, the assumptions made by the model in terms of current enhancement and Na flow are not directly applicable when the crack approaches the cathode/electrolyte interface. However, as a first approximation the Virkar model for 3-D crack propagation will be assumed to be approximately true for cracks of similar length to the electrolyte wall thickness.

The volume flow rate (V) of Na in the crack is then given by:

$$\dot{V} = \frac{\pi P}{4nl} \frac{c^3 b^3}{(c^2+b^2)}$$

where: P is the pressure of the Na at the crack tip
2c is the width of the crack
b is the thickness of the crack
n is the viscosity of the Na
and l is the length of the crack through the tube wall

Dividing by the x-sectional area of the crack (ellipse), and bearing in mind that c >>b the velocity of Na in the crack is given by:

$$\bar{v} = \frac{P\, b^2}{4nl}$$

From Virkar et al.:

$$b = \frac{(1-\nu^2)\, c\, P}{E}$$

where: ν is the Poissons ratio of beta-alumina
E is the Young's Modulus of beta-alumina
ie.

$$\bar{v} = \frac{P^3 (1-\nu^2)^2 c^2}{4\, n\, l\, E^2}$$

If we assume that the pressure (due to the Na) in the region of the crack tip is the critical pressure for crack propagation, P_{crit}, then from Virkar et al.(1983) for a 3-d ribbon shaped crack is;

$$P^2_{crit} = \frac{\pi E \gamma eff}{2\, c\, (1-v^2)}$$

where: γeff is the effective surface energy of liquid Na on beta-alumina.

In addition let us assume that the area ahead of the crack is the sole source of Na being fed into the crack. In effect we are examining a flow situation for a point a distance from the crack tip where no Na is being fed into the crack via the electrolyte (ie. preceding region of the crack is the only source of Na for the point).

Now when the crack penetrates the tube wall the $NaAlCl_4$ is immobile (v=0) relative to the Na in the crack. The rapid flow of Na from the crack tip would result in a suction of the $NaAlCl_4$ into the crack.

The pressure difference (ΔP) due to the velocity of sodium in the region of the crack tip is given by

$$\Delta P = \frac{\rho \bar{v}^2}{2}$$

where ρ is the density of the sodium

Now if $\Delta P > P_{crit}$ (ie. the suction due to the velocity of the liqiud Na > pressure of Na at the crack tip) then suction of $NaAlCl_4$ into the crack will occur. If $\Delta P < P_{crit}$ the liquid Na will tend to burst out from the crack into the cathode. The model is shown schematically in figure 9.8.

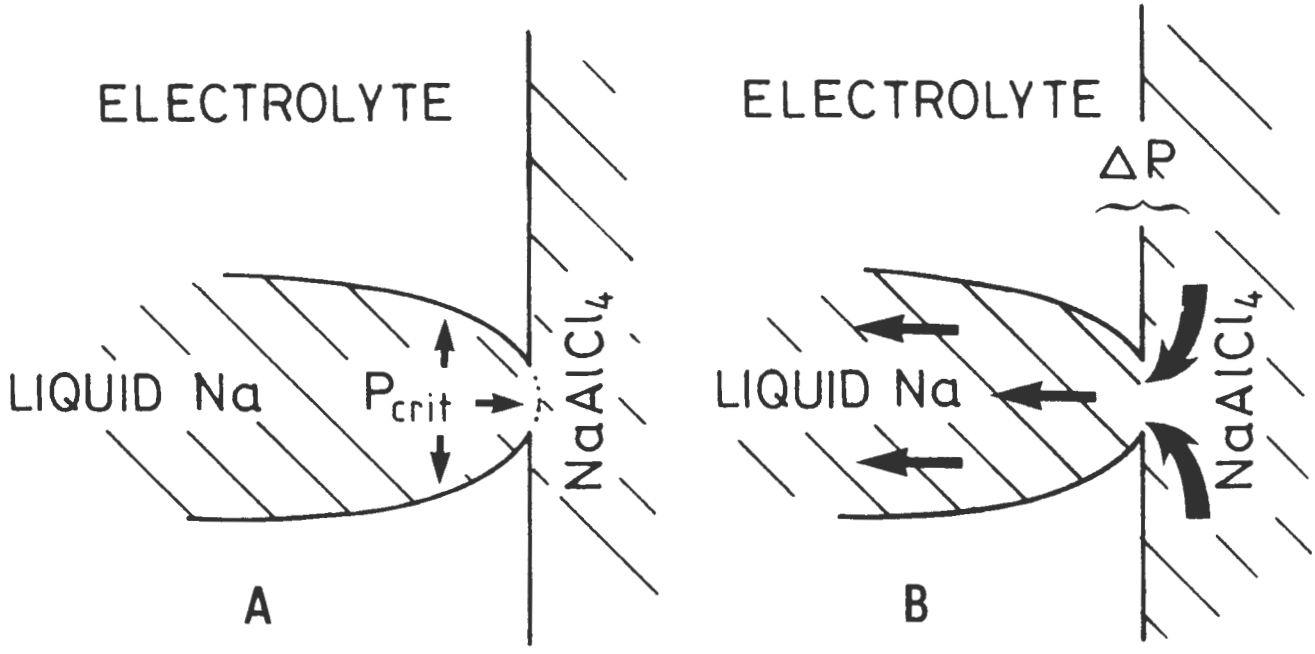

FIGURE 9.8. A SCHEMATIC ILLUSTRATION OF THE VENTURI MODEL FOR THE SUCTION OF $NaAlCl_4$ INTO THE CRACK:
(a) AT THE THE MOMENT WHEN THE CRACK PENETRATES THROUGH THE CATHODE/ELECTROLYTE WALL THE Na IS UNDER PRESSURE, P_{CRIT}
(B) THE HIGH VELOCITY OF THE Na IN THE CRACK CAUSES A PRESSURE DIFFERENTIAL AT THE CRACK TIP: SUCKING $NaAlCl_4$ INTO THE CRACK.

Substituting gives the criteria for suction to occur:

$$\frac{c^{3/2}}{l^2} > \left[\frac{2}{\pi \gamma_{eff}}\right]^{5/2}\left[\frac{E}{(1-\nu^2)}\right]^{3/2}\left[\frac{n^2}{\rho}\right]$$

ie.

$$\frac{c^{3/2}}{l^2} > \text{constant}$$

This equation implies that the probability of $NaAlCl_4$ entering the crack is strongly dependent on the width of the crack tip, and inversely dependent on the crack length.

Substituting an l of 1.5 mm , E of 207 GPa, n of 3.4×10^{-4} poise, γ_{eff} of 5 J m, ν of 0.25 and ρ of 882 kg m^{-3} yields a critical c of > 3.1773 m. The model thus predicts that suction of $NaAlCl_4$ into the crack is unlikely

The original assumption that the feeding of the point is only due to the crack itself is obviously incorrect. In fact most of the Na is not taken in at the tip but the region behind the tip. The model thus does not represent the true conditions at the crack tip. The velocity calculations though are representative of an area a small distance from the crack tip.

Taking a crack of width 3 microns at penetration of the crack into the cathode the Na has a calculated velocity of 1178.15 m sec^{-1} (approximately 4000 km/hour). The speed the Na in the crack is thus of the order of the speed of sound in liquid metals (speed of sound in Hg is 1450 m sec^{-1}). This implies that the flow is supersonic. If this is the case the dependence of ΔP on velocity is not valid.

The true effect of the drag due to the sides in a crack of such small dimensions is not taken into account in the Virkar model. The extra drag would tend to increase the pressure of the Na at the crack tip, and decrease the velocity of the Na in the crack ie. increase the critical crack width (c) necessary for suction of the $NaAlCl_4$ into the crack to occur.

The Venturi effect does not, therefore appear to be likely in the sealing of the cracks.

10. CONCLUSIONS

1) No large scale impurity pickup occurs in the beta-alumina electrolyte of the Zebra cell during charge and discharge cycling.

2) A cell which underwent early failure appears to have failed due to moisture pickup by the cathode, or internal shorting in some part of the cell other than the beta-alumina electrolyte. The cell did not fail as a direct result of the passage of an Na^+ current through the electrolyte

3) Overdischarged cells do not appear to lose capacity due to poisoning, or breakdown of the beta-alumina electrolyte.

4) The beta-alumina electrolyte from a cell which had shown progressive capacity loss with cycling appears to have reacted with atmospheric moisture prior to being installed in the cell. This reaction with the atmosphere would have caused a progressive internal resistance rise which may explain the progressive capacity loss.

5) The beta-alumina electrolyte is not contaminated by impurity pickup from the cathode of the Zebra cell, even after standing at operating temperature for 1 year.

6) The Pb wetting agent is adherent to the beta-alumina tube, irrespective of the number of cycles performed. On the first cycle the amount of Pb detected on the interface decreases rapidly, but thereafter appears to remain relatively constant.

7) The Pb coating applied prior to cycling is not present as a discrete layer after cycling.

8) The Pb wetting agent does not appear to promote cracking in the electrolyte.

9) Cracking in the Zebra cell is not primarily caused by bad wetting of the beta-alumina electrolyte by the sodium.

10) All the cracking observed in failed beta-alumina tubes appears to have originated exclusively from sodium dendrite formation in the beta-alumina electrolyte, rather than interaction of the beta-alumina with the cathode. The cracking appears to have initiated from flaws in the electrolyte and may have been enhanced by internal stresses in the beta-alumina electrolyte.

11) Cracks in the beta-alumina electrolyte of the Zebra cell seal via the formation of a plug in the crack consisting mainly of sodium and chlorine.

11. RECOMMENDED FUTURE RESEARCH

The cells in this thesis were not specifically constructed or cycled for failure mode studies. It has become clear to the author that in order to systematically study failure mechanisms in the Zebra cell such cells must be constructed.

The cells would need to be constructed with known compositions, under rigorously controlled conditions to ensure that the failures may be systematically compared. Several cells from each of the failure modes would need to be examined to obtain a fair sample of each of the modes. This would enable one to be more general with conclusions from a particular failure mode.

The cycling histories of the cells would have to be carefully monitored, particularly with respect to the charge and discharge rates as well as the cell capacity on each cycle. In addition the internal cell resistance must be carefully monitored during cycling. The exact criteria used for removing the cells from service will need to be carefully noted.

The study of the cells in this thesis was solely concentrated on the beta-alumina electrolyte tube. The tubes studied in this thesis seem to suggest that at least some of the blame for failure may well be located in the cathode. In any future studies it is therefore suggested that the tubes be studied in conjunction with the Zebra cathode. Emphasis must be laid on the phases present in the cathode as well as the general morphology of the Fe matrix.

Furthermore the most promising research area would appear to be a study of the Na\electrolyte and the cathode\electrolyte interfaces. All of the tubes studied in this thesis were cleaned with alcohol before studying. As a result any interfacial layers were probably washed off. However by carefully removing the outer casing and cathode from the tube at room temperature may enable one detect interfacial layers. As the layers are likely to be very thin, a study using SIMS would probably be necessary.

The area of failure modes in the Zebra cell remains largely unexplored and it is strongly suggested by the author that research be continued in this area.

REFERENCES

R.D. Armstrong, T.Dickinson and J.Turner: Electrochimica Acta Vol 19 (1974) pp 87-192

N.Baffier,J.C. Badot, Ph Colomban: Mat Res Bull Vol.16 (1981) pp 259-265

J.B.Bates, Herbert Engstrom, J.C.Wang, B.C.Larson, N.J.Dudney and W.E.Brundage: S.S.Ionics Vol 5 (1981) pp 159-162

M.F. Bell, M Sayer ,D.S. Smith and P.S. Nicholson: Solid State Ionics Vol 9 & 10 (1983) pp 731-734

A.C.Beuchele and L.C.De Jonghe: Ceramic Bull. Vol 58 (1979) pp 861-864

A.C.Beuchele, J.C.De Jonghe and D.Hitchcock: J Electrochem Soc Vol 130 (1983) pp 1042-1150

J.P.Boilot, G.Collin, Ph Colomban and R.Comes: Phys Rev B Vol 22 No 12 (1980) pp 5912-5923

J.P.Boilot, Ph Colomban, R Collongues, G.Collin and R.Comes: J Phys Chem of Solids Vol 41 (1980) pp 253

R.J.Bones, J.Coetzer,R.C.Galloway and D.A.Teagle: Extended Abstracts 170th Meeting Electrochemical Society in San Diego, October 1986 Abstract No 763

M.W.Breiter, N.S.Choudhury and E.L.Hall: J Electrochem. Soc Vol 133 No 10 (1976) pp 2064-2068

M.W. Brieter, N.S. Choudhury and E.L. Hall: Solid State Ionics Vol.133 (1984) pp 225-230

J.A.Bruce, R.A.Howe and M.D.Ingram: Solid State Ionics Vol 18 & 19 (1986) pp 1129-1133

N.S. Choudhury, M.W. Brieter and E.L. Hall: Electrochemical Acta Vol 31 No. 7 (1986) pp.771-776

J.Coetzer: J Power Sources Vol 18 (1986) pp 377-380

G.Collin, Ph Colomban, J.P. Boilot and R.Combs: in Fast Ion Transport in Solids Eds P. Vishishta, J.N.Mundy and G.K.Shenoy (North Holland, Amsterdam 1979) pp 309-314

R.Collongues, D Gourier, A.Kahn, J.P.Boilot, P.Colomban and A Wicker: J Phys Chem Solids Vol 45 (1984) pp 981-1013

R. Davidge, G. Tappin, J.R. Mc Tappin and G.J. May: Ceramic Bull Vol. 58 No.8 (1979) pp 771-774

L.C.De Jonghe: Ceramic Bull. Vol 65 No 8 (1986) pp 1158-1160

L.C. De Jonghe: J. Electrochem Soc Vol 129 No 4 (1982) pp 752-755

L.C.De Jonghe and A.Beuchele: Journal of Materials Science Vol 17 (1982) pp 885-892.

L.C. de Jonghe and L. Feldman: Mat. Res. Bull Vol 15 (1980) pp 777-782

L.C. De Jonghe, L. Feldman and A.C. Beuchele: Solid State Ionics Vol 5 (1981) pp 267-270

L.C.De Jonghe, L.Feldman and A Beuchele: Journal of Materials Science Vol 16 (1981) pp 780-786.

R.M.Dell and R.J.Jones in the Extended Abstracts 22nd IECEC Meeting in Philidelphia (1987)

J.S.Demott and A.R.Tilley in "The Sodium Sulphur Battery" Edited by J.L.Sudworth and A.R.Tilley (Chapman and Hall 1985)

G.Evans Private Correspondance (Fellow student in the Department of Materials Engineering at the University of Cape Town)

G.C.Farrington and B.Dunn: Solid State Ionics 7 (1982) pp 267-281

L.A.Feldman and L.C.De Jonghe: Journal of Material Science Vol 17 (1982) pp 517-524.

A.Gibson in "Power Sources" Vol 6; Edited by D.H.Collins; published by Achademic Press,London (1977) pp 673

D.C. Hitchcock and L.C. De Jonghe: J Electrochem Soc Vol 133 No 2 (1986) pp 355-358

D.C. Hitchcock and L.C. De Jonghe: J Electrochim Soc Vol 133 (1986) pp 6-9

A.Hooper: J Phys D Appl. Phys 10 (1977) pp 1487

M.Y.Hsieh and L.C.De Jonghe: J. American Ceramic Soc. Vol 61, No.5-6 (1978) pp 185-191

K.K.Kim, J.N.Mundy and W.K.Chen: J Phys Chem Solids Vol 40 (1979) pp 757

W. Koch and C. Wagner: Z Phys Chem B38 (1937) pp 295

J.T. Kummer: Prog in Solid State Ionics Vol.7 (1972) pp 141-175

Y.Lezennec, C.Lasne, P.Margotin and T.Fally: J Electrochem Soc Vol 122 No 6 (1975) pp 734-737

J.Ni, Y.Tsai and D. Whitmore: Solid State Ionics Vol 5 (1981) pp 199-202

R.W.Powers and D.S.Park: J Electrochem Soc Vol 133 No 7 (1978) pp 1353-1359

R.H. Richman and G.J. Tennenhouse: J Am. Cer. Soc. Vol 58 No 1-2 (1975) pp. 63-67

W.L.Roth, F.Reidinger and S.La Placa: in Superionic Conductors edited by G.D.Mahan and W.L.Roth (Plenum Press New York) (1976) pp 223-241

J.C. Russ(1) in Fundamentals of Energy Dispersive X-Ray Analyses (Butterworths & Co (Publishers) Ltd) (1984) pp 202-203

J.C. Russ(2) in Fundamentals of Energy Dispersive X-Ray Analyses (Butterworths & Co (Publishers) Ltd) (1984) pp 45-46

C.Schmid: J Mat Sci Letters Vol 5 (1980) pp 263-266

L.Y.Shen,G.A.Pasteur and D.E.Aspens: Phys Rev.B Vol 16 (1977) pp 3742

D.H.Shetty, A.V.Virkar and R.S.Gordon in the proceedings of an international symposium on fracture mechanics of ceramics entitled "Fracture Mechanics of Ceramics" Vol 4 Edited by R.C.Bradt Published by Plenum Press, New York (1978)

M.M.Thackeray and K.T.Adendorf in the Proceedings of Electochemical Soc Meeting May 1987 (Philidelphia)

T.Tsurumi, G.Singh and P.Nicholson: S S Ionics Vol 22 (1987) pp 225-230

A.V.Virkar and L.Viswanathan: J Mat Sci Vol 18 (1983) pp 1202-1212

A.V. Virkar, L. Viswanathan and D.R. Biswas: J Mat Sci Vol 15 (1980) pp 302-308

L. Viswanthan and A.V. Virkar: J. Mat Sci Vol 17 (1982) pp 753-759

J.C.Wang: J Chem Phys vol 73 no.11 (1980) pp 5786-5795

J.C.Wang, J.B.Bates, T.Kaneda, E.Enstan, D.F.Pickett and Sang-il Choi: in Fast Ion Transport in Solids Eds P. Vishishta, J.N.Mundy and G.K.Shenoy (North Holland, Amsterdam 1979) pp 379-382

F.G.Will: J Electrochem Soc Vol 123 (1976) pp 834

D.Wolf: J Phys Chem Solids Vol 40 (1979) pp 757-773

G.Yamaguchi and K.Suzuki: Bull. Chem Soc Japan Vol 41 (1968) pp 93-99

P.D.Yankulov, G.Staikov, A.Yanakiev, R.Kvachkov, P.V.Angelov and E.Budevski: Journal of Solid State Chemistry Vol 63 (1986) pp 1-7

I.Yasiu and R.H. Doremus: J Electrochem Soc Vol 125 No 7 (1978) pp 1007-1010

I Yasui and R.H.Doremus J Americam Ceramic Soc Vol 60 No 7-8 (1977) pp 296-300

G.E.Youngblood, G.R.Miller and R.S.Gordon J Amer Ceram Soc Vol 61 (1978) pp 86-87

APPENDIX 1: THE EDS SEMI-QUANTITATIVE ANALYSES

Elemental analyses done using EDS are subject to certain limitations. Some of these limitations, and the methods used by the author to standardise the analyses obtained are detailed in this appendix.

All the x-ray spectra were acquired on a Cambridge Sterioscan 200 with a Tracor Northern 5400 spectral analyser attached.

A1.1. CONDITIONS USED FOR ACQUIRING SPECTRA.

The optimum conditions (in terms of background shape and count rate) for acquiring spectra were at a SEM accelerating voltage of 20 KeV, a working distance (ie. distance from the sample to pole piece in the SEM) of 25 mm, and (for the x-ray detector configuration on the SEM used) a take-off angle of between 51.181^0 to 54.743^0. To minimise detector dead time and simultaneously optimise counts the dead time was adjusted manually (using the resolution of the microscope) to be 20 %.These conditions were used on all the flat, polished standard samples examined to make quantitative comparison of the spectra possible.

However the take-off angle of the detector relative to the sample cannot be easily ascertained when studying the fracture surfaces of samples. The conditions used for the analyses were set up to as closely mirror those used for the polished samples as possible, nevertheless there is a far greater inaccuracy expected from these results than from those of the polished samples.

A1.2. COMPARISON OF SSQ RESULTS WITH MICROPROBE ANALYSES

All the chemical analyses quoted in the thesis were obtained from EDS analyses using the SSQ (Standardless Semi-Quantitative) package for the Tracor 5400. To estimate the uncertainty associated with the chemical analyses the results were compared to microprobe values obtained on a Cameca Camebax Microanalyser. The results are shown in table A1.1.

	EDS Analyses*		Microprobe *	
Na O	6.35	0.48	12.58	1.26
Al O	92.72	0.52	85.46	0.32
CaO	0.00	0.00	0.00	0.00
K O	0.58	0.43	1.23	0.50
FeO	0.00	0.00	0.00	0.00
Cl	0.09	0.06	0.12	0.01
SiO	0.24	0.08	0.10	0.02
Pb	0.00	0.00	0.00	0.00

* All analyses in weight percent

TABLE A1.1. COMPARISON OF CHEMICAL ANALYSES.

As can be seen differences of up to 20% in the results occur.

A1.3 INACCURACIES IN ANALYSING THE SPECTRA.

a) Inaccuracies due to the acquire process

Better statistics (and hence more reliable results) are obtained for longer acquire times. However in beta-alumina the electron beam interacts with the Na in the conduction planes of the sample, resulting in the formation of Na metal globules on the surface being analysed. Globule formation was not found to be a factor for analyses done at magnifications of 1000X, but for analyses done at high magnifications to determine the compositions of small artifacts the amount of Na detected increased rapidly with acquire time. A nominal standard acquire time of 300 seconds detector live time was used throughout and no high magnification analyses were done such that any effect due to Na globule formation could be avoided.

One of the difficulties of the EDS analyses is that the silicon/lithium detector may produce an extraneous Si peak. This peak is caused by Si being ionised on the front silicon dead layer by high energy X-rays. If the Si K x-rays being fluoresced enter the detector they will result an extraneous increase in the number of counts in the silicon which is not representative of the the amount of Si in the sample.

The effect could be quantified by acquiring several spectra at lower and lower SEM acceleration voltages thus successively decreasing the number of high energy X-rays

which could ionise the Si This was done by performing a series of analyses between 10 and 20 KeV, maintaining a dead time of 20 %. The fraction of SiO_2 was found to be virtually unaffected by the change in electron energy (0.16 $^{w}/_{0}$ at 20 KeV, 0.20 $^{w}/_{0}$ at 10 KeV) in the beam striking the sample, and in fact the reverse of the expected trend was found (possibly just due to background fitting during the semi-quantitative analyses).

b) Inaccuracies due to the use of the SSQ package:
Standard EDS quantitative analyses are essentially computed by ratio of the number of counts in the peak acquired to those from a previously acquired standard peak of the pure element under the same conditions (corrections are then done for atomic number, secondary fluorescence and absorbance effects). The SSQ package, on the other hand, mathematically computes the theoretical shape and size of the pure element peak for the relevant conditions. However, when different atomic shells are involved in a single analysis or when light elements are involved, SSQ is not really suitable for quantitative analyses (Russ; 1984).

The SSQ package computes the size of the peaks by fitting a complete background to the spectrum and then studying the portions of the peaks above the background. The equation used to calculate the background is a function of take-off angle, KeV at which the spectrum was acquired, as well as the height and slope of two user defined "regions of interest" on the spectrum.

The two optimum "regions of interest" for background fitting were determined (by trial and error) to be from 1.890 to 2.330 KeV and from 5.490 to 6.070 KeV. The position of these regions relative to the peaks, and the background calculated from them by the SSQ package is shown in figure A1.1.

It will be noted from the background in figure A1.1 that the region in which the greatest inaccuracy in background fitting occurred was in the vicinity of the Al and Na peaks. This was an inherent problem in the background fitting of the SSQ package and was probably caused by the extremely large slope of the spectrum (and indeed the background) in this region. The inaccuracy could not be decreased by either increasing acquire times or moving one of the selected "regions of interest".

To normalise the error involved in background fitting the region of interest used to calculate the background were the same for all the spectra analysed.

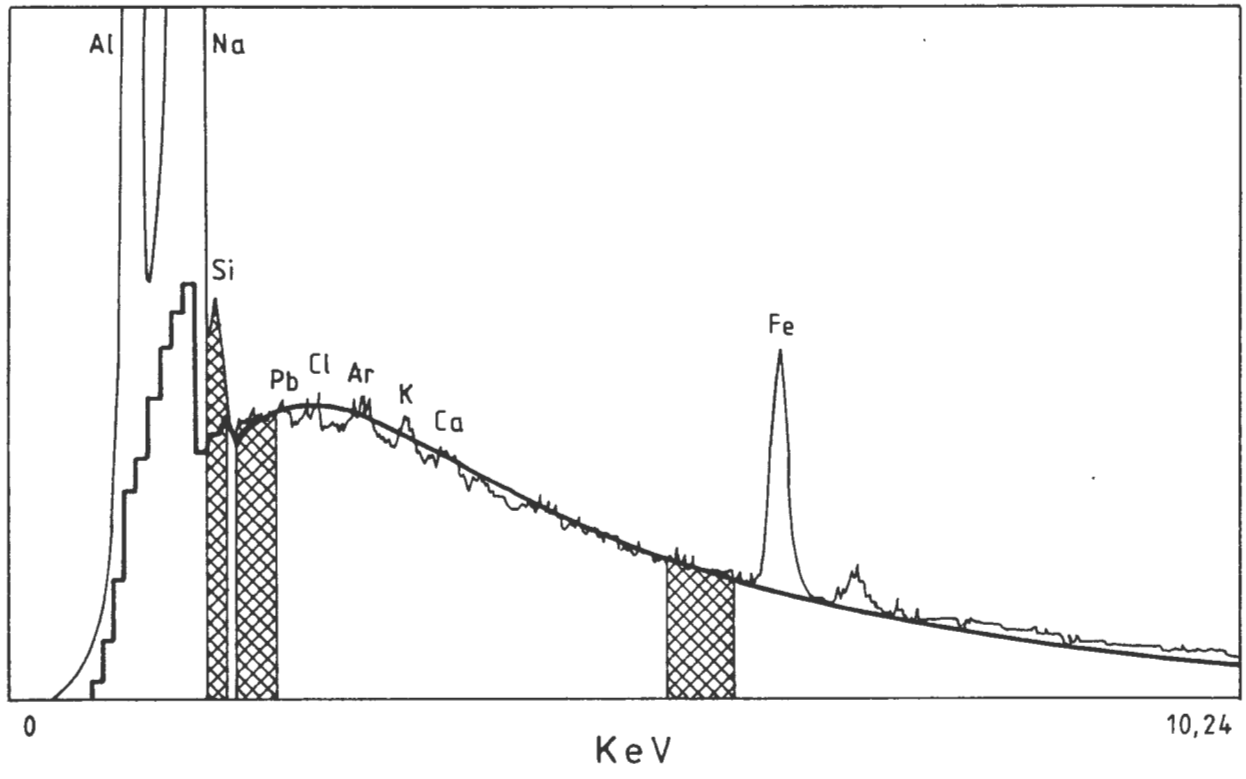

FIGURE A1.1. AN EDS SPECTRUM WITH A BACKGROUND FITTED FROM THE REGIONS OF INTEREST INDICATED.

APPENDIX 2 NOMOGRAM TO ESTIMATE THE THICKNESS OF THE Pb COATING

The maximum electron range in a particular sample in a SEM is dependant on:
1) The acceleration voltage of the SEM E_0
2) The elemental absorption edge energy E_c
3) The sample density

These factors have been combined to produce a nomogram from which the electron range may be determined. This nomogram is shown in figure A2.1.(Russ; 1984)

The maximum depth to which an element can be detected by EDS is obviously less than the electron range in the sample. Hence the maximum electron range in a particular sample may be used to give an order of magnitude estimate of the maximum depth to which a particular element may be being detected.

If we assume that the Pb coating is a discrete layer on the surface of the sample, we can (from figure 8.5.) be reasonably certain that the maximum thickness of the coating is at the maximum electron range in Pb at an acceleration energy of less than 10 KeV. Taking 10 KeV as the E_0 it is possible to estimate from figure A2.1. the maximum possible thickness of the coating

Taking an acceleration voltage E_0 of 10 KeV, elemental absorption edge for Pb (M line) of 10.55 KeV, and a density of 11.343 g cm^{-3}, the thickness from figure A2.1. is less than 0.2 microns.

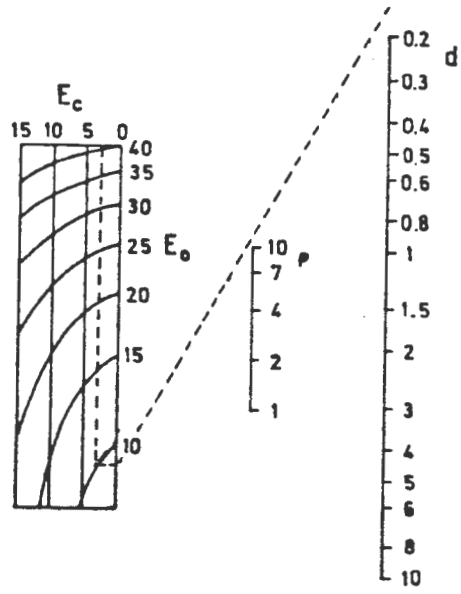

FIGURE A2.1. NONOGRAM TO ESTIMATE ELECTRON RANGE IN BULK SAMPLES AS A FUNCTION OF ACCELERATING VOLTAGE E_O, ELEMENTAL ABSORPTION EDGE ENERGY E_C, AND SAMPLE DENSITY